

REDUCTION OF SO₂ BY CO OVER GOLD SUPPORTED CATALYSTS

Mphumzile Thelma Ngwenya

Doctor of Philosophy

A thesis submitted to the Faculty of Engineering and the Built Environment,
University of the Witwatersrand, Johannesburg, in fulfilment of the requirements
for the degree of Doctor of Philosophy.

Johannesburg, 2018

Declaration

I declare that this thesis is my own, unaided work. It is being submitted for the Degree of Doctor of Philosophy in the University of the Witwatersrand, Johannesburg. It has not been submitted before for any degree or examination in any other University.

(M. T. Ngwenya)

_____ day of _____ 2018

Abstract

Sulphur dioxide is a toxic air pollutant that affects the environment and human life. The catalytic reduction of SO₂ to produce the less harmful elemental sulphur has been investigated since the 1940s. This offers a single step flue gas desulphurization process compared to using wet or dry flue gas desulphurization methods. In this research, the catalytic reduction of SO₂ by CO was investigated over gold nanoparticles supported on an easily reducible amphoteric metal oxide (TiO₂), an alkaline metal oxide (ZnO) and an acidic metal oxide (γ -Al₂O₃). In comparison, Au/TiO₂ catalyst had the highest SO₂ conversion of 86.4 % at 300 °C and a gas hourly space velocity of 3 600 mL.g_{cat}⁻¹.h⁻¹ and 2 000 ppm of SO₂, with Au/ZnO and Au/Al₂O₃ having very low average SO₂ conversions of 1.8 and 1.4 %, respectively. The optimum reaction temperature was found to be 300 °C as irreversible deactivation of the catalyst by sintering of the Au nanoparticles occurs above 300 °C as observed from the high resolution transmission electron microscopy images of catalysts after the reaction.

The products of the reaction, CO₂ and sulphur, identified as crystalline sulphur in the form of S₈, were observed in the reactor product stream, however, the reaction intermediate carbonyl sulphide was not observed. The optimum feed ratio, CO:SO₂, for high SO₂ conversions was the stoichiometric ratio of 2:1 over Au/TiO₂. The flue gas concentrations of SO₂ and CO of 420 ppm and 50 ppm

were also used to investigate the activity of the catalysts. Very high SO₂ conversions were observed at these low concentrations despite the limiting CO.

The surface analysis of Au/TiO₂ after the reaction showed that there was 1 % atomic concentration of S species which was later identified as SO_x, where x is 2, 3 or 4; however, there was no accumulation on the catalyst observed after 144 hours. This observation confirmed that the redox reaction mechanism was probably followed with SO₂ dissociating into S via adsorbed SO_x on the catalysts surface and CO oxidation occurring on the Au-support interface with the excess O adatoms on the support surface.

Pre-treatment of Au/TiO₂ with 0.5 vol% SO₂ enhanced the activity of the catalyst at reaction temperatures less than 150 °C, yet the untreated catalyst showed higher activities at 300 °C. The addition of O₂, which is present in flue gas, to the reaction feed stream reduced the conversion of SO₂ by 51.9 % as this offered a competing reaction, the direct oxidation of CO. When the O₂ feed was removed, the conversion of SO₂ increased showing that its effect was reversible.

Publications and Presentations related to this work

Conference Presentations

1. Ngwenya, T. and Jewell, L., 2010, *The Catalytic Behaviour of Au/TiO₂ for the Reduction of SO₂ by CO*, (Poster) at the CATSA conference in Bloemfontein, South Africa, 7-10 November
2. Ngwenya, T., Franklyn, P. and Jewell, L., 2011, *Activity of Gold Supported Catalysts for the Reduction of SO₂ by CO*, (Poster) at the EuropaCat X conference in Glasgow, Scotland, 28 August - 2 September
3. Ngwenya, T., Franklyn, P. and Jewell, L., 2011, *A Comparison of Gold Supported on TiO₂, Al₂O₃ and ZnO for SO₂ Reduction*, (Poster) at the CATSA conference in Muldersdrift, South Africa, 13-16 November
4. Ngwenya, T. and Jewell, L., 2012, *Au/TiO₂ for the Reduction of SO₂ using CO*, (Poster) at the SAICChE conference in Drakensberg, South Africa, 16-19 September
5. Ngwenya, T. and Jewell, L., 2013, *The Catalytic Behaviour of Au/TiO₂ for the Reduction of SO₂ by CO*, (Poster) at the CATSA conference in Port Edward, South Africa, 17-20 November
6. Ngwenya, T. and Jewell, L., 2014, *SO₂ Abatement using Au/TiO₂ and Au/ZnO*, (Oral) at the ICCT/SAICChE conference in Durban, South Africa, 31 July -3 Aug
7. Ngwenya, T., Beas, I., and Jewell, L., 2014, *Dissociation of SO₂ by Au/TiO₂*, (Poster) at the CATSA conference in Johannesburg, South Africa, 9-12 November

Publications

1. Ngwenya, T., Beas, I. and Jewell, L., 2016, *Reduction of Sulphur Dioxide using Carbon Monoxide over Gold Supported Catalysts*, in final preparation.

To my sister,
Dr. Sharol Ngwenya

Acknowledgements

The journey from the beginning to the end of this project has been very long and challenging. I have dedicated many hours to this work, but I could not have been successful without the unwavering support and assistance of the following people:

- My supervisor, Prof. Linda Jewell, for her dedication, support and guidance throughout the duration of this project.
- Basil Chassoulos for the technical instrumentation assistance and guidance.
- Mintek, for the financial support through their bursary programme and the supportive bursary officers.
- The University of the Witwatersrand and the National Research Fund (NRF) for funding this project.
- Project AuTEK and the Mintek Advanced Materials Division staff for support and providing the catalyst materials (AUROLite™ catalysts which are available commercially through STREM Chemicals Inc.).
- Jason McPherson, formerly from Mintek, for his guidance at the beginning of this project.
- Prof. Neil Coville for his support and guidance.
- The School of Chemical and Metallurgical Engineering at the University of the Witwatersrand (Wits) support staff, in particular, Bruce Mothibedi, Doctor Mbense, Reghana Burns, Sibongile Maswanganye.
- The School of Chemical and Metallurgical Engineering (Wits) workshop staff.
- The School of Chemistry (Wits) technical and chemistry stores staff.

Acknowledgements

- The Catalysis, Organometallic and Materials group members of the School of Chemistry at the University of the Witwatersrand for providing a working environment and catalyst characterization assistance.
- Thomas Bigala, of the Climatology Research Group (Wits) for his assistance at the beginning of this project.
- Mr. Werner Jordaan of NMISA Pretoria for XPS analysis.
- Prof. H. Swart, University of the Free State, for the XPS analysis.
- Dr. Isaac Beas, for his support and assistance towards the completion of this project.
- Dr. Paul Franklyn for the HRTEM and EDS analysis.
- Natsayi Chiwaye for the PXRD analysis.
- Dr Sabelo Mahlangu for the BET analysis.
- Hiafeng Xiaong for the TEM analysis.
- Michael Kganyago for his support and patience in seeing me through this work.
- My friends who helped in any way they could.
- Finally to my God and Goddess for guidance and protection.

Citation Declaration

All the citations, referencing and bibliography in this work have been done using Mendeley referencing software, Version 1. 15. 3 via the Mendeley Cite-O-Matic citation MSWord Plug-in. In the case of multiple citations, the references are listed in ascending year of publication.

Contents

Declaration	i
Abstract	ii
Publications and Presentations related to this work.....	iv
Conference Presentations	iv
Publications	v
Acknowledgements	vii
Citation Declaration	ix
List of Figures	xv
List of Tables.....	xviii
Nomenclature	xix
List of Symbols	xx
Chapter 1. Introduction	1
1.1 Introduction to Air Pollution	1
1.2 Sources of SO _x Pollution	3
1.3 SO ₂ in the Atmosphere	5
1.3.1 Acid Precipitation and Particulate Matter	6
1.3.2 Effects of SO ₂ on Human and Animal Health	7
1.3.3 Effects of SO ₂ on Plants	8
1.4 CO Effects and Sources in the Atmosphere	9
1.5 Legislation on Emissions.....	11
Chapter 2. SO ₂ Abatement Methods.....	14
2.1 Sulphur-free Energy Sources.....	14

2.1	Change fuel source	16
2.2	Removal of Sulphur Compounds	18
2.2.1	Sulphur- removal before combustion.....	18
2.2.2	Sulphur- removal during combustion	19
2.2.3	Sulphur- removal after combustion.....	20
2.2.4	Review of Sulphur removal processes	25
Chapter 3:	Catalytic abatement.....	27
3.1	Introduction to Reduction of SO ₂	27
3.2	Reduction using Hydrogen	28
3.2.1	Characterization of the Reaction	30
3.2.2	Reaction products and by-products	33
3.2.3	Effect of additional reactants on SO ₂ reduction.....	34
3.3	Reduction using Methane	35
3.3.1	Effect of Reaction Temperature	37
3.3.2	Effect of CH ₄ :SO ₂ feed ratio	37
3.3.3	Production of the by-products H ₂ S, COS and CO	38
3.4	Reduction by Carbon Monoxide	39
3.4.1	Characteristics of the Reaction.....	41
3.4.2	Effect of CO:SO ₂ Feed Ratio	45
3.4.3	Effects of additional reactants.....	46
3.5	Conclusion.....	48
Chapter 4:	Gold Catalysis	51
4.1	Characteristics of Au-supported catalysts	51
4.2	Characterization of Au-supported catalysts	53

4.2.1	The size of Au nanoparticles.....	53
4.2.2	Surface of supported Au catalysts.....	54
4.2.3	Structure of Au supported catalysts	54
4.2.4	BET Surface Area of Au supported catalysts	55
4.3	Gold catalysts for CO Oxidation	56
4.3.1	Characteristics of the Reaction.....	57
4.3.2	Deactivation and Sintering of Au-supported Catalysts.....	58
4.4	Conclusion.....	60
Chapter 5.	Aims and Objectives	62
5.1	Reducing agent	62
5.2	Metal Oxide Support	63
5.3	Effect of Feed Ratio	64
5.4	Reaction Products.....	65
Chapter 6:	Research Methods	68
6.1	Preparation of the Catalysts.....	68
6.2	Activity Measurements.....	69
6.2.1	Gas Mixtures and Feed Compositions	69
6.2.2	Reactor system	70
6.3	On-line Analysis.....	71
6.4	Interpretation of Data	74
6.5	Characterization Techniques	75
6.5.1	X-ray Diffraction (XRD) Analysis.....	75
6.5.2	Brunauer-Emmett-Teller (BET) Surface Area Analysis.....	76
6.5.3	X-ray Photoelectron Spectroscopy (XPS).....	76

6.5.4	Transmission Electron Microscopy (TEM)	77
Chapter 7.	Characterization and Support Effects.....	78
7.1	Catalyst Characterization	78
7.1.1	Surface Area Analysis.....	78
7.1.2	X-Ray Diffraction (XRD) Patterns	78
7.1.3	Transmission Electron Microscopy (TEM)	81
7.2	Effect of Au nanoparticles and Reaction Temperature	85
7.2.1	Activity of Au/Al ₂ O ₃ and Al ₂ O ₃	85
7.2.2	Activity of Au/ZnO and ZnO.....	87
7.2.3	Activity of Au/TiO ₂ and TiO ₂	89
7.3	Conclusion.....	92
Chapter 8.	Product Selectivity and Feed Ratio Effects.....	94
8.1	Analysis of Reaction Products	94
8.2	Effect of Feed Ratio on Au-supported catalysts.....	98
8.3	Conclusion.....	103
Chapter 9.	Effect of time on-stream, pre-treatment and adding oxygen on Au/TiO ₂	104
9.1	Introduction	104
9.2	Effect of Time-On-Stream.....	105
9.3	Effect of Pre-treatment	108
9.4	Effect of adding Oxygen to feed gas	111
9.5	Conclusion.....	114
Summary and Conclusions.....		116
References		121

Appendix A: Research Methods	136
A.1 Thermodynamic Calculations.....	136
A.2 Gas Mixtures and Feed Compositions.....	137
A.3 Mass Balance Calculations.....	139
Appendix B: Characterization Results	141
B.1 TEM Images	141
B.2 XRD Analysis.....	143
B.3 XPS Analysis.....	146
B.4 EDS Peaks	147
Appendix C: Reaction Tests.....	149
C.1 Effect of varying SO ₂ feed concentrations	149
ANOVA Tables.....	151

List of Figures

Figure 1.1: Global SO ₂ emissions (<i>Klimont, Smith & Cofala, 2013</i>)	5
Figure 1.2: 2011 global CO emissions (<i>Yin et al., 2015</i>).....	9
Figure 2.1: Percentage of the world's electricity generation from non-renewable and renewable sources (<i>Berga, 2016</i>)	14
Figure 2.2: Illustration of dry scrubber system (<i>adapted from De Nevers, 2000</i>)	21
Figure 3.1: Relationship between equilibrium constant K_a and the inverse of temperature for SO ₂ reduction by H ₂ (Calculations as shown in Appendix A)....	29
Figure 3.2: Logarithm of equilibrium K_a versus the inverse of temperature for the reduction of SO ₂ by CH ₄ (Calculations as shown in Appendix A).....	36
Figure 3.3: Chemical equilibrium constants as a function of the inverse of temperature for the reduction of SO ₂ by CO (Calculations as shown in Appendix A)	41
Figure 4.1: Illustration of spherical and hemispherical Au clusters on metal oxide support.....	52
Figure 4.2: Relationship between the log ₁₀ of the equilibrium constant K_a and the temperature for CO oxidation (Calculations as shown in Appendix A)	56
Figure 6.1: Illustration of experimental set up	71
Figure 6.2: GC peaks of air and SO ₂ at an oven temperature of 200 °C.....	72
Figure 6.3: GC peaks of air and CO with the oven at room temperature	73
Figure 6.4: GC peaks of air, CO and SO ₂ fully separated using a temperature programmed GC.....	74
Figure 7.1: XRD pattern of 1% Au/Al ₂ O ₃	79
Figure 7.2: XRD pattern of fresh ZnO	80
Figure 7.3: XRD patterns of fresh 1% Au/TiO ₂ displaying the peaks for the anatase phase (red) and rutile phase (green)	81
Figure 7.4: TEM image of Au/Al ₂ O ₃	82
Figure 7.5: TEM image of Au/ZnO	83
Figure 7.6: TEM image of Au/TiO ₂	83

Figure 7.7: Au cluster size distribution for Au/ZnO	84
Figure 7.8: Au cluster size distribution for Au/TiO ₂	85
Figure 7.9: Activity test for Au/Al ₂ O ₃ and Al ₂ O ₃ for SO ₂ reduction as temperature was increased in 50 °C steps at 8 h intervals at a GHSV of 3 600 mL.g _{cat} ⁻¹ .h ⁻¹	86
Figure 7.10: Activity test for Au/ZnO and ZnO for SO ₂ reduction as temperature was increased in 50 °C steps at 8 h intervals at a GHSV of 3 600 mL.g _{cat} ⁻¹ .h ⁻¹	87
Figure 7.11: HRTEM images of (a) fresh and (b) after-reaction Au/ZnO.....	88
Figure 7.12: EDX analysis of after-reaction Au/ZnO showing presence of S species	89
Figure 7.13: Activity test for Au/TiO ₂ and TiO ₂ for SO ₂ reduction as temperature was increased in 50 °C steps at 8 h intervals at a GHSV of 3 600 mL.g _{cat} ⁻¹ .h ⁻¹	90
Figure 7.14: Activity test for TiO ₂ for SO ₂ reduction as temperature is increased in 50 °C steps at 8 h intervals at a GHSV of 3 600 mL.g _{cat} ⁻¹ .h ⁻¹	91
Figure 7.15: HRTEM images of (a) fresh and (b) after-reaction Au/TiO ₂	92
Figure 8.1: GC peaks of separated reactor exit gas stream for CO:SO ₂ ratio of 3:1, reaction over Au/TiO ₂ at 300 °C	94
Figure 8.2: XRD peaks of sulphur product identified as S ₈	95
Figure 8.3: HRTEM image of sulphur product.....	96
Figure 8.4: EDS peaks of the sulphur product sample.....	96
Figure 8.5: Effect of feed ratio on the activity of Au/TiO ₂ at 300 °C, TOS of 72 h and GHSV of 3 600 mL.g _{cat} ⁻¹ .h ⁻¹	100
Figure 8.6: Effect of temperature on activity of Au/TiO ₂ at a feed ratio of 0.12, GHSV of 3 600 mL.g _{cat} ⁻¹ .h ⁻¹ and SO ₂ feed concentration of 420 ppm.	102
Figure 9.1: EDS analysis of after-reaction Au/TiO ₂ (“a.u.” refers to arbitrary units).....	105
Figure 9.2: HRTEM image of an after-reaction Au/TiO ₂ sample.....	106
Figure 9.3: XPS analysis peak of S2p (“a.u.” denotes arbitrary units)	107
Figure 9.4: Effect of pre-treatment temperature on conversion of SO ₂ with time over Au/TiO ₂ at CO:SO ₂ feed ratio of 2:1, as temperature was increased in 50 °C steps at 8 h intervals at a GHSV of 3 600 mL.g _{cat} ⁻¹ .h ⁻¹	109

List of Figures

Figure 9.5: Conversion versus time over Au/TiO₂ at 300 °C, O₂ feed concentration of 2 000 ppm, CO concentration of 4 000 ppm and CO:SO₂ = 2:1 112

Figure 9.6: Effect of removal of O₂ from reactor feed gas on SO₂ and CO percentage conversion at CO:SO₂ = 2, 2 000 ppm O₂ and reaction temperature of 300 °C..... 113

List of Tables

Table 1.1: Some Gaseous Air Pollutants <i>extracted from Vesilind & Morgan, 2004</i>	2
Table 1.2: Concentration of sulphur in fossil fuels	3
Table 1.3: Sulphur forms in selected bituminous coal-Worldwide (<i>extracted from Yen, 1999</i>)	4
Table 1.4: Health effects of CO and COHb	10
Table 1.5: Previous Air emissions Acts of South Africa	12
Table 2.1: Concentration of sulphur in biomass and coal (<i>Yen, 1999; Ren, Sun, et al., 2017</i>)	17
Table 2.2: Comparison of SO ₂ removal processes	26
Table 3.1: Summary of literature results for reduction of SO ₂ using CO at a feed ratio of 2:1	49
Table 6.1: Catalysts information	68
Table 6.2: SO ₂ and CO feed ratios and concentrations	69
Table 6.3: Feed gas mixture ratios and concentrations	70
Table 7.1: BET surface area and pore volume	78
Table 8.1: EDS peaks from figure 7.4 for S, Ti, O, Au and Cu	97
Table 8.2: Effect of feed ratio on the conversion of SO ₂ at a reaction temperature of 300 °C and SO ₂ concentration of 2 000 ppm	99
Table 8.3: ANOVA of the SO ₂ conversions over the catalysts and the supports	100
Table 8.4: Effect of reaction temperature on the conversion of SO ₂ at a feed ratio of 0.12	101
Table 9.1: XPS results of Au/TiO ₂ at different TOS	107

Nomenclature

Brunauer, Emmet and Teller	BET
Direct sulphur reduction process	DRSP
Flue gas desulphurization	FGD
Fluidized bed combustor	FBC
Gas chromatography	GC
Gas hourly space velocity	GHSV
Haemoglobin	Hb
High resolution transmission electron microscopy	HRTEM
Internal diameter	ID
Particulate Matter	PM
Powder X-ray diffraction	PXRD
Standard Gravity	s.g.
Thermal conductivity detector	TCD
Time on-stream	TOS
Transmission electron microscopy	TEM
Weight hourly space velocity	WHSV
X-ray diffraction	XRD
X-ray energy-dispersive spectroscopy	XEDS/EDS
X-ray photoelectron spectroscopy	XPS

List of Symbols

Concentration	C
Feed Ratio	<i>FR</i>
Molar flow rate	<i>n</i>
Molar gas constant	R
Parts per million	ppm
Reaction equilibrium constant	K_a
Standard Gibbs free energy change	$\Delta G^\circ_{\text{rxn}}$
Stoichiometric coefficient	<i>v</i>
Temperature	T
Volume	vol
Volumetric flow rate	V
Weight	wt

Chapter 1. Introduction

1.1 Introduction to Air Pollution

Air pollution control is a major factor that most industries face due to the harmful effects which air pollutants have on human health and the natural and built environment. Developing countries however depend on industrial activities for economic growth and are most affected by air pollution due to fewer resources dedicated to its control. The historical documented episodes of air pollution disasters that led to detrimental human health effects include;

- In Manchester, England, 1931, more than 500 people died from exposure to particulates and acids in the atmosphere (Ray, 1995)
- In Donora, Pennsylvania, 1948, approximately 20 people died and 6 000 people were ill due to the effects of airbourne contamination (Ray, 1995), (Masters, 1998)
- In London , 1952, there was a report of a killer smog (Vesilind, Pierce & Weiner, 1994; Masters, 1998)
- In New York in the mid-1950s the burning of sulphur-containing oil to generate electricity resulted in dirty air (Vesilind, Pierce & Weiner, 1994)

It is worth noting firstly that these above mentioned episodes pertaining to the adverse effects of air pollution are all caused by anthropogenic pollutants that are both gas and particulate matter. Occasionally natural phenomena such as volcanic eruptions and sulphur-containing geothermal sources such as geysers and hot springs also contribute to emissions of pollutants into the atmosphere (Strauss, 1972; Vesilind, Pierce & Weiner, 1994). There are various types of gaseous air

pollutants, of which all are asphyxiants, and these are listed with their effects in the air by Vesilind & Morgan (2004) in the Table 1.1.

Table 1.1: Some Gaseous Air Pollutants *extracted from Vesilind & Morgan, 2004*

Name	Formula	Properties of Importance	Significance as Air Pollutants
Sulphur Dioxide	SO ₂	Colourless gas, intense choking, highly soluble in water-forming sulphurous acid, H ₂ SO ₃	Damage to property, health and vegetation
Sulphur trioxide	SO ₃	Soluble in water-forming sulphuric acid H ₂ SO ₄	Highly corrosive
Hydrogen sulphide	H ₂ S	Rotten egg odour at low concentrations, odourless at high concentration	Highly poisonous
Nitrous oxide	N ₂ O	Colourless, used as carrier gas in aerosol bottles	Relatively inert, not produced in combustion
Nitric oxide	NO	Colourless gas	Produced during high-temperature, high-pressure combustion; oxidises to NO ₂
Nitrogen dioxide	NO ₂	Brown to orange gas	Major component in the formation of photochemical smog
Carbon monoxide	CO	Colourless and odourless, very toxic	Product of incomplete combustion
Carbon dioxide	CO ₂	Colourless and odourless	Formed during complete combustion; greenhouse gas
Ozone	O ₃	Highly reactive	Damage to vegetation and property; produced mainly during the formation of photochemical smog
Hydrocarbons	C _x H _y or HC	Many	Emitted from automobiles and industries; formed in the atmosphere
Methane	CH ₄	Combustible, odourless	Greenhouse gas
Chlorofluorocarbons	CFC	Nonreactive, excellent thermal properties	Deplete ozone in upper atmosphere

Secondly, the one of the most common pollutants in these episodes are sulphur oxides (SO_x), mainly sulphur dioxide (SO₂). SO₂ is emitted into the atmosphere

by both industrial activity and volcanic activity (Strauss, 1972) which are classified as stationary sources.

1.2 Sources of SO_x Pollution

Sulphur is the 16th most abundant element in the earth's crust with a concentration of approximately 260 ppm (De Nevers, 2000) and is found in all organic fuels. It is present as both inorganic form (pyritic) and organic form. Table 1.2 and Table 1.3 both obtained from (Yen, 1999) show the sulphur content in fossil fuels and the forms and concentrations of sulphur in coals respectively.

Table 1.2: Concentration of sulphur in fossil fuels

Fuel	Sulphur (wt %)
Qayarah (Iraq) heavy oil	8.4
Boscan (Venezuela) asphaltene	5.6
Athabasca (Canada) tar sand	4.9
Trinidad Lake bitumen	6.2
Mexico residua	6.4
Kuwait residua	5.5
Alberta crude oil	2.63
Bituminous coal	1.72 (organic sulphur only)

In industry or domestic use, fossil fuels are combusted in air to generate energy which results in the oxidation of the sulphur and other elements via a simple reaction (Masters, 1998) shown in Reaction 1.1.

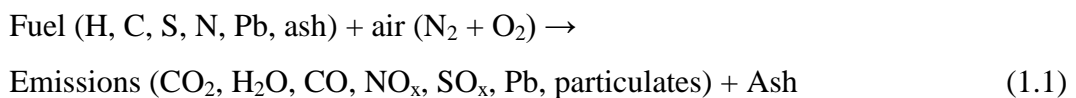


Table 1.3: Sulphur forms in selected bituminous coal-Worldwide (extracted from Yen, 1999)

Region and Country	Location or Mine	Sulphur, Percent w/w			Ratio of Pyritic to organic Sulphur
		Total	Pyritic	Organic	
ASIA					
USSR	Shakhtersky	0.38	0.09	0.29	0.0031
China (mainland)	Taitung	1.19	0.87	0.32	2.7
India	Tipong	3.63	1.59	2.04	0.78
Japan	Miike	2.61	0.81	1.80	0.45
Malaysia	Sarawak	5.32	3.97	1.35	2.9
NORTH AMERICA					
U.S.	Eagle No. 2	4.29	2.68	1.61	1.7
Canada	Fernie	0.60	0.03	0.57	0.053
EUROPE					
Germany	-	1.78	0.92	0.76	1.2
United Kingdom	Derbyshire	2.61	1.55	0.87	1.8
Poland	-	0.81	0.30	0.51	0.59
AFRICA					
S. Africa	Mpumalanga	1.39	0.59	0.70	0.84
AUSTRALIA					
	Lower Newcastle	0.94	0.15	0.79	0.19
SOUTH AMERICA					
Brazil	Santa Caterina	1.32	0.80	0.53	1.5

In 2014, 41 % of the worldwide electricity production was from coal which is low compared to South Africa's 92 % ("IEA report", 2017). Areas abundant in coal and water are hence ideal for the erection of large power stations. The Vaal Triangle in South Africa is a good example of such a location and with a population of approximately 1.2 million people presented an ideal location for the study on the effects of air pollution on human health conducted by Terblanche in 1998 (Terblanche, 1998).

1.3 SO₂ in the Atmosphere

Air is known to be composed of approximately 78% nitrogen (N₂), 20.1 % oxygen (O₂), 0.9 % argon (Ar), 0.03 % carbon dioxide (CO₂), 0.002 % neon (Ne) and 0.0005 % helium (He) (Vesilind & Morgan, 2004). The concentration of SO₂ in unpolluted parts of the world is approximately 0.2 ppb (De Nevers, 2000) which is unlikely to cause any severe damage to human health and the environment. However due to human activities that contribute to the rise in SO₂ levels in the atmosphere, the concentrations have increased. Figure 1.1 shows the global SO₂ emissions for the decade between 1990 and 2010 and the sources of the emissions (Klimont, Smith & Cofala, 2013).

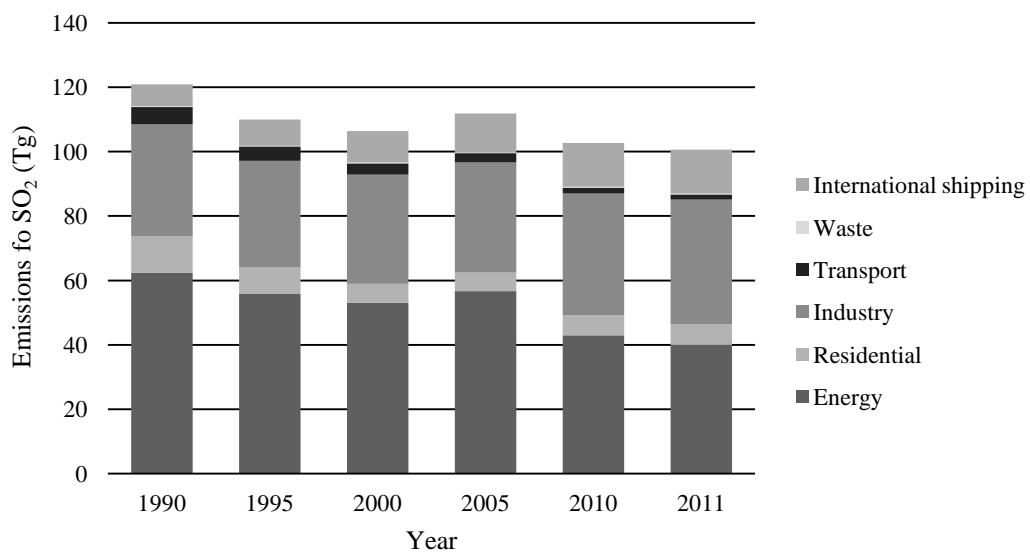


Figure 1.1: Global SO₂ emissions (Klimont, Smith & Cofala, 2013)

As seen in Figure 1.1, the SO₂ emissions decreased by 15 % from 121 Tg/year in 1990 to 2010. The energy sector, as the highest contributor to these emissions, decreased its emissions from 52 % to 42 % from 1990 to 2010.

In South Africa, power generation from coal is the largest sector responsible for the SO₂ emissions (Patel, 2012). Terblanche (1998) in their study of the pollution over a 4-year period in the Vaal Triangle in South Africa found that the ambient SO₂ levels monitored were higher than the indicated health standards. The levels were higher in winter when many households used coal for heating especially in the densely populated areas. They also studied the levels of particulate matter (PM) and found the annual PM₁₀ (particulate matter with an average size less or equal to 10µm) concentration to be 70 µg.m⁻³ annually which is higher than the U.S. standard of 50 µg.m⁻³ per year.

1.3.1 Acid Precipitation and Particulate Matter

SO₂ is very soluble in water and easily gets washed out of the atmosphere by precipitation once released into the atmosphere (Strauss, 1972). In the presence of sunlight, it reacts with the oxygen and water in air to form sulphurous acid and sulphuric acid aerosol droplets via Equations 1.2 to 1.4



The acid formed dissolves in rain water and decreases its pH from approximately 5.6 to 2 (Vesilind & Morgan, 2004) and falls as acid rain. This in turn decreases the pH of water bodies such as rivers and lakes leading to the loss of fish life and aquatic plants at a pH below 4.5. The lakes in Scandinavia and North America have no fish life due to acid precipitation (Vesilind, Pierce & Weiner, 1994) resulting from sulphuric acid aerosol formation in the atmosphere.

Acid rain can also cause minor to severe damage to built structures such as exposed pipe lines, limestone buildings and motor vehicles by corroding the surfaces. It can also alter the pH of ground water and affect the growth and development of plants and ground animals. The lower pH can also lead to the increased leaching of metals bound in soil (Ray, 1995).

SO₂ can also combine with olefins and NO₂ to form particulate matter with a size of less than or equal to 2.5 µm and 10 µm (noted as PM_{2.5} and PM₁₀, respectively) in the presence of sunlight and H₂SO₄ aerosol particles (Strauss, 1972). Particulate matter that is suspended in the air causes visibility and respiratory problems. These fine particles reduce visibility by scattering sunlight. When fine particles enter the respiratory system they become trapped in the alveoli (air sacs) in the lungs which are 0.6 mm in diameter (Ray, 1995) and have no cilia (small finger-like projections lining the respiratory tract) to “sweep” them out (Vesilind et al., 1994). Short and long-term exposure to PM_{2.5} in bronchial epithelial cells induced changes in the gene expression leading to asthma pathogenesis (Tripathi et al., 2017). Some of these particles are soluble in water and dissolve in blood, the insoluble particles cannot be removed hence scar tissue forms around them, reducing the capacity of the lungs and bronchioles. This may result in emphysema.

1.3.2 Effects of SO₂ on Human and Animal Health

Gaseous SO₂ affects the respiratory system by paralyzing cilia (Vesilind et al., 1994) which are fine finger-like projections that sweep out impurities from the respiratory tract. It was found to reduce the frequency of cilia oscillation in rabbits and other animals and to constrict bronchi. This resulted in more fine particles

accumulating the respiratory tract and alveoli therefore decreasing the capacity of the lungs.

Terblanche (1998) found that children who live in the Vaal Triangle had significantly higher risks of developing respiratory tract symptoms and illness. This was due to exposure to atmospheric concentrations of SO₂ and particulate matter higher than the health standards. The exposure to both SO₂ and PM_{2.5} poses a potential risk to neuronal dysfunction (Ku et al., 2017).

1.3.3 Effects of SO₂ on Plants

SO₂ affects plant health and growth indirectly via acid precipitation which leads to leaching of certain minerals in the soil necessary for plant growth (Yunus & Iqbal, 1996). When plants are exposed to SO₂ in the atmosphere they absorb and internally convert the excess sulphur compound into H₂S (Yunus & Iqbal, 1996). However some plants show water stress when exposed to high levels of SO₂ (Mansfield, 1998) which damages the epidermal cells close to the stomata and as a result, increase their aperture, which leads to water loss.

These effects are also evidenced in the agricultural sector especially in developing countries. One such example is China which depends on fossil fuel dependent industries. With the highest output of grain in the world, agriculture is the main source of income in parts of China. Wei et al.(2014) analysed the agricultural losses caused by 2 069 industries located close to the farming area and found that US\$1.5 billion was lost due to air pollution in 2008.

1.4 CO Effects and Sources in the Atmosphere

CO is a colourless, odourless, tasteless and poisonous gas yielded from the incomplete combustion of fuel (Vesilind et al., 1994; Masters, 1998; De Nevers, 2000). The following conditions are necessary for the production of CO as listed in Masters (1998);

- Low supply of oxygen
- Low temperature of combustion
- High temperature with low gas residence time
- Low turbulence in combustion chamber

The 2011 global CO emissions from different anthropogenic sources were as shown in Figure 1.2 (Yin et al., 2015) with the residential burning of biomass as the largest source of CO emissions. The iron and steel production were responsible for 19.26 % of the global CO emissions.

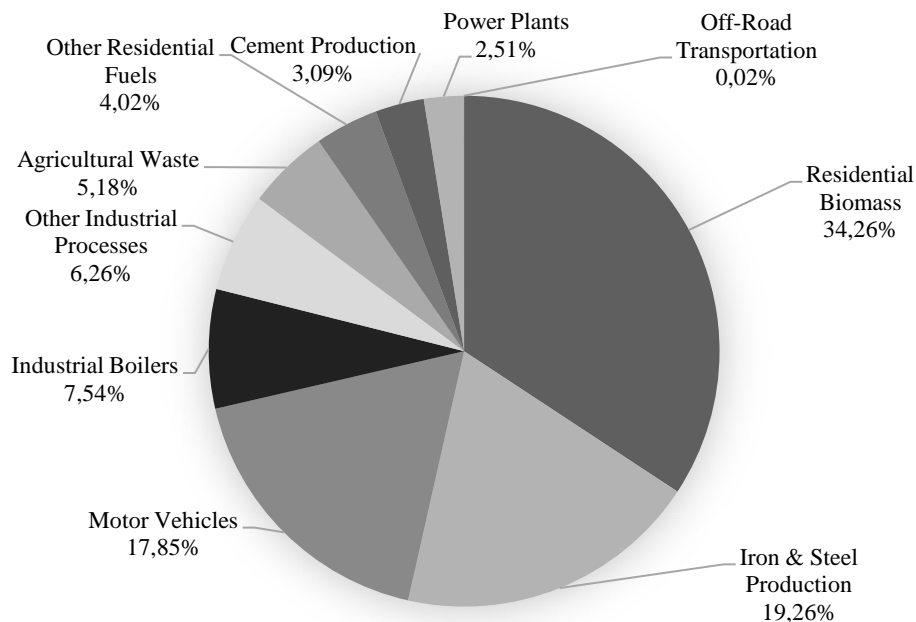


Figure 1.2: 2011 global CO emissions (Yin et al., 2015)

In the atmosphere CO reacts with the oxygen in air to form CO₂ (Vesilind et al., 1994) via Reaction 1.5.



The direct effects of CO, before oxidising to CO₂, on plants and materials is insignificant (Masters, 1998), but is fatal to humans at very high levels of exposure for prolonged times. In the blood, haemoglobin (Hb) transports oxygen to all organs and tissues in the body by binding the iron atoms in Hb loosely to the oxygen molecule. CO has an affinity to bind to Hb 220 times higher than oxygen (Masters, 1998; Yen, 1999).

Upon exposure, the formation of carboxyhaemoglobin (COHb) inhibits the transport of vital oxygen to major organs and can result in death. CO exposure is a major cause of death in residential fires and coal mine fires however the effects from acute exposure are reversible (De Nevers, 2000) with the administration of pure oxygen. The health effects at different exposure concentrations of CO are shown in Table 1.4 extracted from Vesilind et al. (1994).

The CO released as industrial flue gas oxidises in the atmosphere into CO₂ as shown in Equation 1.5. This however cannot be seen as a contributing factor to the high CO₂ emissions as this CO would have been fully oxidised in the combustion chamber to CO₂.

Table 1.4: Health effects of CO and COHb

Condition of CO exposure	Effects of CO
9 ppm, 8-hour exposure	National air ambient standard
50 ppm, 6-week exposure	Structural changes in heart and brain of animals
50 ppm, 50-minute exposure	Changes in relative brightness threshold

	and visual acuity
50 ppm, 8 to 12-hours exposure, non-smoker	Impaired performance on psychomotor tests
COHb Concentration	Effects
<1.0 %	No apparent effect
1.0 % to 2.0 %	Some evidence of effect on behavioural performance
2.0 % to 5.0 %	Central nervous system effects. Impairment of time-interval discrimination, visual acuity, brightness discrimination and other psychomotor functions
5.0 % to 10.0 %	Cardiac and pulmonary functional changes
10.0 % to 80.0 %	Severe headaches, fatigue, drowsiness, coma, respiratory failure, death

1.5 Legislation on Emissions

To regulate the emissions in the atmosphere various legislations has been enforced to mitigate the harmful effects of air pollution. This may differ from one country to another with less strict laws in developing countries, while developed countries have better technologies and vast resources to assist in the abatement and prevention of air pollution.

South Africa is a good example of a developing country relying on coal combustion for power generation which results in emissions of harmful gases. The legislation on emissions control has been developed over the years as shown in Table 1.5 extracted from *National Environment Management: Air Quality Act [No. 39 of 2004]*, (2005).

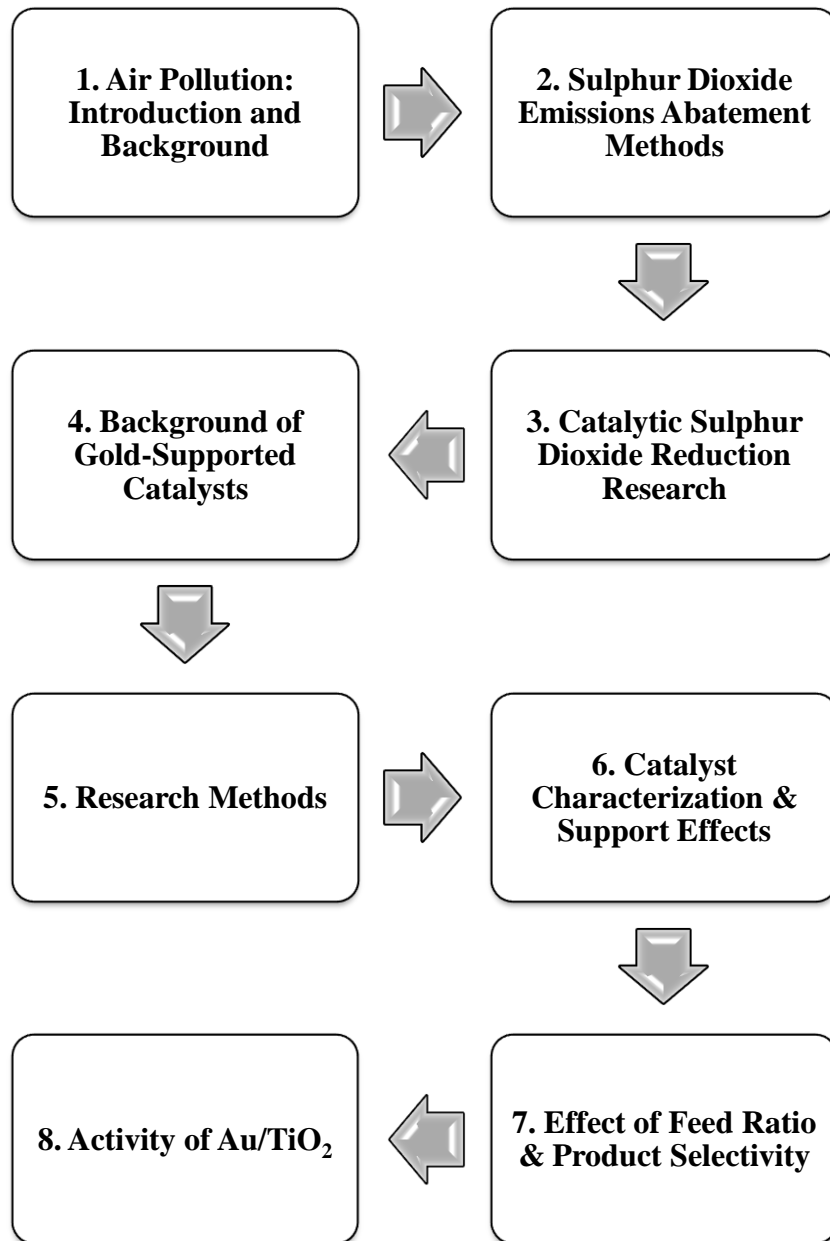
Table 1.5: Previous Air emissions Acts of South Africa

No. and year of Act	Title of Act
Act No. 45 of 1965	Atmospheric Pollution Prevention Act. 1965
Act No. 17 of 1973	Atmospheric Pollution Prevention Amendment Act. 1973
Act No. 21 of 1981	Atmospheric Pollution Prevention Amendment Act. 1981
Act No. 15 of 1985	Atmospheric Pollution Prevention Amendment Act. 1985
Act No. 107 of 1998	National Environmental Management Act. 1998

National Environment Management: Air Quality Act [No. 39 of 2004], (2005) lists the standards of ambient air for ozone (O₃), oxides of nitrogen, nitrogen oxide, SO₂, lead and PM₁₀ levels. It states that annual average for SO₂ and PM₁₀ may not exceed 50 µg.m⁻³ and 60 µg.m⁻³ respectively. The United States however invalidated the 24 hour and annual standards and lists a 150 µg.m⁻³ emission level for a 24-hour interval instead.

These standards are to regulate the emissions of air pollutants into the atmosphere and are based on safe levels that will not cause severe damage to the environment and human/animal health. In order for industries to achieve the set standards for emissions, the methods described in Chapter 2 have been employed to reduce SO₂ emissions.

The following map shows the outline of the literature review work, research methods and results and discussions of the research of the reduction of SO₂ by CO over gold-supported catalysts.



Chapter 2. SO₂ Abatement Methods

2.1 Sulphur-free Energy Sources

The main source of SO₂ emissions into the environment in developing countries is from burning coal for electricity. With respect to emissions control, it would be ideal to avoid burning fossil fuels, as this would diminish the generation of air pollutants. However, energy is required to sustain and grow the economies of countries; hence, alternatives to burning coal have been proposed and implemented. Figure 2.1 shows the percentages of the world's electricity generated from non-renewable and renewable energy sources.

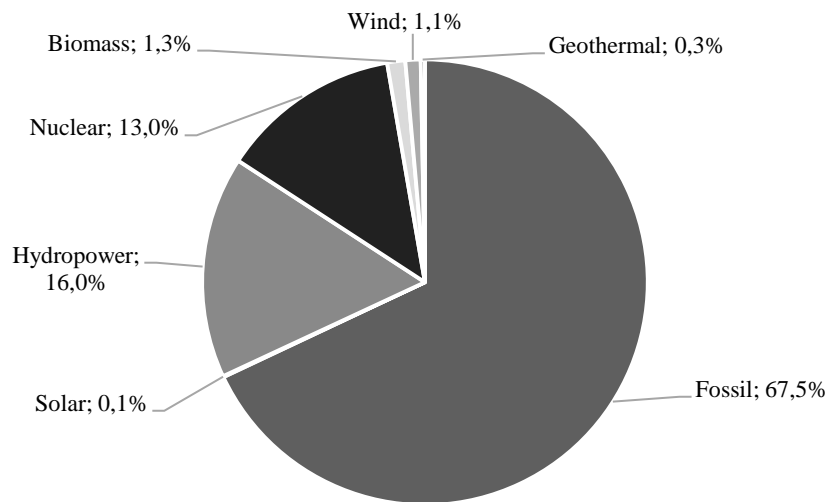


Figure 2.1: Percentage of the world's electricity generation from non-renewable and renewable sources (*Berga, 2016*)

Some of the renewable energy sources from Figure 2.1 have not been used to their full potential due to technological, economical and/or environmental reasons (*Kannan & Vakeesan, 2016; Yu & Xu, 2016; Chandel & Agarwal, 2017;*

González-Roubaud, Pérez-Osorio & Prieto, 2017; Novacheck & Johnson, 2017; Singh & Singal, 2017; Zerrahn, 2017). The advantages of some of these non-combustion energy sources are:

- 1) *Solar power*: The sun radiates energy to the earth at a rate 7 000 times greater than the energy currently consumed globally (Seifried & Witzel, 2010). This radiated solar energy can be captured and converted directly into electrical energy by photovoltaic cells or captured and converted into chemical or thermal energy (Guney, 2016; Kannan & Vakeesan, 2016). Industrially, concentrated solar power has been coupled with thermal energy storage and used since 1985 (González-Roubaud, Pérez-Osorio & Prieto, 2017). There is currently a need to increase the efficiency and to reduce the operating costs of the thermal storage of concentrated solar power (Stein & Buck, 2017).
- 2) *Wind Power*: This utilizes wind mills, previously used for mechanical power, as turbines to generate electricity (Seifried & Witzel, 2010). The major disadvantage with wind power is its intermittency which affects the grid operation, operation costs and the efficiency of the generators (Novacheck & Johnson, 2017; Ren, Liu, et al., 2017; Zerrahn, 2017). These issues can be mitigated by interconnecting wind farms with different wind patterns and applying technological and managerial approaches that are specific to each region and wind farm (Novacheck & Johnson, 2017; Ren, Liu, et al., 2017).
- 3) *Hydroelectric Power*: This is the largest source of renewable energy generating 16 % of the world's electricity generation (Seifried & Witzel, 2010; Berga, 2016). Hydroelectric power is generated by converting the potential energy of water into mechanical energy that turns turbines and finally into electrical energy (Singh & Singal, 2017).

Hydroelectric power plants are classified as small and large, with the small as renewable and sustainable while large plants are not sustainable (Yu & Xu, 2016). Large hydroelectric power plants require the construction of large dams and reservoirs that impair river ecosystems by changing their flow regime (Kummu & Sarkkula, 2008). This impact together with the displacement of indigenous people and cultural or tourists sites, and the destruction of land for agriculture and mining has led to the opposition to large hydroelectric power plants (Yu & Xu, 2016).

Another way to reduce emissions is to increase the efficiency of electrical appliances as this will reduce the demand of electric power (De Nevers, 2000). Effort is made by governments in partnerships with industry to inspire citizens to reduce energy usage. An example is the demand side management called the 49M initiative in South Africa where the government has partnered with Eskom and other companies (“About 49M”, 2014). Initiatives such as these may be effective with the full cooperation of all citizens and businesses involved. Nonetheless, the majority of the world still depends on fossil fuels as the main source of energy.

2.1 Change fuel source

Fossil fuels have different concentrations of impurities such as sulphur as shown in Chapter 1. Alternative fuel sources such as biomass can be burnt in place of coal as some forms have lower sulphur content as shown in Table 2.1 (Ren, Sun, et al., 2017).

Rice husks derived from corn have a sulphur content of 0.09 %, which is 19 times less than that of bituminous coal and 4.8 times less than that of sub-bituminous

coal. However, some biomass types, miscanthus, corn DDGS, and beech wood have a sulphur content greater than sub-bituminous coal.

Table 2.1: Concentration of sulphur in biomass and coal (Yen, 1999; Ren, Sun, et al., 2017)

Biomass fuel type		Percentage sulphur content (%)
Herbaceous	Corn straw	0.21
	Miscanthus	0.54
	Sugarcane bagasse	0.12
Corn-derived waste	Corn distiller's dried grain with solubles(DDGS)	0.93
	Olive residue	0.17
	Rice husks	0.09
	Beech wood	0.63
Coal	Sub-bituminous coal	0.43
	Bituminous coal	1.72 (organic sulphur only)

Natural gas found in shale can be extracted by a process known as fracking which was developed in the 1970s (Thornton, 2014). In Pennsylvania 1365 natural gas wells were drilled for fracking with earnings of US\$1.2 billion in 2012 (Sovacool, 2014). Added benefits of using natural gas include less gaseous emissions from burning. Yet, the advantages of using natural gas are overcome by environmental and health impacts. The drilling/fracking solution, usually water-based, contains a mix of chemicals that can contaminate ground water (Thornton, 2014). Some residents have also raised concerns about how fracking was related to and responsible for their families' severe health problems and about noise pollution associated with fracking (Foster, 2013).

In an effort to reduce SO₂ emissions, coal-fired power generators can switch to burning coal with a low sulphur content (Vesilind et al., 1994). The USSR Shakhtersky coal has the lowest sulphur content of 0.39 %, as shown in Table 1.3, and would be ideal but problems arise with respect to supply and cost as most low sulphur coals are expensive. This may also affect the economy and politics as job losses may occur at high-sulphur content coal mines (De Nevers, 2000).

2.2 Removal of Sulphur Compounds

Desulphurization is the term used for processes that remove sulphur and/or its compounds either from the coal or during coal combustion or after combustion from the flue gas streams. Several methods have been and are presently employed in industry in order to reduce SO₂ emissions as stricter legislative laws are applied.

2.2.1 Sulphur- removal before combustion

Pyritic sulphur, usually found as FeS₂ is easily removed from coal prior to combustion as it is heavier than coal (Ray, 1995). The coal, with a specific gravity (s.g) between 1.1 and 1.3, is ground into small particles and separated from pyrites (s.g. = 5.0) by gravity methods (De Nevers, 2000). This results in very finely ground pyrite free coal, which is used in the combustion chamber. Pyritic sulphur can also be removed by washing the coal with concentrated acid (Vesilind et al., 1994).

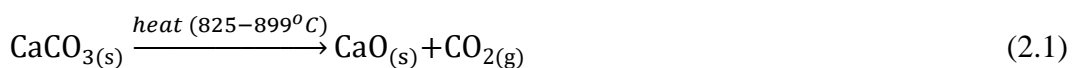
The sulphur in coal can also be removed by dissolving the coal in a strong enough solvent such as tetralin and quinolone (Rivolta Hernández et al., 2012). The

solution is then treated by a catalytic hydrogenation process that removes sulphur producing a solvent-refined coal which is ash and sulphur free (De Nevers, 2000).

2.2.2 Sulphur- removal during combustion

Stationary combustors are responsible for the generation of SO₂ during combustion. These include coal-fired electric boilers, gas turbines, glass furnaces, kilns, and municipal waste incinerators (Heinsohn & Kabel, 1999). With the problems faced with using low-sulphur coal, the combustion process can be modified to remove sulphur during combustion. This is done by the development of fluidized bed combustors (FBC) that help in reduce SO₂ pollution (Singh, Brink & Hupa, 2013).

FBC burn gravel-sized coal in a hot fluidized bed of lime or limestone particles suspended by incoming air (Ray, 1995). The operating temperature of a FBC is low (approximately 850°C) thus, the formation of nitrogen oxides is prevented. When limestone is used, it undergoes the following decomposition in the bed (Heinsohn & Kabel, 1999);



The lime then removes sulphur dioxide as it is formed in the combustor by the following reaction (Heinsohn & Kabel, 1999);



Dolomite (CaCO₃•MgCO₃) can also be used in place of limestone which also produces [CaSO₄ + MgO]. This process can lead to the removal of 90 % of the

SO₂ produced hence there is no need to add scrubbers on the flue gas. In the combustor, the limestone is steadily replaced while the dry product is continuously removed and can be land filled due to its high pH. However this process requires large amounts of lime/limestone as it has to be in excess, meaning high reagent costs, a high volume of solids disposed and an increased load on the particle collector (De Nevers, 2000).

2.2.3 Sulphur- removal after combustion

Flue Gas Desulphurization (FGD)

Flue gas desulphurization is the most commonly used process for the removal of gaseous SO₂ from the stack gas lines of coal-burning facilities. The stack lines usually have a low SO₂ concentration of approximately 1 000 ppm which is too low to be economically recovered as H₂SO₄ (De Nevers, 2000) therefore scrubbers are used (Ray, 1995).

Dry Scrubbing

In the removal process, dry alkaline particles are injected into the flue gas stream to react with the SO₂. Various reagents can be used to react with the dilute SO₂ flue gas stream and most can be regenerated by a series of steps. The FBC process in Section 2.2.2 is a good example of a dry scrubbing system where alkaline reagent is added to the furnace. Figure 2.2 below shows an illustration of a dry scrubbing unit (De Nevers, 2000).

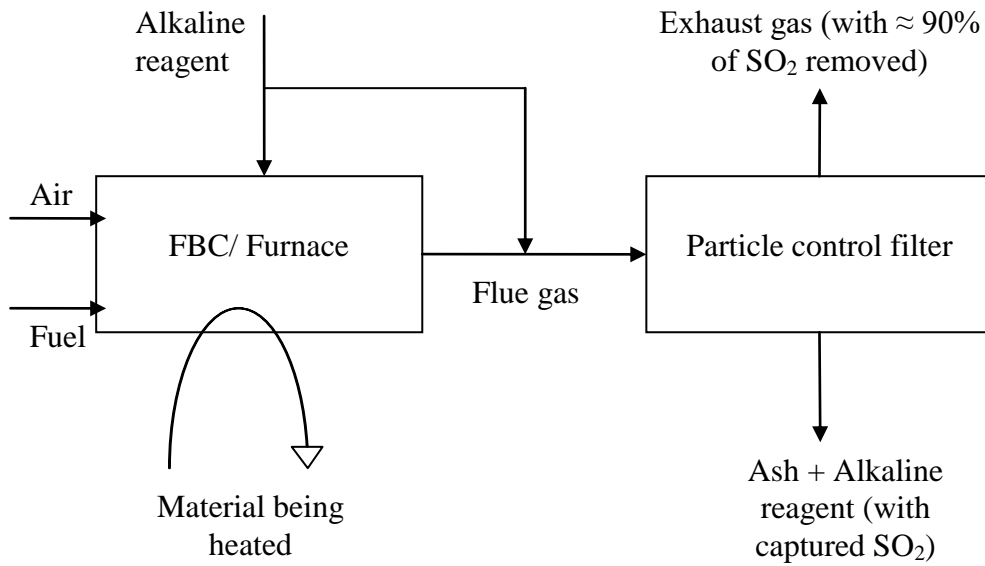


Figure 2.2: Illustration of dry scrubber system (*adapted from De Nevers, 2000*)

For scrubbing after combustion, lime/limestone can be sprayed into the hot flue gas stream to produce particles of CaSO_3 and CaSO_4 (Heinsohn & Kabel, 1999) which can be captured by a fabric filter downstream. Alternatively, $\text{Ca}(\text{OH})_2$ and dolomite can be used instead of lime or limestone.

Sodium salts such as trona (naturally occurring Na_2CO_3) and nahcolite (naturally occurring NaHCO_3) are used to remove SO_2 in the dry scrubbing process via the following reactions (Heinsohn & Kabel, 1999):



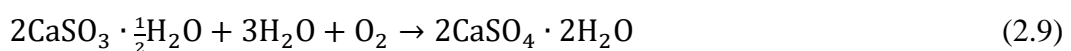
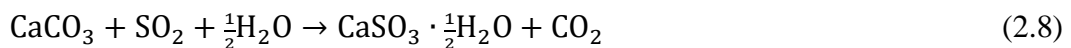
The main advantage of this process over the wet scrubbing method is that there are no disposal problems created by a wet sludge by-product. Yet due to the large volume of dry solid matter required for the scrubber, there is a high volume of dry solids to be disposed of.

Wet Scrubbing

Wet scrubbing is commonly used for the removal of SO₂ from lean flue gas streams since it also removes particulate matter. In this process, an alkali solution is sprayed onto the acidic gas stream generating a wet sludge as the product (Ray, 1995). Prior to this, all the fly ash has to be removed. The actual process depends on the alkali solution used with calcium-based processes being the most common due to the availability of lime/limestone.

Calcium-based processes

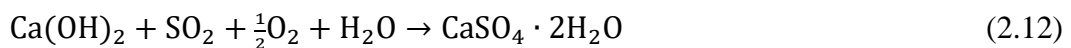
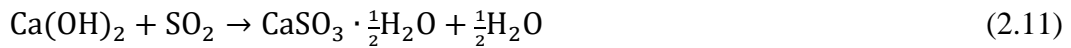
Limestone is an inexpensive mineral that forms naturally, is composed mainly of calcium carbonate (CaCO₃), and is slightly soluble in water (Heinsohn & Kabel, 1999). In limestone scrubbing, the limestone is mixed with water to form slurry, which is passed counter-current to the flue gas in a scrubber unit. Upon contact, the dissolution of SO₂ in the slurry is followed by its reaction with the limestone as shown in the reaction (Schnelle & Brown, 2002).



Lime (CaO) is produced by calcining limestone and can be used for SO₂ scrubbing.



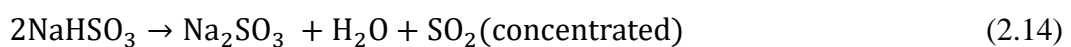
In the slurry the lime is converted to slacked lime, Ca(OH)₂, which is more soluble in water and reacts with SO₂ via the following equations (Schnelle & Brown, 2002).



The limestone/lime scrubber produces one mole of CO₂ per mole of SO₂ scrubbed. The product generated by both methods is a wet sludge that can be converted to gypsum and used in various other processes such as the manufacture of dry wall. The solid dry waste product mainly made up of 25 % CaSO₄ and 75 % CaSO₃ causes serious waste disposal problems, as it has to be land filled.

Sodium-based processes

Sodium compounds are used in the double-alkali scrubbing process to help curb the problem of solid disposal. Single-alkali scrubbing is also used to concentrate SO₂ via the reaction (Vesilind et al., 1994).

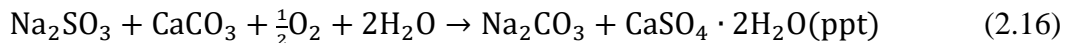


The concentrated SO₂ produced is then used in other processes such as the sulphuric acid manufacture and the pulp and paper industry.

The double alkali process (De Nevers, 2000) was developed in response to the problems associated with the slurry scrubbing method. These include scaling, plugging and solid deposition on the process equipment. Sodium carbonate or bicarbonate is used together with a low concentration of calcium ions. The Na salts have a higher solubility in water than Ca salts hence the scrubbing material is in liquid form. The scrubber reaction for this process is as follows:



The spent scrubber fluid is regenerated by reaction with CaCO₃ via the following equation:



This product is sent to a thickener unit to remove the CaSO₄ precipitate and the remaining Na solution is recycled back to the scrubber.

SO₂ can also be removed by dissolving it in an aqueous solution of sodium citrate, which does not react but acts as a buffer keeping the reactions 2.17 and 2.18 progressing to the right (Vesilind, Pierce & Weiner, 1994; Schnelle & Brown, 2002). In this case, sodium citrate is regenerated, as it is not involved in the reaction.



Alkali scrubbing processes such as these have a removal efficiency of 75 % and are economically favourable due to the regeneration of the buffer salt.

2.2.4 Review of Sulphur removal processes

The processes used for the removal of SO₂ from coal to reduce pollution are widely implemented in industry. It is then necessary to review the advantages and disadvantages of each process in detail in the hopes of finding a less wasteful yet economical way to remove SO₂ from coal either prior, during or after combustion. Table 2.2 summarizes and compares these sulphur removal processes.

Table 2.2: Comparison of SO₂ removal processes

SO ₂ Removal Process					
	Coal Cleaning	Fluidised Bed Combustion (FBC)	Sulphuric Acid Recovery	FGD	
				Dry Scrubbing	Wet Scrubbing
Raw materials required	Concentrated acid or solvent	Limestone/lime Dolomite	Vanadium oxide catalyst Water	Limestone/lime Trona/nahcolite	Limestone/lime Sodium carbonate/bicarbonate Sodium citrate
Products and Disposal	Solution is treated by catalytic hydrogenation	CaSO ₄ CaSO ₄ •MgO Products are a basic solid and land filled	98 % grade H ₂ SO ₄ which is used in other processes	Dry CaSO ₃ /CaSO ₄ or Na ₂ SO ₄ solids which are land filled	Wet sludge which has to be land filled
Efficiency	100 % efficient in removing pyritic sulphur	90 % of Sulphur is removed	99 % of SO ₂ is converted	90 % of SO ₂ is removed from the flue gas stream	Over 90 % of SO ₂ is scrubbed out of the flue gas 75 % efficiency with alkali scrubbing
Advantages	Produces crushed coal which is ideal for combustion	No additional scrubber required downstream	High efficiency Produces reusable products	No wet sludge disposal problems	Can removes SO ₂ at very low concentrations Reagent can be regenerated in some processes
Disadvantages	Only removes pyritic sulphur	High reagent costs as lime/limestone is added in excess High volume of solids disposed Increased load on the particle collector downstream	Only economical at high SO ₂ concentrations in the gas stream	Produces large volumes of solids to be disposed of High reagent costs due to large volumes of scrubbing solid required	Disposal of wet sludge High volumes of water required Scaling and plugging of scrubbing unit In a boiler process, 5% of energy generated is used in the scrubber unit

Chapter 3: Catalytic abatement

A catalyst is a substance that increases the rate of reaction between reactants without being consumed in the overall reaction by lowering the activation energy of the reactants and reacting to form intermediate products.

This chapter deals with heterogeneous catalysis, a process of catalysis where the catalyst and the reactants are in different phases, for example, gaseous reactants and solid catalyst particles. Generally, an active species (A) of a catalyst is supported on a species (Support) typically with a high surface area. The notation for these supported catalysts is generally A/Support, for example, gold nanoparticles supported on titania and noted as Au/TiO₂.

3.1 Introduction to Reduction of SO₂

Catalytic abatement of SO₂ via the direct sulphur reduction process (DSRP) has gained attention due to the problems faced with the current abatement methods (Table 2.2). It is necessary to point out that with the dry or wet scrubbing technique, one mole of CO₂ is released with every mole of SO₂ scrubbed when the limestone converts to lime as shown in Reaction 2.8. Typical flue gas from a coal-fired plant is composed of 12.5 % to 12.8 % CO₂, 6.2 % H₂O, 4.4 % O₂, 50 ppm CO, 420 ppm NO_x, 420 ppm SO₂, and 76 % to 77 % N₂ (Xu et al., 2003). This composition varies depending on the combustion conditions and the type of coal used in the combustion process. At this low SO₂ concentration of 420 ppm, it is uneconomical to convert the SO₂ into H₂SO₄, as the processing costs would be greater than the product sale costs due to low yield. As a result, researchers have been studying the reduction of SO₂ into elemental sulphur as early as the 1940s (Lepsoe, 1940). This single stage process is economically ideal as the sulphur dry

product is safe to handle, transport and store and can be sold (Zhu et al., 1999). Through the early decades of research on SO₂ reduction it was found that the reduction is very slow without a catalyst (Khalafalla et al, 1971) even at temperatures as high as 950 °C. Consequently, various studies have been carried out to investigate the activity of various catalysts and reducing agents on the reduction of SO₂.

3.2 Reduction using Hydrogen

Hydrogen gas has been used by a number of researchers (Paik et al., 1997; Chen et al., 2004; Han et al., 2008) as a reducing agent for the catalytic abatement of SO₂. This is owing to its high reducibility and availability, and is one of two components found in coal-derived gas with CO. The reduction of SO₂ by H₂ for the yield of elemental sulphur ideally follows Reaction 3.1.



The standard Gibbs free energy change ($\Delta G_{\text{rxn}}^{\circ}$) for this reaction is -117.5 kJ.mol⁻¹.K⁻¹ (calculated in as shown in Appendix A) when S₂ product is generated. A side reaction producing H₂S may also occur as shown in Reaction 3.2 (Paik et al., 1997).



The equilibrium K_a is the ratio of the product of the activities of the products to the activities of the reactants and can be expressed in terms of $\Delta G_{\text{rxn}}^{\circ}$ in Equation 3.3 (Devoe, 2014).

$$K_a = \exp\left(-\frac{\Delta G_{\text{rxn}}^{\circ}}{RT}\right) \quad (3.3)$$

The almost linear relationship between reciprocal of temperature ($T \times 10^{-4}$) and the log of the equilibrium constant K_a is shown in Figure 3.1 (“NIST Standard Reference Database Number 69”, n.d.). The positive slope of both lines indicates that the forward reaction is favourable in both cases. For the production of S_2 and water vapour, the value of $\log_{10} K_a$ approaches zero from 20.5 as the temperature increases from 25 K to 3 000 K, equivalently the temperature reciprocal decreases from 33 K^{-1} to 3 K^{-1} at which point the forward reaction becomes unfavourable. Both reactions are exothermic for temperatures up to 6 000 K as shown by a negative enthalpy of reaction. Following Le Châtelier’s principle (Devoe, 2014), an increase in temperature results in the reverse reaction becoming favourable as K_a approaches zero.

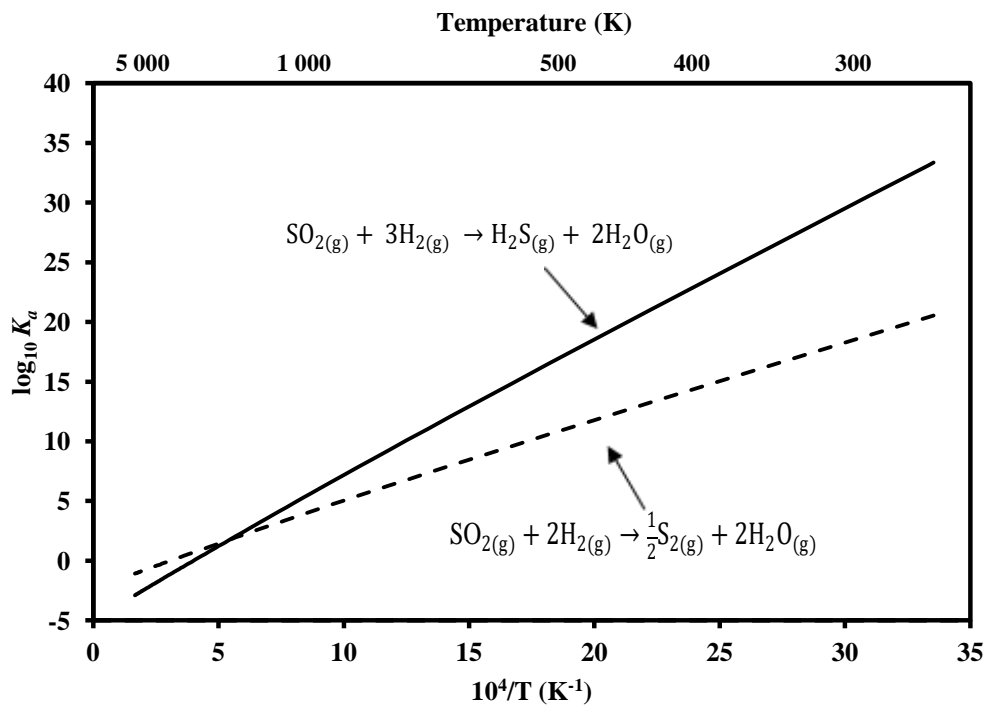


Figure 3.1: Relationship between equilibrium constant K_a and the inverse of temperature for SO_2 reduction by H_2 (Calculations as shown in Appendix A)

3.2.1 Characterization of the Reaction

H₂:SO₂ Feed Ratio

Previous studies have mostly used the stoichiometric feed ratio of H₂:SO₂ of 2:1 at different concentrations for the reactor feed gas. Chen et al., (2004) investigated the effect of different H₂:SO₂ feed molar ratios on the conversion of SO₂ and sulphur and H₂S yields. When comparing the ratios from 1:1 to 4:1, they found that the feed ratios of 3:1 and 4:1 had the highest SO₂ conversion of 100 % at both 300 °C and 320 °C over a 16 wt% Ni/γ-Al₂O₃ at a weight hourly space velocity (WHSV) of 5 040 mL.h⁻¹.g⁻¹. However, at these ratios, lower sulphur yields (≈ 55 %) were observed when compared to the feed ratio of 2:1. This led to the conclusion that the feed ratio of 2:1 was the optimum feed ratio with a conversion of ≈ 98% and a sulphur and H₂S yield of ≈ 70 % and ≈ 30 % respectively at 320 °C. The feed ratio of 1:1 showed the lowest SO₂ conversion, sulphur, and H₂S yields. The catalyst having a higher affinity for the adsorption of SO₂ than H₂ may explain this result, therefore, a higher H₂ concentration in the reactor gas is essential for higher rates of H₂ adsorption (Chen et al., 2004). Paik et al., (1997) also used a feed ratio of 2:1 in order to minimize the selectivity of SO₂ to H₂S and in turn increase the sulphur yield.

Effect of Pre-treatment

The reaction mechanism mentioned by Paik & Chung (1995), Paik et al.(1997) and Chen et al.(2004) may involve the formation of H₂S, which is an intermediate in the reduction of SO₂ by H₂. Hence, for the reduction over a metal oxide catalyst, pre-treatment with the reaction intermediate may be required for the reaction to proceed. This presulphidation has been done by Chen et al., (2004) by placing the Ni/Al₂O₃ catalyst in a reactor and flowing 50 000 ppm H₂ and

50 000 ppm H₂S in He gas at 500 °C for 2 hours. The activity of the presulphided catalyst was compared to the activity of the catalysts pre-treated with He gas and H₂ gas separately. They found that an SO₂ conversion of 100 % was achieved within 2 hours of coming on-stream for the presulphided catalysts rather than the 3.5-hour and 5-hour time lapse for H₂ and He gas pre-treated catalysts respectively. This was attributed to the formation of NiS₂ species, as analysed by an X-ray diffraction (XRD) on-stream analyser, on the γ -Al₂O₃ support from exposure to the presulphidation gas mixture, which is the active species in the conversion of SO₂.

Paik et al., (1997) exposed a Co/Al₂O₃ catalyst to 10 vol% H₂S in He gas at 400 °C for 20 hours. In situ XRD analysis was done to track the changes in the Co phases as the reaction proceeded. They found that presulphidation produced the Co₉S₈ phase which, when exposed to 5 % SO₂ from the reactor feed gas, converted to Co₃S₄ and eventually CoS₂ in 3 hours at 300 °C. This observation was also supported by the high initial uptake of SO₂ hence the conclusion that CoS₂ is the active species in the conversion of SO₂ for the Co/Al₂O₃ catalyst.

Paik & Chung(1995) compared the effects on the reduction of SO₂ by H₂ of the following pre-treatment conditions on Co-Mo/Al₂O₃:

- i. Pre-treatment with heating the catalyst in a He atmosphere to 400 °C followed by presulphidation with 10 % H₂:H₂S gas for 2 hours at 400 °C;
- ii. Pre-treatment with heating the catalyst in a He atmosphere to 400 °C followed by pre-reduction with pure H₂ gas at 400 °C; and
- iii. Pre-treatment with heating to 300 °C in an O₂ atmosphere.

The activities of the catalysts were compared under the following reaction conditions: reaction temperature of 300 °C, 5% SO₂ feed gas at a ratio of H₂/SO₂ and GHSV of 3 000 L.kg_{cat}⁻¹.h⁻¹. The results they obtained showed that the presulphided catalyst had the highest conversion of SO₂, which decreased with

time on-stream while the pre-reduced and pre-oxidized catalysts showed very low conversion, which increased slowly with time. The results implied that this increase in activity for the metallic and metal oxide catalysts was due to sulphidation of the catalysts by H₂S, which was a by-product of the reaction and thus, increased the conversion of SO₂. A further analysis via XRD for the pre-reduced and pre-oxidized catalysts after reaction showed the presence of MoS₂ which was reported to be the active species in SO₂ reduction.

Reaction Temperature Effects

The optimum reaction temperature is highly dependent on the catalyst used in the reduction of SO₂, as it has to be high enough for the reaction to occur but also not so high as to deactivate the catalyst by sintering. Paik & Chung (1995) investigated the effect of temperature with changing SO₂ feed concentrations over a temperature range of 260 °C to 350 °C over Co-Mo/Al₂O₃. They found that the selectivity to sulphur depends on the sulphur feed concentration at temperatures below 300 °C and decreases above 300 °C yet the conversion of SO₂ remained above 90 %.

The effect of different supports for 10 wt% NiO supported catalysts was investigated over a temperature range of 280 °C to 400 °C (Chen, Wang & Weng, 2004). Under the following reactor conditions: WHSV of 5 040 mL.g⁻¹.h⁻¹ and H₂:SO₂ feed ratio of 2:1, NiO/Al₂O₃ showed the best activity with high SO₂ conversions and yields to sulphur for the temperature range investigated. However, the selectivity to sulphur also declined with increasing temperature due to increased conversion of SO₂ to the reaction by product H₂S.

Han et al., (2008) studied the temperature effects over Ce_{1-x}Zr_xO₂ at a gas hourly space velocity (GHSV) of 30 000 mL.g_{cat}⁻¹.h⁻¹ and molar feed ratio of H₂:SO₂ of

2:1. The temperatures at which the catalytic reactions were initiated (light-off temperatures) of 575 °C, 500 °C and 625 °C were found for x values of 0.2, 0.5 and 0.8 respectively. The conversion of SO₂ increased rapidly below 700 °C and stabilized at approximately 95 % between 700 and 800 °C. Similar reaction characteristics were observed in all three Ce-Zr based catalysts with Ce_{0.5}Zr_{0.5}O₂ having the highest activity and the lowest light-off temperature.

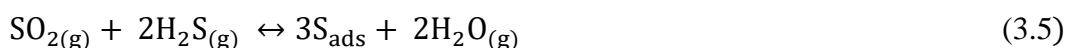
3.2.2 Reaction products and by-products

Ideally, the reaction products expected for the reduction of SO₂ by H₂ are water vapour and elemental sulphur as shown by Reaction 3.1. Due to the high temperatures used in the reactor for the reduction of SO₂, the sulphur produced is in the gas phase and typically is condensed out of the effluent stream (Paik & Chung, 1995; Paik et al., 1997). Hydrogen sulphide is produced as a reaction intermediate and depending on the catalyst and reaction conditions (such as reactant feed ratio and reaction temperature) it can be released as a reaction by-product. The selectivity for the formation of H₂S can be expressed as shown in Equation 3.4.

$$\text{Selectivity for H}_2\text{S (\%)} = \frac{\text{amount of H}_2\text{S produced}}{\text{amount of SO}_2 \text{ reacted}} \times 100 \quad (3.4)$$

Paik & Chung, (1995) suggested two main reactions that occur in the reduction of SO₂ in the presence of H₂ over two different catalyst sites of the Co-Mo/Al₂O₃ catalyst. The first reaction is as shown in Reaction 3.2 and results in the production of the reaction by-product, H₂S, when SO₂ reacts with H₂ over the metal sulphide site CoS₂ (Paik, Kim & Chung, 1997). This reaction was reported to have a very small equilibrium constant, K_a in the range of 10⁻¹⁵ to 10⁻²⁵ and is therefore nearly irreversible (Paik & Chung, 1995). It can also be seen as the

reaction that determines the effect of varying the feed ratio of H₂:SO₂ on the selectivity to H₂S, since a ratio larger than 2:1 would result in a higher selectivity to H₂S. The H₂S produced then reacts with SO₂ on the metal oxide site to produce elemental sulphur via the Claus reaction shown in Reaction 3.5 (Li et al., 2008).



From this reaction, it can be seen that if SO₂ were the limiting reactant the H₂S produced by Reaction 3.2 would be released as a reaction by-product and not consumed in Reaction 3.5. The sulphur produced desorbs from the metal oxide catalyst site as gas phase S₂ or S₄ and typically condenses and crystallizes upon cooling at the reactor exit to form S₈. The selectivity to S can be controlled not only by the reactor feed ratio of H₂:SO₂ but also by adjusting the reaction conditions so that the forward Claus reaction occurs. It is then necessary to understand how the addition of other reactants such as oxygen and water would affect the reduction of SO₂ by H₂.

3.2.3 Effect of additional reactants on SO₂ reduction

Effect of adding Water Vapour

Water vapour is a product of the reduction of SO₂ by H₂ as shown in Reactions 3.1 and 3.2 and can be added to the reaction feed. Paik & Chung, (1995) studied the effect of different concentrations (from 0 % to 56.0 %) of water vapour on the activity of Co-Mo/Al₂O₃ at 300 °C with a feed gas consisting of 5 % SO₂ and 15 % H₂. Their results showed very little to no effect on the SO₂ conversion and the selectivity to sulphur for water vapour concentrations ranged from 11 % to 56 %. This effect was also investigated (Chen, Wang & Weng, 2004) by adding 30 vol% H₂O to a reaction gas mixture of 12 000 ppm SO₂ and 24 000 ppm H₂ at

320 °C over 16 wt% NiO/ γ -Al₂O₃. They found that this reduced the SO₂ conversion by 20 % and the S yield by 39 %. This minor adverse effect of water vapour on the reduction of SO₂ was due to the addition of water vapour causing the reverse Claus reaction to become favourable (Reaction 3.5).

Effect of adding Oxygen

Han et al.(2009) investigated the effect of adding 1 vol% oxygen to the feed gas on the activity of SnO₂-ZrO₂ catalysts at various temperatures and H₂:SO₂ feed molar ratios. When varying the temperature, it was found that the presence of O₂ increased the light-off temperature from 250 °C to 375 °C. In the absence of O₂, the optimum temperature was found to be 450 °C with an SO₂ conversion of 82 % and sulphur yield of 56 %. This optimum temperature increased in the presence of O₂ to 600 °C with an SO₂ conversion and sulphur yield of 90 % and 57 % respectively.

3.3 Reduction using Methane

Methane is widely used in various industrial reducing processes due to its availability, abundance and low price. The ideal reaction for the reduction of sulphur dioxide proceeds as shown in Reaction 3.6 where [S] is an S₂, S₄ or an S₈ species.



The standard Gibbs free energy of reaction for the production of S₂ is -120.9 kJ.mol⁻¹.K⁻¹ indicating a spontaneous reaction. A side reaction that produces H₂S is also possible with a $\Delta G^\circ_{\text{rxn}}$ of -48.2 kJ.mol⁻¹.K⁻¹.

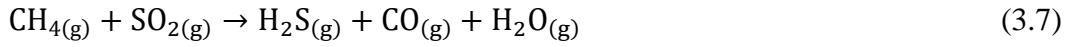


Figure 3.2 shows the relationship between the log of the equilibrium constants and the inverse of temperature (plotted via calculations shown in Appendix A). The forward reaction for the production of S₂ via Reaction 3.6 is favoured due to the positive slope of the log of K_a versus temperature. Both reactions are exothermic with the reaction via Reaction 3.6 having a greater negative enthalpy of reaction than the reaction via Reaction 3.7.

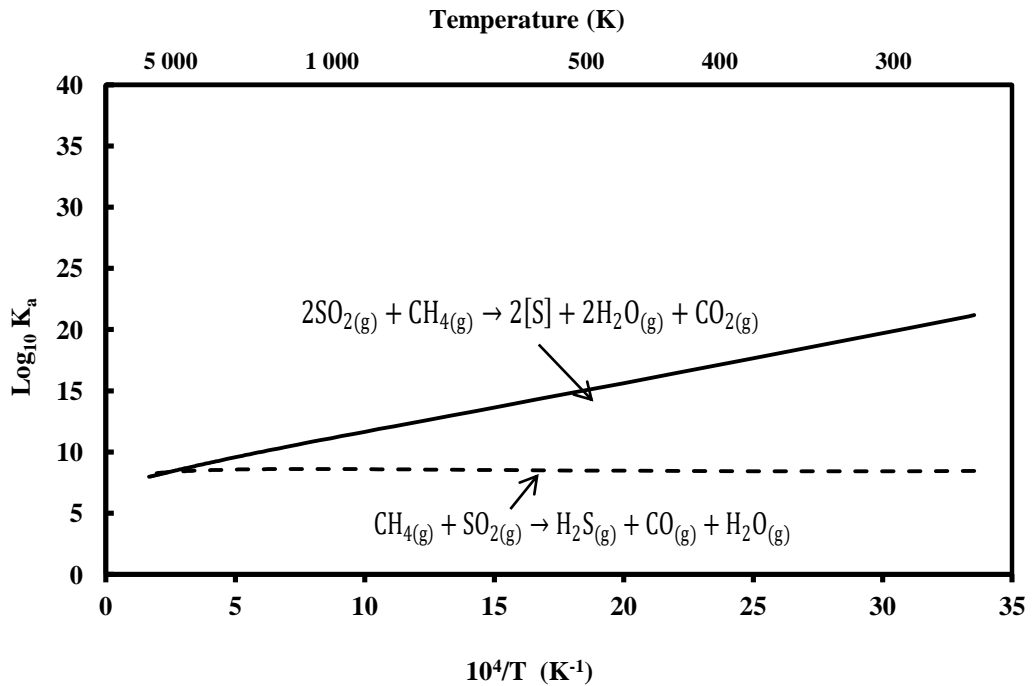


Figure 3.2: Logarithm of equilibrium K_a versus the inverse of temperature for the reduction of SO₂ by CH₄ (Calculations as shown in Appendix A)

3.3.1 Effect of Reaction Temperature

The analysis of the activity of $\text{Co}_3\text{O}_4/\gamma\text{-Al}_2\text{O}_3$ catalyst at a stoichiometric $\text{SO}_2:\text{CH}_4$ feed ratio and space velocity of 5000 h^{-1} showed an increase in the SO_4 conversion as the temperature increased from $720\text{ }^\circ\text{C}$ to $840\text{ }^\circ\text{C}$ (Yu et al., 1997). The selectivity to H_2S and COS only increased slightly above $780\text{ }^\circ\text{C}$ but remained below 5 %. Ceria-based catalysts were also shown to be active in the reduction of SO_2 with a light-off temperature of $600\text{ }^\circ\text{C}$ at the stoichiometric feed ratio (Zhu, Dreher & Flytzani-Stephanopoulos, 1999). A 90 % SO_2 conversion and 80 % sulphur yield were observed at $700\text{ }^\circ\text{C}$ particularly over CeO_2 calcined at $650\text{ }^\circ\text{C}$, which is higher than that of 4 to 10 % La-doped ceria (calcined at $750\text{ }^\circ\text{C}$), however CeO_2 is less resistant to sintering at high temperatures. Mulligan & Berk (1989) found the highest SO_2 conversions and selectivity to sulphur at $750\text{ }^\circ\text{C}$ at a feed ratio of 0.5:1 over both MoS_2 and WS_2 catalysts.

Shikina et al. (2015) investigate the effect of reaction temperature over ferromanganese (Fe-Mn) catalysts with different binders for the following reaction conditions: 67 % SO_2 , $\text{SO}_2:\text{CH}_4$ feed ratio of 2:1, a WHSV of $1\ 200\text{ h}^{-1}$ and a temperature range of 600 to $900\text{ }^\circ\text{C}$. The conversion of SO_2 over Fe-Mn (Al) was 40 % at $600\text{ }^\circ\text{C}$ and increased to 100 % at $700\text{ }^\circ\text{C}$ while the sulphur yield increased from 40 % to 80 % from 600 to $700\text{ }^\circ\text{C}$ followed by a decrease to approximately 40 % at $900\text{ }^\circ\text{C}$. The yield of H_2S increased from 0 % at $600\text{ }^\circ\text{C}$ to 50 % at $900\text{ }^\circ\text{C}$ while the yield of COS remained at approximately 0 % throughout.

3.3.2 Effect of $\text{CH}_4:\text{SO}_2$ feed ratio

The effect of the $\text{SO}_2:\text{CH}_4$ feed ratio on the selectivity to S of MoS_2 and WS_2 catalysts was investigated at temperatures from 650 to $750\text{ }^\circ\text{C}$ by Mulligan &

Berk (1989). The MoS₂ catalyst was found to have a selectivity to sulphur approximately 3 to 4 times higher at 650 °C and 675 °C than at 750 °C at a feed ratio of 2:1. Both MoS₂ and WS₂ showed an increase in selectivity with increasing feed ratio from 0.5:1 to 2:1. A previous study by Sarlis & Berk (1988) showed that an increase in the SO₂:CH₄ feed ratio (0.5:1 to 2.5:1) with decreasing reaction temperature (750 °C to 600 °C) over activated alumina catalyst resulted in a decrease in the production of the by-products carbonyl sulphide (COS) and hydrogen sulphide (H₂S). Yu et al. (1997) found that as they increased the SO₂:CH₄ feed ratio from 1.2:1 to 3.0:1 the conversion of SO₂ decreased by 34.5 % from 99.5 % while the selectivity to sulphur increased from 13.7 % to 96.5 % (over Co₃O₄/γ-Al₂O₃ catalysts at 840 °C). The respective increases in the production of H₂S and COS at low feed ratios were due to the excess CH₄ leading to the secondary reactions that produce these by-products. It was concluded that the optimum feed ratio is the stoichiometric ratio as it resulted in high SO₂ conversions, high sulphur yields and low selectivity to by-products. Zhu, Kundakovic, et al. (1999) observed the production of H₂S and CO at SO₂:CH₄ feed ratios above 1:1 and a reaction temperature above 650 °C over CeO₂-based catalysts.

3.3.3 Production of the by-products H₂S, COS and CO

The by-products H₂S, COS and CO can be produced under certain reaction conditions leading to low sulphur yields. When methane was in excess, that is at a SO₂:CH₄ feed ratio much less than 2:1, there was a notable increase in the rate of production of H₂S and CO at temperatures above 725 °C (Sarlis & Berk, 1988; Mulligan & Berk, 1989). Alongside H₂S, COS can also be produced in the presence of excess CH₄ by means of secondary reactions over Co₃O₄/γ-Al₂O₃ at 840 °C (Yu et al., 1997). When comparing the amount of CH₄ consumed to the amount of CO₂ produced at temperatures ranging from 550 °C to 750 °C over

Ce(4.5%La)O_x and 5%Cu-Ce(4.5%La)O_x catalysts, it was observed that the difference between the actual amount of CO₂ produced and the amount that should have been produced based on the amount of CH₄ consumed (assuming complete conversion of the C in CH₄ to CO₂) increased with increasing temperature from 650 °C (Zhu et al., 1999). This difference was accounted for by the presence of CO in the product gas stream due to the partial oxidation of CH₄ to CO and H₂ (Zhu et al., 1999). The H₂ then reacted with the sulphur produced to form H₂S as shown in Reaction 3.7 resulting in low sulphur yields.

Yu et al., (1997) investigated the effect of adding 10 % H₂S to the reactor feed and found that the presence of H₂S increased the production of elemental sulphur as it reacted with SO₂. However, this did not result in an increased production of H₂S or COS by supported Co catalysts. Shikina et al.(2015) found that the amount of COS produced over Fe-Mn (Al) catalyst at a GHSV of 1 200 h⁻¹ remained relatively low, at approximately 0 vol%. The concentration of H₂S increased up to 50 vol% as the temperature increased to 900 °C over the untreated and sulphided forms of Fe-Mn (Al) catalysts.

3.4 Reduction by Carbon Monoxide

Carbon monoxide is formed as a by-product from the combustion of coal under low oxygen conditions, which is known as the partial oxidation of C to CO. In the generation of power via coal combustion, the air/coal ratio can be varied to increase the production of CO which can then be used for the reduction of SO₂ (Khalafalla & Haas, 1972). The reaction can be expressed as shown in the Reaction 3.9.



The standard change in Gibbs free energy of reaction for this reaction is $-173.7 \text{ kJ.mol}^{-1}.\text{K}^{-1}$, showing that the reaction with gaseous S_2 product is feasible. However, a side reaction that produces the undesirable and more toxic by-product carbonyl sulphide, COS (Reaction 3.10) can also occur with a $\Delta G_{\text{rxn}}^{\circ}$ of $-285.04 \text{ kJ.mol}^{-1}.\text{K}^{-1}$.



Further analysis of the thermodynamics of the two reactions followed in the reduction of SO_2 by CO shows a linear relationship between the logarithm of the equilibrium constant K_a and $T \times 10^{-4}$ for temperatures ranging from 298 to 6 000 K in Figure 3.3 (“NIST Webbook”, n.d.). Note that values of T in K are indicated along the top of the graph.

The positive slope of the log of K_a indicates that the forward reaction is favoured as shown in the Figure 3.3. For the production of S_2 and CO_2 , as the temperature reciprocal decreases from 33 K^{-1} to 5 K^{-1} , (equivalent of temperature increasing from 298.15 K to 2 000 K), the value of $\log K_a$ approaches zero. This trend shows that as temperature increases the value of ΔG_{rxn} moves from a negative to a positive value hence the production of the CO_2 and S_2 is lowered. Below 5 K^{-1} , the forward reaction is not spontaneous as shown by the negative values of $\log K_a$. The same trend is observed for Reaction 3.10, which produces COS instead of elemental sulphur however this reaction has a greater slope of $\log_{10}K_a$ versus $T \times 10^{-4}$ than for Reaction 3.9.

Other reaction conditions also affect the production of elemental sulphur and/or COS such as reactor feed ratio, catalyst used, which in turn can determine the reaction mechanism followed, and the presence of additional reactants such as water and oxygen (Mulligan & Berk, 1989; Liu et al., 1996; Ma et al., 1997; Paik et al., 1997; Flytzani-stephanopoulos et al., 2000; Zhuang et al., 2000; Wang et

al., 2002; Chen & Weng, 2005; Han et al., 2008; Han et al., 2008; Han et al., 2009).

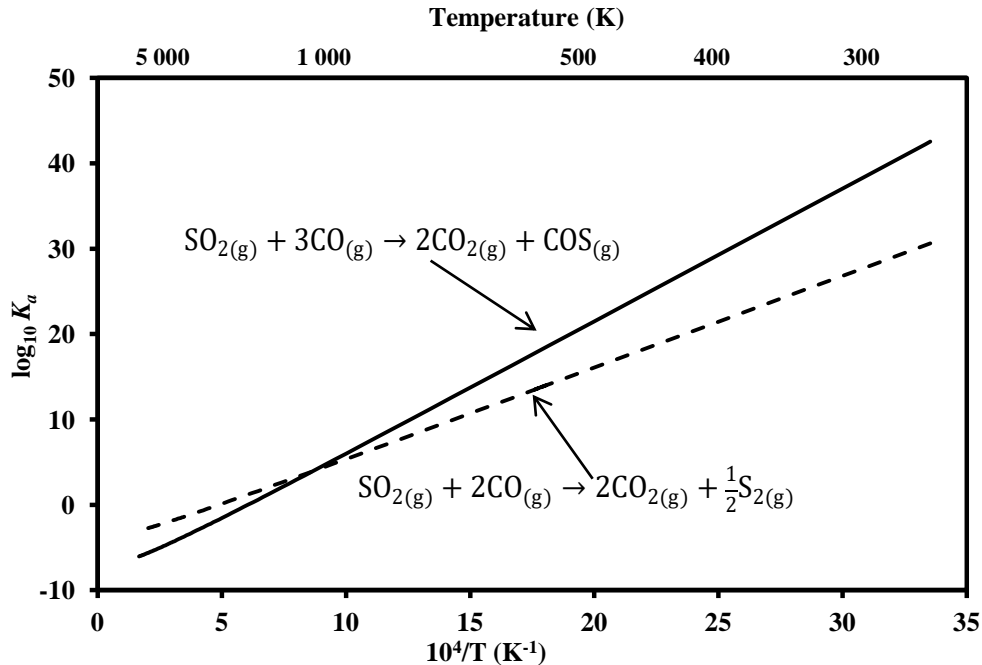


Figure 3.3: Chemical equilibrium constants as a function of the inverse of temperature for the reduction of SO_2 by CO (Calculations as shown in Appendix A)

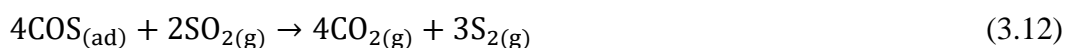
3.4.1 Characteristics of the Reaction

Pre-treatment of Catalyst

Pre-sulphidation of the catalyst is a necessary step that activates the catalysts for the reduction of SO_2 using CO most likely via the COS intermediate reaction mechanism. Paik et al. (1997) presulphided a $\text{Co}/\text{Al}_2\text{O}_3$ catalyst in a flow of 10 % H_2S in He for 2 hours at 400 °C. This step in the catalyst preparation yielded CoS_2 , which was thought to be the active species in the generation of COS via Reaction 3.11:



They reached this conclusion by observing the reduction of SO₂ by CoS₂, which showed a constant production of COS with very low SO₂ consumption. Further analysis by XRD showed there was a transformation of CoS₂ into CoS. Previous studies (Haas & Khalafalla, 1973a) also showed the same effect over an Fe-supported catalyst where the Fe was transformed into FeS₂ in-situ by the S₂ initially generated. The COS produced then reacted with SO₂ via Reaction 3.12 to produce elemental S and CO₂.



The effects of pre-sulphidation on CoMo-supported on Al₂O₃ was investigated by (Zhuang et al., 2000) by analysing the activity of 4.4% Co -15.9% Mo/Al₂O₃. Upon increasing the temperature from 100 °C to 550 °C, both the consumptions of CO and SO₂ were very low initially followed by a rapid increase between 350°C and 450 °C while COS production was almost zero. The reaction was then cooled down and showed a complete removal of SO₂ and CO at 350 °C. This was followed by an increase in COS produced as the reactor was cooled further from 300 °C to 200 °C. These results show that the S species on the catalyst was formed in situ between 350 °C and 450°C by reaction between SO₂ and COS to produce S₂. The reaction between S₂ and the catalyst produced MoS₂, which appeared to be the active species in the reduction of SO₂ as shown by the increase in its consumption with small quantities of COS generated. At temperatures below 350 °C, a low activity was observed as the SO₂ and CO consumption rates increased. The activity of the sulphided CoMo/Al₂O₃ was not only higher but it was also active at a lower temperature of 300 °C as compared to the unsulphided catalyst.

Chen & Weng (2005) pre-treated Cr₂O₃/nano-CeO₂ with different gases to illustrate the effects of pre-sulphidation. After pre-treatment with He, CO, SO₂ and a mixture of SO₂ and CO, the activities of these catalysts were analysed at

320 °C at a WHSV of 12 000 mL.g⁻¹.h¹ over 30 hours. The lowest SO₂ conversion of approximately 20 % was achieved by the catalyst treated in He, while the catalyst treated in a mixture of SO₂ and CO showed the highest activity, namely 90 % to 100 %, and the lowest deactivation rate. Analysis of the sulphur yield showed the same trend with the catalyst pre-treated with SO₂ and CO having the highest yield of approximately 100 %. This was due to the partial conversion of the Cr₂O₃/nano-CeO₂ catalyst into a chromic sulphide species while maintaining the active Cr₂O₃ species that stabilized the catalyst making the catalyst more resistant to deactivation. The Fe₂O₃/CeO₂ catalyst also exhibited similar activity with the SO₂ and CO pre-treated catalyst having the highest activity and lowest deactivation rate (Wang et al., 2002).

Wang et al. (2014) investigated the effect of presulphidation temperature on the conversion of SO₂ and yield of S over Fe₂O₃ supported on activated carbon (AC). In their study, Fe₂O₃/AC was pre-treated with a gas mixture of 1 % SO₂ and 2 % CO in N₂ at a flow of 58 mLmin⁻¹ for 2 hours at 300 °C, 400 °C, and 500 °C. They found that the higher pre-treatment temperatures of 400 °C and 500 °C resulted in higher SO₂ conversion and S yield rates. Analysis of their catalysts using X-ray diffraction after each pre-treatment showed that Fe₂O₃ on the catalysts converted to FeS₂. This sulphidation of the Fe species was a necessary step to activate the catalyst for the reduction of SO₂, thus pre-treatment at 300 °C resulted in the partial conversion of Fe₂O₃ hence the lower SO₂ conversion and S yield rates.

Zhang et al. (2016) achieved SO₂ conversions of 93 % and sulphur yields of 99 % over Ce_{0.7}Ti_{0.3}O₂ at 500 °C without any catalyst pre-treatment. They found that the active species in the reduction of SO₂ was due to CeO₂ with labile oxygen vacancies, while TiO₂ stabilized the structure of the catalysts.

Reaction Temperature Effects

Early studies (Khalafalla et al., 1971) show that at SO₂ and CO concentrations lower than 10 %, there is no reaction between SO₂ and CO in the absence of a catalyst even when the temperature is raised to 950 °C. The introduction of the Buehler alumina catalyst increased the conversion of SO₂ to approximately 60 % at 900 °C with a light-off temperature of 675 °C as shown by Khalafalla & Haas (1972). The effect of temperature on the activity of the physical mixture of La₂O₂S and CoS₂ was investigated (Ma et al., 1996) by heating the catalyst from room temperature in 50 °C steps to 600 °C and then cooling in a similar manner to room temperature. The light-off temperature in the heating cycle was found to be 350 °C while the maximum amount of COS was generated at approximately 450 °C. The successive cooling cycle however showed activity at lower reaction temperatures with the catalyst remaining active down to 300 °C and a lower maximum amount of COS generated at a lower temperature, *viz.* 375 °C. The lower activity observed in the heating phase compared to the cooling phase at a particular temperature was attributed to the sulphidation of the catalyst. The sulphur species remain on the catalyst during the subsequent cooling phase and allow the reaction to continue happening at lower temperatures.

Further work on La₂O₂S prepared from La₂O₃ powder (Ma et al., 1997) showed a light-off temperature of 350 °C followed by a sharp increase in the conversions of SO₂ and CO and the formation of COS. A conversion of 98 % was reached and maintained from 450 °C to 600 °C while COS production peaked at 375 °C and declined thereafter. Han et al. (2008) also observed a light-off temperature of 375 °C using SnO₂ at a GHSV of 10 000 h⁻¹ and CO:SO₂ feed ratio of 2:1. Below 425 °C, the SO₂ conversion and selectivity increased monotonically with temperature while the sulphur selectivity decreased monotonically. Above 425 °C, the selectivity to COS decreased to 20 % while sulphur selectivity increased to a maximum of 80 % with the highest SO₂ conversion of 45 % at 550 °C. In other

work on SnO₂Park et al., (2011) observed that the catalyst became active at temperatures above 350 °C.

CoMo/ γ -Al₂O₃ was found to have high SO₂ conversions of 100 % and high S yields of 100 % at temperatures above 350 °C (Zhao et al., 2015) at a GHSV of 6 000 ml.g_{cat}⁻¹.h⁻¹. At 200 °C, the selectivity of the CoMo/Al₂O₃ was greater than 60 % and it decreased to 0 % as the reaction temperature increased to 350 °C.

3.4.2 Effect of CO:SO₂ Feed Ratio

The composition of flue gas is highly dependent on the composition of the fuel burnt and the combustion conditions that affect the ratio of CO and CO₂. Querido & Short (1973) reported that the composition of flue gas from the combustion of coal which contained 3.2 wt% sulphur with 1 % excess air was 18 % CO₂, 1.4 % CO, 0.5 % O₂ and 0.2 % SO₂. The presence of other gases may have affected the activity of a catalyst in the reduction of SO₂ with CO. Hence, it was necessary for preliminary studies where the aim was to understand SO₂ reduction to remove the gases not directly involved in SO₂ reduction and to introduce them again later. To produce high sulphur yields, it is vital to reduce the production of by-products such as COS.

The effects of the CO:SO₂ feed ratio on the conversion of SO₂ of pre-sulphided CoMo/Al₂O₃ at 300 °C was investigated (Zhuang et al., 2000) for the range 0.9:1 to 3:1. It was found that when SO₂ is in excess in the reactor feed gas, that is, CO:SO₂ is less than 2:1, there was no COS in the reactor effluent stream. The SO₂ conversion however decreased as CO:SO₂ approaches 2:1. For Cr₂O₃/nano-CeO₂ a low SO₂ conversion and sulphur yield at temperatures ranging from 260 °C to 360 °C when CO:SO₂ is 1:1 was also observed (Chen & Weng, 2005). A similar trend was also observed over Fe₂O₃/ γ -Al₂O₃ over a temperature range of 200 °C to

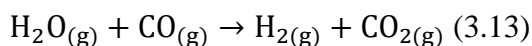
800 °C with both SO₂ conversion and sulphur yield reaching a maximum of 45 % (Wang et al., 2006). When CO:SO₂ was greater than 2:1, that is, when CO was in excess Han et al. (2008) and Wang et al.(2014) found that the conversion of SO₂ increased together with the selectivity to COS. This however decreased the yield to sulphur also observed over CoMo/Al₂O₃ showing an increase in COS selectivity (Zhuang et al., 2000).

Due to the differences in the reaction conditions and catalysts used to investigate the effect of feed ratio, CO:SO₂, on the SO₂ reduction, different values of the feed ratio were found to be the optimum feed ratio. It is however consistent that the feed ratio for which the highest S yield is obtained is close to the stoichiometric feed ratio of 2:1 (Ma et al., 1997; Zhuang et al., 2000; Wang et al., 2006; Han et al., 2008; Wang et al., 2014)

3.4.3 Effects of additional reactants

Effect of Water

Flue gas from the combustion of fossil fuels is known to contain moisture hence studying its effect on the reduction of SO₂ is important. There is also a possibility of the occurrence of the water-gas shift reaction (Reaction 3.13) over catalysts which are active for this reaction (Querido & Short, 1973).



The presence of H₂ may lead to reactions such as Reactions 3.3 and 3.4, the production of H₂S from H₂ and S₂ product and reactions with COS as shown in Reactions 3.14 and 3.15 (Okay & Short, 1973).



Research on the effect of water on the reduction of SO_2 by 8 % $\text{Cu}/\text{Al}_2\text{O}_3$ led to the conclusion that the water-gas shift reaction did not occur due to the absence of H_2 and H_2O in the reactor effluent stream (Okay & Short, 1973). The most significant effect observed was a decrease in the SO_2 conversion for water vapour concentrations less than 10 % (Okay & Short, 1973; Ma et al., 1997; Wang et al., 2006). This adverse effect is however reversible; with the removal of water vapour from the feed stream the activity is restored to its former level.

Effect of Oxygen

It is important to study the effect of oxygen on the reduction of SO_2 by CO as it is present in flue gas. When 0.5 % of O_2 was introduced into the reactor, the activity of $\text{Fe}_2\text{O}_3/\gamma\text{-Al}_2\text{O}_3$ decreased from 100 % SO_2 conversion to 29.41 % (Wang et al., 2006). This negative effect was caused by O_2 reversing the sulphidation of the catalyst transforming it from FeS_2 to the non-active form, Fe_2O_3 . However, this effect is reversible once the oxygen is removed from the reactor feed gas. Ma et al. (1997) also found similar results of $\text{La}_2\text{O}_2\text{S}$ but with a lower decrease in activity at higher temperatures when exposed to up to 2 mol% O_2 . Exposing 1 vol% O_2 to $\text{SnO}_2\text{-ZrO}_2$ at a GHSV of $10\,000\text{ h}^{-1}$ and a $\text{CO}:\text{SO}_2$ feed ratio of 3.5:1 resulted in an increase in the light-off temperature from $250\text{ }^\circ\text{C}$ to $400\text{ }^\circ\text{C}$ (Han et al., 2009). The decrease in activity was attributed to the preferential adsorption of O_2 versus SO_2 on the catalyst surface so that the oxidation of the sulphided catalyst with O_2 and CO to produce SO_2 and CO_2 (Ma, Fang & Lau, 1997). These competing reactions merely inhibited SO_2 reduction but did not stop

it completely hence, the presence of SO₂ may also interfere with the oxidation of CO.

3.5 Conclusion

The catalytic abatement of SO₂ is achieved using various reducing agents such as hydrogen, methane and carbon monoxide on supported and unsupported metal oxide catalysts. The nature of the catalyst and reaction conditions typically determines the reduction mechanism followed. Previous studies have shown that a reaction intermediate can be generated and is dependent on the reducing agent used. Adjusting the reaction conditions such as feed ratio, reaction temperature and reactor feed composition increases the selectivity to sulphur over the reaction intermediate molecule. Table 3.1 summarizes some of the results of the reduction of SO₂ by CO over different catalysts at a feed ratio of 2:1.

Pre-treatment of the catalyst has been shown to improve the activity in the reduction of SO₂. This step results in the formation of a metal sulphide species that acts as the active site for the reaction of the reducing agent. On catalysts such as Co/Al₂O₃ for the reduction of SO₂ by CO, pre-treatment converted the Co to CoS₂ which reacts with CO to form the reaction intermediate COS, adsorbed on the surface (Paik et al., 1997). The overall conversion of SO₂ therefore depends on the rate of reaction between SO₂ and CO and the reaction temperature.

Table 3.1: Summary of literature results for reduction of SO₂ using CO at a feed ratio of 2:1

Reference	Catalyst Employed	% SO ₂ Conversion	% Selectivity to Sulphur	Reaction Temperature (°C)	GHSV
Ma et al. (1997)	La ₂ O ₂ S	98	-	600	10 800 cm ³ /g _{cat} .h
Paik et al. (1997)	CoS ₂ -TiO ₂	98.6	97.6	400	3000h ⁻¹
	TiO ₂	97.9	97.1	400	3 000h ⁻¹
Kim et al. (1998)	Co ₃ O ₄ -TiO ₂	100	≈ 98	400	3 000h ⁻¹
Zhuang et al. (2000)	CoMo/Al ₂ O ₃	100	100	300	6000 mL/g _{cat} .h
Wang et al. (2002)	Fe ₂ O ₃ /CeO ₂	100	100	380	17 280 mL/g _{cat} .h
Zhaoliang et al.(2003)	Ti _{1-x} Sn _x O ₂	> 95	>95	350	2400h ⁻¹
Chen & Weng (2005)	Cr ₂ O ₃ /CeO ₂	90 to 100	≈100	320	12 000 ml/g _{cat} .h
Han et al. (2008)	Ce _{1-x} Zr _x O ₂	92.4	91.8	550	30000 mL/g _{cat} .h
Han et al. (2008)	SnO ₂	45	80	550	10000h ⁻¹
Park et al.(2011)	SnO ₂ -ZrO ₂	68	58	450	-
Wang et al.(2014)	Fe ₂ O ₃ /AC	98	90	450	7 000 mL/g _{cat} .h
Zhang et al. (2016)	Ce _{0.7} Ti _{0.3} O ₂	≈100		500	24 000 mL/g _{cat} .h

The reactor feed ratio of the reducing agent to SO₂ played a vital role in the conversion of SO₂ to elemental sulphur. On most catalysts, SO₂ adsorbs strongly on the catalysts surface and therefore blocks the adsorption of the reducing agent. In order to increase the conversion of SO₂, the reducing agent had to be at the stoichiometric equivalent concentration or in excess to compete with SO₂ for adsorption. The most common result reported from previous researchers was that maintaining the feed ratio at the stoichiometric ratio resulted in higher SO₂ conversions and sulphur yields.

The addition of water vapour and oxygen to the reactor gas stream had an impact on the conversion of SO₂ and selectivity to sulphur. When using H₂ as the

reducing agent, the addition of water caused the conversion to decrease since water is a product of the reduction reaction (Paik & Chung, 1995; Chen, et.al, 2004). However, the presence O₂ led to an increase in the reaction temperature required for high conversions of sulphur when H₂ and CO were used as reducing agents. In addition, the presulphided catalysts went through oxidation resulting in a reduction in the conversion of SO₂. These negative effects were found to be reversible upon removal of the oxygen flow.

The general reaction temperatures for high sulphur yields were found to be 300 °C and above. These high temperatures would require the addition of high amounts of energy to achieve appreciable catalytic abatement of SO₂. Thus, the need to find a catalyst that would be active for the reduction of SO₂ at lower reaction temperatures.

Chapter 4: Gold Catalysis

Gold nanoparticles have been recently shown to produce highly active catalysts for various reactions. This has resulted in a lot of research into the catalytic activity of these Au nanoparticles supported on various supports for a variety of reactions. These include environmental reactions such as its use in catalytic cracking reactions (CO abatement) in vehicles.

4.1 Characteristics of Au-supported catalysts

It is well known that bulk gold is inert and classified as a noble metal with no catalytic activity unlike its neighbouring metals in the periodic table. However, gold nanoparticles dispersed on a metal oxide support exhibit very high catalytic properties. Initial discoveries were observed by Hutchings who found that Au-supported on activated carbon showed higher activity for ethyne hydrochlorination for the synthesis of poly vinyl chloride (PVC) than the commonly used mercuric chloride catalyst (Hutchings, 1985). This gold catalyst was superior due to its greater stability and resistance to thermal deactivation. The most significant application of Au-supported catalyst was the discovery of its catalytic ability in the oxidation of CO at low temperatures (Haruta et al., 1987).

The size of the supported nanoparticles plays a significant role in the catalytic ability of the Au. Early studies show that the highest activity for CO oxidation was achieved by Au-supported catalysts with an Au nanoparticle diameter less than 10 nm (Haruta et al., 1989). Later studies also show that Au nanoparticles with a size less than 5 nm were the most active as shown by Haruta (2004) in the oxidation of CO. Au/TiO₂ with Au cluster sizes ranging from 2 nm to 4 nm were

prepared and tested under excess O_2 at 350 K (Goodman, 2004). It was found that the most active catalyst had an Au nanoparticle size of 3.5 nm and a thickness of 2 atoms. It is thought that the active sites of the catalysts are the step sites, corners or edges of the Au nanoparticles; decreasing the particle size increased the surface area and hence the number of active sites. Furthermore, the atoms adjacent to the support appeared to be particularly active. This meant that hemispherical particles have more active sites than spherical particles, and are therefore more active as illustrated in Figure 4.1 (Haruta, 2008). This shows a spherical and hemispherical Au cluster on the metal oxide support, where the perimeter of the cluster-support interfaces are projected onto a flat surface. This shows that hemispherical cluster offers a larger interface, which was believed to be the active site for CO oxidation.

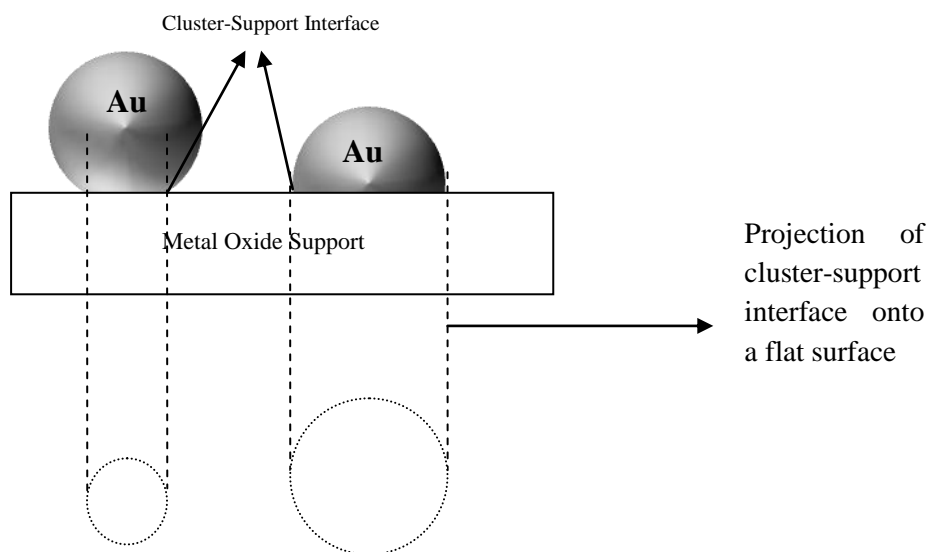


Figure 4.1: Illustration of spherical and hemispherical Au clusters on metal oxide support

Deactivation of the catalyst therefore occurred when the size of the Au nanoparticles increases by sintering (Parker & Campbell, 2007). The activity of Au-supported catalysts also depends on the method of preparation and support

used. Several analytical methods can be used to determine the physical and chemical properties of Au-supported nanoparticles.

4.2 Characterization of Au-supported catalysts

4.2.1 The size of Au nanoparticles

The size and shape of the Au nanoparticles on the metal oxide support is primarily determined using transmission electron microscopy (TEM). For Au-supported nanoparticles, the image generated typically shows hemispherical and/or spherical Au nanoparticles attached to the flat planes of the metal oxide support (Haruta, 1997; Rossi et al., 2008; Soares & Bowker, 2005; Wu et al., 2004). These nanoparticles are visibly distinguished as darker, smaller spherical particles in contrast to the large lighter support particles. The size and distribution of the nanoparticles largely depends on the method of preparation of the catalyst. The Au nanoparticle size of Au/TiO₂ prepared by the deposition-precipitation method was investigated by changing pH of the solution (Haruta, 1997). Analysis by TEM found that the Au nanoparticles size increased with increasing pH as the acidic conditions produced particles over 5 nm in size. The TEM image of Au/ α -Fe₂O₃ prepared by co-precipitation showed Au nanoparticles homogeneously dispersed on the iron oxide support with a standard deviation of 30 % (Haruta, 2004b). Giorgio et al. (2001) prepared Au nanoparticles by condensation in ultra-high vacuum on anatase-TiO₂ at varying deposition times. They found that increasing the deposition time from 2 minutes to 18 minutes results in an increase in the Au cluster size from 2 nm to 5 nm respectively.

4.2.2 Surface of supported Au catalysts

Heterogeneous catalysis mainly occurs on the surface of the catalyst where the substrate molecules adsorb, dissociate and recombine before desorption into the final products. It is therefore necessary not only to identify the atomic species present on the surface of the catalyst but also their quantity and the chemical bonds present. The surface of catalysts can be studied using X-ray spectroscopy (XPS) to determine its atomic composition and the chemical bonds present between ions. This is done by exciting the valence electrons and measuring their kinetic energy, which is specific to each element and bond energy. Impurities that may lead to the inactivity of the catalyst can be detected by XPS. The contamination of the catalyst usually occurs during the preparation of the catalyst. XPS of Au/TiO₂ prepared by deposition-precipitation and incipient-wetness methods showed a higher presence of chlorine in the latter preparation method than in the deposition precipitation method (Soares & Bowker, 2005).

The effect of pre-treatment of Au/TiO₂ using SO₂ for CO oxidation showed that the presence of SO₂ did not affect the binding energy of the metallic Au 4f spectra (Kim & Woo, 2006). However, the O 1s spectra revealed the presence of sulphate created from reaction between SO₂ and the hydroxyl groups, the amount of sulphate increased with increasing pre-treatment temperature.

4.2.3 Structure of Au supported catalysts

X-ray diffraction is not only used to identify the type of crystalline/non-crystalline structures of the catalysts but also to measure the size of the nanoparticles. Both these properties can be used to support the information obtained from TEM and high resolution TEM (HRTEM) studies. Both HRTEM and XRD can give the *d*-spacing of the planes of a crystal. The measured values are compared to the

reference values to identify the crystal. The XRD patterns are a series of peaks specific to each element or compound and can be superimposed if more than one species is present in the sample. Most of the analysed Au-supported catalysts produce XRD patterns of mainly the support and the dopant, if present, since the Au loading is usually $\ll 10\%$. For example, the XRD patterns of 3% Au/Fe(OH)_x calcined at temperatures ranging from 423 K to 623 K showed the presence α -Fe₂O₃ and FeOOH (Wu et al., 2004). The XRD peaks for Au were not observed, as a loading of 3% is too low to detect. Ilieva et al. (2009) also obtained XRD patterns showing peaks of the doped CeO₂ support and no noticeable Au peaks for Au/CeO₂ prepared by the deposition-precipitation method with a gold loading of 2%.

4.2.4 BET Surface Area of Au supported catalysts

Generally, good catalytic properties are attributed to the large surface areas available on the catalyst for the adsorption and reaction of the reactants. Brunauer, Emmet and Teller developed a method to measure the surface area (commonly referred to as the BET surface area) of a catalyst by the volumetric physisorption of an inert gas. In the case of supported nanoparticles, the surface area is largely a property of the support. The addition of nanoparticles may cause a slight change in the surface area. Titania showed an insignificant change in the BET surface area, from 50 m²/g to 47 m²/g, after loading Au nanoparticles (Moma, 2007). Wu et al. (2004) found that the surface area of Fe(OH)_x reduced by 1 m²/g from 277 m²/g after loading 3 wt% Au, note that this change is within experimental error for BET measurements. This surface area reduced to 208 m²/g after calcination and reaction with the support in the form of Fe(OH)_x and iron oxide.

4.3 Gold catalysts for CO Oxidation

Carbon monoxide oxidation is an important environmental elimination reaction that converts CO to a less harmful gas CO₂ via Reaction 1.5. The relationship between the log₁₀ of the equilibrium constant K_a and the temperature of the reaction is shown in Figure 4.2. The reaction is spontaneous as shown by a negative value of ΔG_{rxn} at temperatures higher than 3 350 K as shown by a negative value of log₁₀K_a. Cant & Fredrickson (1975) found that gold is active for CO oxidation at 0 °C at varying partial pressures of O₂ and CO.

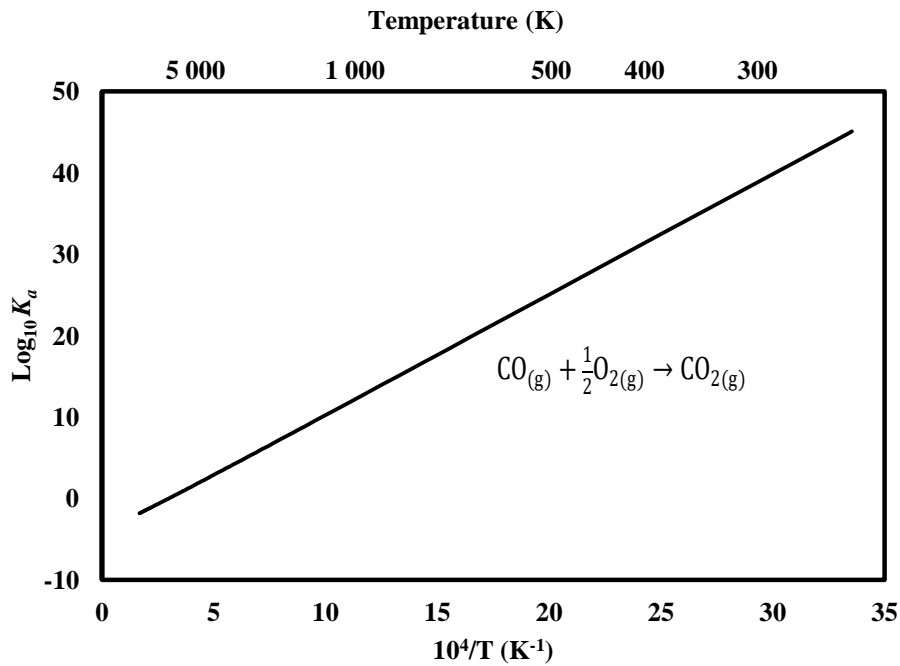


Figure 4.2: Relationship between the log₁₀ of the equilibrium constant K_a and the temperature for CO oxidation (Calculations as shown in Appendix A)

4.3.1 Characteristics of the Reaction

Low Temperature

Early studies by Haruta et al. (1987) found that Au/ α -Fe₂O₃, Au/Co₃O₄ and Au/NiO completely oxidized CO at temperatures as low as -70 °C while showing very high catalytic activities when compared to the metal oxide support and unsupported Au. The tests on 3%Au/Fe(OH)_x showed 100 % conversion, even under saturated moisture for extended time on stream of up to 100 hours (Wu et al., 2004) at room temperature (18 °C to 27 °C). This high activity at low temperatures means that there is a wide range of temperatures that the catalyst will be active before it will be deactivated. This means that Au-supported catalysts are superior catalysts as they not only increase the rate of reaction but also lower the temperature for complete CO oxidation.

Effect of Support Material

The supporting materials of Au nanoparticles can be classified according to their reducibility and position in the periodic table. With respect to CO oxidation, oxides of reducible transition metals tend to have a higher activity than irreducible metal oxides (Schubert et al., 2001). This is due to their ability to absorb and store oxygen at low temperatures. The activities of Au supported on reducible metal oxides like Co₃O₄, Fe₂O₃ and TiO₂ showed that there is still a hierarchy in the activity of these metal oxides with Co₃O₄ exhibiting the highest turnover frequency and TiO₂ the lowest (Haruta, 1997). Irreducible metal oxide supports such as Al₂O₃ and SiO₂ show lower activities for CO oxidation (Bond, Louis & Thompson, 2006). It is impossible to explain why reducible metal oxide supports are superior without discussing the mechanism involved in the oxidation of CO.

Mechanism of CO oxidation

As mentioned earlier, the size of the Au nanoparticle and the type of support characterize the activity of the supported Au catalyst in CO oxidation. It is then necessary to understand the mechanism involved in the oxidation of CO to explain the high activity of the Au supported on reducible metal oxides. Schubert et al. (2001) sought to identify the sites on which O₂ adsorbs using CO–O₂ titrations on Au/ α -Fe₂O₃ and the support, α -Fe₂O₃. In the titrations, O₂ is pre-adsorbed on the catalyst surface resulting in a high amount of O₂ available for reaction when CO is later introduced. The fast reaction response observed led to the conclusion that O₂ adsorbs on the support in close proximity to the Au nanoparticle (where CO adsorbs), specifically on the oxygen vacancy of the support. Azar et al. (2006) concurs with this mechanism for the oxidation of CO on Au/TiO₂, and found that stoichiometric feed ratios of CO:O₂ do not lead to the complete conversion of CO. When they pre-adsorbed O₂ thereby stabilizing the catalyst, the complete conversion of CO was achieved. It was then proposed that oxygen reacts with both CO and the oxygen vacancies on the TiO₂ support hence its insufficiency in stoichiometric proportions in the reaction with CO. A reaction between the adsorbed species of CO and O₂ also resulted in the formation of carbonate species on the catalyst surface that causes deactivation of the catalyst. Several other observations have led to other explanations for the deactivation of Au-supported catalysts.

4.3.2 Deactivation and Sintering of Au-supported Catalysts

Deactivation of a catalyst results in the loss of the ability of the catalyst to adsorb, dissociate or facilitate the generation of reaction products. Many factors may contribute to this loss of activity. As noted in 4.2.1, the size of the Au nanoparticle influences the activity of the catalyst with particles less than 10 nm showing

higher activity. Continuous exposure to the reaction conditions for CO oxidation leads to a loss in activity and has been attributed to the agglomeration of the Au nanoparticles, resulting in larger and less active particles (Goodman, 2004; Haruta, 2004b). This deactivation by sintering yields more thermodynamically stable and larger particles of Au (Parker & Campbell, 2007).

Au/TiO₂ was found to deactivate during storage under various conditions over a period of one year (Raphulu et al., 2009). This deactivation was attributed to agglomeration of Au clusters, Au(III) reduction, loss of hydroxyl groups and moisture, and the accumulation of impurities, such as carbonates and formates on the surface as observed from the infrared spectra. They proposed that storage under an inert, cool and dark atmosphere might reduce the deactivation during storage.

With respect to CO oxidation, the formation of carbonates on the surface of the catalyst has been reported to be one of the causes of Au/TiO₂ deactivation (Haruta, 2004b; Azar et al., 2006). Stabilized Au/TiO₂ also produced the carbonates yet remained active due to the sub-surface migration and consequent storage of the carbonates in the TiO₂ support (Azar et al., 2006). Other impurities on the catalyst surface can also adsorb irreversibly and deactivate the catalyst. These could be on the catalyst surface from the catalyst preparation step, such as chlorides. Sulphates have also been incorporated into Au-supported catalysts to determine their effect on the activity on CO oxidation (Ruth et al., 2000; Lai et al., 2004; Kim & Woo, 2006).

Poisoning by S Species

Gold supported catalysts are known for their high activity in the oxidation of CO at very low temperatures (Haruta et al., 1987). It has however been found that the presence of SO₂ inhibits this catalytic activity to an appreciable degree (Kim &

Woo, 2006). The effect of SO₂ on CO oxidation was investigated by Ruth et al. (2000) over Au and Pt supported on TiO₂. Both Au/TiO₂ and Pt/TiO₂ were pre-treated with 0.05 % SO₂ in air at 300 °C for 1 h then flushed with air before cooling for the CO oxidation. They initially found that this pre-treatment had no effect on the activity of Au/TiO₂ and therefore introduced 0.05 % SO₂ into the reactor feed gas. This pre-treatment of the catalysts resulted in the highest activities achieved (at higher temperatures) compared to untreated catalysts. The Au/TiO₂ catalysts suffered irreversible deactivation with continuous exposure to 0.05 % SO₂ in the feed stream. Ruth et al. (2000) suggested the deactivation to be due to SO₂ adsorbing on the Au-TiO₂ interface, which is where the active sites for oxygen activation are thought to be located. A similar effect was observed over Au/TiO₂ pre-treated with 0.5 % SO₂ in He at room temperature and 300 °C (Kim & Woo, 2006). This was due to an increase in the strength of the adsorption of CO on Au after pre-treatment, which restrains the migration of CO to the interface of Au and TiO₂ where CO₂ is formed (Kim & Woo, 2006).

4.4 Conclusion

Research has shown that supported Au nanoparticles are very active for low temperature CO oxidation. This is mainly due to the reactive properties of Au nanoparticles, unlike the noble state of bulk Au, and their interactions with the supporting metal oxide. The size of the Au nanoparticles also plays an important role as shown by higher activities achieved by clusters less than 10 nm.

A large amount of the research into the catalytic properties of Au supported catalysts has been done for the oxidation of CO. Deactivation of the catalyst can occur by sintering caused by continuous exposure to CO reaction conditions, prolonged storage, sintering at high temperatures and exposure to impurities. It was found that reducible metal oxide supports have a higher activity than non-

reducible metal oxide supports due to their ability to adsorb and store oxygen. This means that they play a role in the overall reaction other than provide a support for the Au nanoparticles. Researchers have proposed the following reaction mechanism involved in the oxidation of CO: adsorption of O on the support, migration of O to Au-support interface, reaction with CO adsorbed on Au.

Chapter 5. Aims and Objectives

Gold supported catalysts have been reported to be highly active for low temperature CO oxidation with a high dependency on the size of Au nanoparticles and support material (Haruta, 2004a; Hutchings, 2004). As observed in 4.4 the introduction of SO₂ to CO oxidation resulted in the loss of activity of Au/TiO₂ due to SO₂ adsorbing strongly on the O adsorption sites and inhibiting its migration to CO active sites. This preferential adsorption of SO₂ on Au/TiO₂ led to the idea that SO₂ abatement via catalytic reduction over Au-supported catalysts using CO could be done. This was also supported by work done Rodriguez et al.(2002) and Chalom (2009) that showed that Au/TiO₂ was active in the dissociation of SO₂.

On studying the adsorption of SO₂ on Au/TiO₂, it was found that SO₂ dissociates into elemental sulphur via the formation of adsorbed sulphate on the catalyst surface (Rodriguez et al., 2002). It was explained that the presence of Au increases the mobility of O₂ vacancies between the bulk and the surface of the TiO₂ support (Bond, Louis & Thompson, 2006). This increased mobility of the O₂ vacancies is a characteristic that is necessary for the dissociation of SO₂.

5.1 Reducing agent

The majority of research into the catalytic reduction of SO₂ has been done over various supported and unsupported catalysts as shown in Chapter 3 using various reducing agents. Wang et al. (2003) tested three different reducing agents, (ethylene, hydrogen and carbon monoxide) over Fe₂O₃/CeO₂ and showed that carbon monoxide was the better reducing agent. Thus, in this research CO was chosen as the reducing agent as it can be found in flue gas under certain combustion conditions that allow its production.

5.2 Metal Oxide Support

Previous research using supported catalysts found that the support played a very important role in the activity of the catalyst (Wang et al., 2003; Chen et al, 2004). The choice of the supporting metal oxide for Au nanoparticles in the reduction of SO₂ by CO was based mainly on previous studies on either CO oxidation or SO₂ reduction. With respect to CO oxidation, easily reducible metal oxide supports have higher activities due to their ability to absorb and store oxygen (Schubert et al., 2001). Other metal oxides, such as alumina, silica and magnesia, interact poorly with oxygen and therefore are poor oxidation catalysts and used more in dehydration reactions (Reddy, 2006). Thus, a reducible metal oxide and a non-reducible metal oxide were chosen for comparison of support effects in this study. The acidity of the supports also plays an important role in their ability to adsorb molecules. Acidic metal oxides do not adsorb acidic molecules such as SO₂ to form sulphites and CO₂ to form carbonates, and vice versa.

TiO₂ (reducible) and Al₂O₃ (non-reducible) are commonly used in the hydrodesulphurization process via the Claus reaction (Equation 3.5) (Rase, 2000) and are both popular choices as supports (Khalafalla & Haas, 1972; Haas & Khalafalla, 1973a; Paik & Chung, 1995; Paik et al., 1997; Zhuang et al., 2000; Wang et al., 2003; Chen et al., 2004; Zhao et al., 2007; Li et al., 2008). TiO₂ and Al₂O₃ supports also differ in their acid properties with the former reported as amphoteric while the acidity of alumina is dependent on its phase. The main phases of alumina are: α-Al₂O₃, with low Lewis acidity, low activity in oxidation reactions, it is thermally stable and mechanically strong; and γ-Al₂O₃ which is a strong Lewis acid with a high surface area (Busca, 2006). Thus, γ-Al₂O₃ is the main phase of alumina used as either a catalyst or a support material. The three main phases of TiO₂ are rutile, anatase and brookite which differ in their crystalline structures. A mixture of anatase and rutile are the main phases involved in the applications of TiO₂ such as heterogeneous catalysis and photo

catalysis (Diebold, 2003). This is due to the more catalytically active phase, anatase, being thermodynamically unstable thus the difficulty in synthesising the pure phase (Hanaor & Sorrell, 2010).

In this work, the amphoteric TiO_2 and acidic $\gamma\text{-Al}_2\text{O}_3$ supports were compared to a basic metal oxide support, viz. ZnO . ZnO is a transition metal oxide that is a strong Lewis base (Busca, 2006) and is commonly used as a photo catalyst, as is titania (Yu et al., 2013). Due to its basicity, it was expected that ZnO will adsorb the acidic SO_2 molecules used in this study. The addition of Au nanoparticles to these metal oxides results in highly active catalysts for CO oxidation as shown in Chapter 4. Thus, Au/TiO_2 , Au/ZnO and $\text{Au/Al}_2\text{O}_3$ were donated by Project AuTEK in Mintek and used in the reduction of SO_2 by CO. The catalysts used in this study were prepared using the deposition-precipitation method with an Au loading of 1 wt% as explained further in Chapter 6. This was done to ensure small Au nanoparticles with high dispersion on the surface of the metal oxide support since smaller clusters have high activities (Haruta et al., 1989).

5.3 Effect of Feed Ratio

The ratio of SO_2 to CO in flue gas streams is highly dependent on the fuel combusted and the combustion conditions. The concentration of sulphur in the fuel determines the amount of SO_2 present in the flue gas as explained in Chapter 1. On the other hand, the concentration of CO in the flue gas is usually kept at a minimum to increase the energy output of the combustor, however certain factors can lead to high CO levels (Masters, 1998). The stricter monitoring of industrial emissions also encourages low concentrations of CO in flue gas streams. Consequently, the concentrations of SO_2 and CO in the flue gas stream vary and the addition of CO to the flue gas may be necessary to achieve catalytic reduction

of SO₂. A feed ratio of CO to SO₂ of 0.12 was derived from the following flue gas composition; 12.5-12.8% CO₂, 6.2% H₂O, 4.4% O₂, 50 ppm CO, 420 ppm NO_x, 420 ppm SO₂, and 76-77% N₂ (Xu et al., 2003). In general, the research into the catalytic reduction of SO₂ by CO has utilised synthetic gas mixtures with fixed feed ratios in order to determine the ideal conditions for high reduction rates of SO₂ and selectivity to S. Some researchers concluded that the optimum feed ratio was the stoichiometric feed ratio of 2:1 (Ma et al., 1997; Zhuang et al., 2000; Wang et al., 2006; Han et al., 2008). As stated in Section 3.4.2, the optimum feed ratio varied depending on the reaction conditions such as catalyst used (reaction mechanism) reaction temperature and reactant feed concentrations. Therefore, in this study, the feed ratio was varied to determine the optimum ratio and also compared to the CO:SO₂ ratio in the flue gas.

5.4 Reaction Products

The activity of Au/TiO₂ on the reduction of SO₂ by CO was studied by Chalom (2009) who showed that the reactants, SO₂ and CO, were consumed yet did not confirm the absence of COS in the product stream as the infra-red analyser which was used cannot detect COS. With the possibility of the formation of the reaction intermediate COS (Haas & Khalafalla, 1973a), which is more toxic than SO₂, it was necessary to confirm the identity of the products of this reaction. The dependency of the catalysis on the support was also not explored by Chalom (2009). Understanding the nature and structure of the support may assist in identifying the factors required in the reduction of SO₂ using CO.

The expected reaction products of the reduction of SO₂ by CO are elemental sulphur and carbon monoxide as shown in Reaction 3.9 in Chapter 3. However, other reaction by-products are possible depending mainly on the reduction

mechanism followed. Two main reaction mechanisms have been proposed, namely: the COS reaction intermediate mechanism and the redox reaction mechanism (Haas & Khalafalla, 1973a; Ma et al., 1996; Ma et al., 1997; Han et al., 2008). The former reaction mechanism proceeds via the following steps (Equations 5.1) where the metal sulphide species (Cat [S]) is generated from the product elemental S reacting with either the supported metal or metal oxide (Ma et al., 1996; Han et al., 2008)



Where Cat [S] is the sulphided catalyst.

The reaction intermediate COS can also be produced by a side reaction between CO and S or Reaction 3.10 (section 3.4) and in turn reduces SO₂ via Reaction R.1b which occurs on the Lewis and Brönsted acid sites of the catalyst (Haas & Khalafalla, 1973b; Han, Park, Yoon & Lee, 2008). Overall, the reactions rates of Reactions 5.1a and 5.1b determine the amount of COS by-product generated and thus the selectivity to the production of S.

The redox mechanism typically results in very little or no generation of COS and occurs over a redox metal oxide (Paik et al., 1997; Han et al., 2008). Reactions 5.2 show the steps followed in the reduction of SO₂ by CO via the redox mechanism (Ma et al., 1996).



Where Cat [O] is metal oxide,

Cat [] is the reduced metal oxide or oxygen vacancy

And ads refers to adsorbed species

Therefore, the reaction mechanism, which is in turn dependant on the catalyst employed and the characteristics of the reaction, determines the reaction products of the reduction of SO₂ by CO.

Chapter 6: Research Methods

6.1 Preparation of the Catalysts

The gold supported catalysts used for the reduction of SO₂ by CO in the study were synthesised via the deposition-precipitation method. This method of preparation involves loading Au on the metal oxide support from tetrachloroauric acid. The pH of the solution during loading is kept at 7.5 by balancing the addition of an acid and basic solution. Pre-treatment of the washed catalysts was then done in a nitrogen/hydrogen environment at 110 °C for 30 minutes in order to reduce the Au oxidation to Au⁰. The Au loading can be calculated to a specific value however it depends highly on the conditions of the loading process. Due to this matter, the reproducibility of these catalysts is low; therefore industrially manufactured catalysts were used. These were donated by Project AuTEK in the Advanced Materials Division in Mintek, Randburg, South Africa.

The metal oxide supports were also tested for their catalytic activity on the reduction of SO₂ to compare with the Au loaded supports. Table 6.1 shows the catalysts used and the analysis provided with them.

Table 6.1: Catalysts information

Catalyst Name	Catalyst Type	Au loading (wt %)	Support Chemical Analysis
AUROLite TM BC8	Au/TiO ₂	1	TiO ₂ > 99 wt% Anatase >70 wt%
AUROLite TM BC2	Au/ZnO	1	ZnO > 90 wt%
AUROLite TM BC8	Au/Al ₂ O ₃	0.9	Al ₂ O ₃ > 99 wt%

6.2 Activity Measurements

6.2.1 Gas Mixtures and Feed Compositions

A synthetic gas mixture was used to investigate the activity of the catalyst specified. These gases were supplied by AFROX with the following certified compositions:

- 1 vol% (10 000 ppm) SO₂ in He
- 2 vol% (20 000 ppm) CO in He
- Pure He
- 1 vol% (10 000 ppm) O₂ in He

Preliminary studies were carried out to determine the effect of SO₂ concentration. Therefore, the feed ratio was adjusted by varying both SO₂ and CO feed compositions as shown in Table 6.2.

Table 6.2: SO₂ and CO feed ratios and concentrations

Feed Ratio	Feed Concentration (ppm)	
	SO ₂	CO
2:1	5 000	10 000
4:1	3 333	13 333
6:1	2 500	15 000
8:1	2 000	16 000

The feed concentration of SO₂ into the reactor was later maintained at 2 000 ppm with the CO feed concentration varied accordingly to increase the CO:SO₂ feed ratio from 0.5:1 to 4:1 to investigate the activity of the catalyst when CO was limiting to when it is in excess. The concentration of SO₂ was determined from preliminary studies based on Table 6.2 as shown in Appendix C. The flow rates

required to obtain each feed ratio were calculated from the cylinder concentration while maintaining a gas-hourly-space-velocity (GHSV) of $3\,600 \text{ mL.g}_{\text{cat}}^{-1}.\text{h}^{-1}$, these are shown in Table 6.3.

Table 6.3: Feed gas mixture ratios and concentrations

Feed Ratio	Feed Concentration (ppm)	
	SO ₂	CO
0.5:1	2 000	1 000
1:1	2 000	2 000
2:1	2 000	4 000
3:1	2 000	6 000

To investigate the effect of oxygen on the catalysts activity, oxygen was added to the reactor feed gas mixture to give a CO:O₂ feed ratio of 2:1 with changing CO:SO₂. Helium was added to keep the total volumetric flow rate at 60 mL.min^{-1} at all times, by adjusting the flow rates on the mass flow controllers.

6.2.2 Reactor system

Figure 6.1 shows an illustration of the reactor system used to test the activity of Au-supported catalysts for the reduction of SO₂ over CO. The reactor system consists of four Alicat MC Series mass flow controllers supplied by Action Instruments SA CC (AISA) based in Braamfontein, Johannesburg, South Africa, that regulate the mass/volumetric flow rate of each gas from an Afrox gas cylinder filled with one of the four gases specified. The mixed gases then flowed to a vertically mounted 10 mm ID glass reactor fitted with a glass frit 15 mm from the top of the reactor. This 15 mm distance was determined from optimising the catalyst bed to be situated at the hottest part of the heating coil and jacket around the reactor. A thermostat inserted into the reactor-heating jacket was used to

regulate the temperature of the reactor. The exit gases from the reactor flow through a sulphur trap that condensed the sulphur produced before entering a Hewlett Packard® gas chromatogram (GC) through a 12 m long and 0.069 in ID sample loop. The GC was equipped with a 2 m long 1/8 inch diameter Carboxen® packed column (Sigma-Aldrich) and a thermal conductivity detector (TCD). The exit gases then pass through a bubble meter before being sent to a fume hood after passing through a water trap that prevented the back diffusion of air into the system. This occurs due to the extremely low concentrations used in this work. The bubble meter was used to confirm the total gas volumetric flow rate.

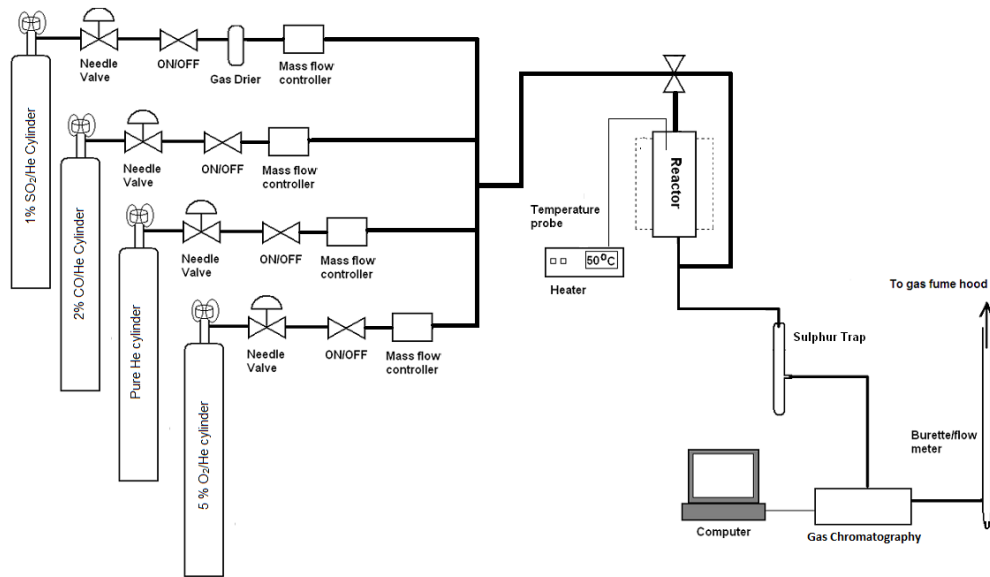


Figure 6.1: Illustration of experimental set up

6.3 On-line Analysis

The calibration of the GC had to be carried out with known concentrations of gas to determine the retention time for each specific gas. In the GC oven, the

Carboxen® column separated the gases using He as a carrier gas while the TCD detector identified the gas according to their thermal conductivity in reference to He gas. The TCD detector was kept at a constant temperature of 200 °C. The signal from the detector was sent to an online computer equipped with Clarity™ software that displayed and determined the retention time, height and area under each peak corresponding to a quantity of gas analysed. This implies that when there was no gas other than He passing through, a flat baseline was displayed since He gas was the reference gas for the TCD detector.

Each gas was analysed individually first from room temperature to 200 °C in the GC oven to determine the retention time and to calibrate the peak area relative to the corresponding known concentration. With the individual analysis of SO₂ and CO, it was found that both cylinders contained a small amount of air, which could not be avoided by the manufacturer, Afrox. The individual cylinder calibrations were done without any temperature ramping.

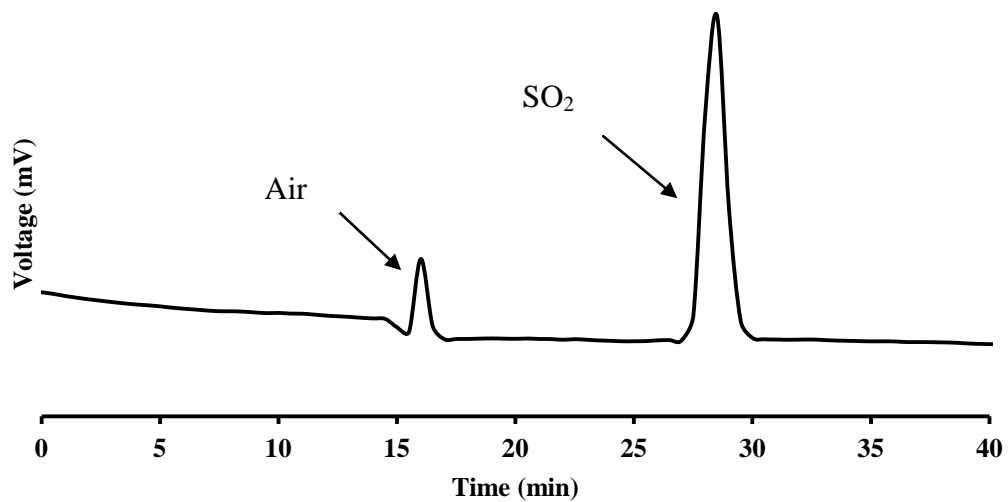


Figure 6.2: GC peaks of air and SO₂ at an oven temperature of 200 °C

Figure 6.2 and Figure 6.3 show the GC peaks of 1 % SO₂ and 2 % CO respectively, with the previously mentioned air peaks. The SO₂ peak was only observed when the GC oven temperature was at 200 °C. At this temperature, CO and air were not separated and both gases were observed as one peak. To obtain a full separation of CO and air, the GC oven had to be operated at room temperature.

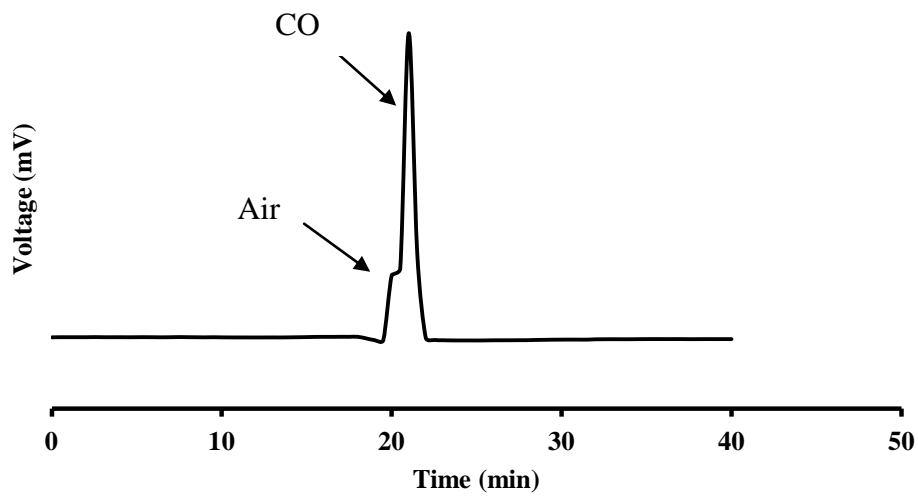


Figure 6.3: GC peaks of air and CO with the oven at room temperature

Figure 6.4 shows the peaks for both CO and SO₂ calibrated simultaneously. To obtain a full separation, the CO gas and air have to be separated with the GC oven at room temperature followed by ramping the temperature to 200 °C in 20 min where the SO₂ peak appeared after 6 min once the oven was at 200 °C.

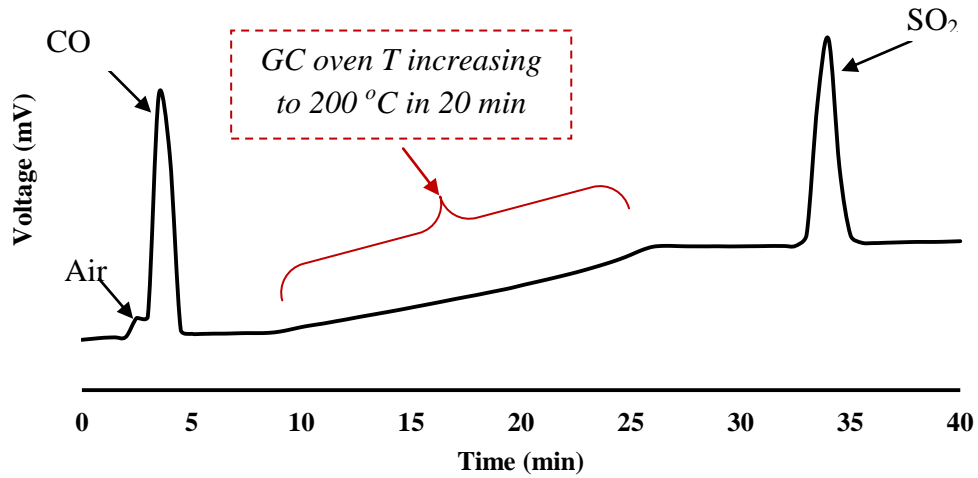


Figure 6.4: GC peaks of air, CO and SO₂ fully separated using a temperature programmed GC

6.4 Interpretation of Data

The mean of the calibrated peaks were used as a baseline that determines the amount of reactants consumed by the reaction and the products generated (Appendix A2). Each peak area corresponds to a volumetric concentration of that particular gas in the sample loop and can then be related to molar flow rate via the conversion factor in Equation 6.1, determined by assuming ideal gas behaviour (Appendix A3).

$$\frac{\dot{n}}{V} = 3.53 \times 10^{-5} \text{ mol. cm}^{-3} \quad (6.1)$$

Where \dot{n} is the molar flow rate and V is the volumetric flow rate.

The percentage conversion of each gas was calculated via Equation 6.2 where the moles of gas reacted was determined by the difference between moles of gas into the reactor and moles of gas exiting the reactor.

$$\% \text{ Conversion} = \frac{\text{moles of gas reacted}}{\text{moles of gas in}} \times 100 \quad (6.2)$$

Selectivity is defined as the fraction of a particular reactant that is converted into a desired product. With respect to sulphur, it is expressed as:

$$\% \text{ Selectivity to S} = \frac{\text{Amount of S produced (mol)}}{\text{Amount of SO}_2 \text{ reacted mol}} \times 100 \quad (6.3)$$

Equation 6.3 holds if and only if all the sulphur produced is from the reduction of SO₂ and no other sulphur containing reactants.

The stoichiometric Equation 6.4 can then be used to complete the mass balance for the feed and products of the reactor for each reaction occurring in the reactor.

$$\frac{\text{Amount of reactant consumed } i}{v_i} = \frac{\text{Amount of product generated } j}{v_j} \quad (6.4)$$

Where v is the stoichiometric coefficient of each reaction reactant i and reaction product j .

6.5 Characterization Techniques

6.5.1 X-ray Diffraction (XRD) Analysis

The XRD patterns of the catalysts were analysed to obtain information on their composition and structure. Each catalyst was ground for the preparation of

samples for powder X-ray diffraction (PXRD). PXRD analysis of the catalysts was done on the Bruker D2 phaser. This bench top type diffractometer was operated at 30 kV and at a current of 10 mA with a copper X-ray source. The resulting patterns were analysed and identified using the Diffrac_{plus} Eva software and a powder diffraction file (PDF) database that uses a search-match algorithm.

6.5.2 Brunauer-Emmett-Teller (BET) Surface Area Analysis

The surface area and pore diameters of the catalysts were determined by BET surface area measurements. The catalyst samples were degassed in a flow of nitrogen at 120 °C prior to analysis in order to remove impurities such as moisture. After 4 hours, the sample was cooled to room temperature before the surface area analysis was done. In the analysis pot, the sample was exposed to liquid nitrogen and from the amount of nitrogen adsorbed, the surface area and pore volume could be determined.

6.5.3 X-ray Photoelectron Spectroscopy (XPS)

XPS analysis of one sample of Au/TiO₂ was carried out at the National Metrology Institute of South Africa and for the other samples at the University of the Free State in Bloemfontein, South Africa. XPS analysis was necessary to analyse the atomic surface of both fresh and spent catalysts. This was done using a PHI 500 Versaprobe scanning ESCA microprobe system. The XPS surveys and high resolution spectra were done with a 100 µm, 25 W, 15 kV Al monochromatic X-ray beam. The sputtering was done with an argon ion gun (2 kV, 2 µA, 1×1 mm raster) at a sputter rate of 17 nm.min⁻¹.

6.5.4 Transmission Electron Microscopy (TEM)

TEM micrographs of the catalysts were used to determine the particle size and particle dispersion of the Au nanoparticles on the supporting metal oxides. A Tecnai Spirit Transmission Electron Microscope was used at 120 kV to analyse gold supported catalyst samples loaded onto a copper grid. This technique was done at the Electron Microscopy Unit at the University of the Witwatersrand, Johannesburg. A JEOL 2010 was used in the HRTEM analysis of each sample loaded on a carbon coated copper grid.

Chapter 7. Characterization and Support Effects

7.1 Catalyst Characterization

7.1.1 Surface Area Analysis

The surface area and pore diameter of each of the three catalysts used was determined by BET surface area analysis and the results are shown in Table 7.1 below.

Table 7.1: BET surface area and pore volume

Sample name	Analysed Au Loading (wt%)	BET surface area (m ² /g)	Pore volume (cm ³ /g)
Au/ZnO	1	38	0.23
Au/TiO ₂	1	45	0.35
Au/Al ₂ O ₃	0.9	224	0.61

Au/Al₂O₃ has a surface area approximately five times larger than for Au/ZnO and Au/TiO₂ and a correspondingly higher pore volume. The low Au loading of 1 % at these surface areas would still result in the highly dispersed clusters over the metal oxide surface.

7.1.2 X-Ray Diffraction (XRD) Patterns

The XRD patterns for Au/Al₂O₃, Au/ZnO and Au/TiO₂ are shown in Figure 7.1, Figure 7.2 and Figure 7.3, respectively. The patterns were analysed and the

Chapter Seven: Characterization and Support Effects

sample compounds were identified using Diffrac_{plus} Eva software together with a powder diffraction file (PDF) database. The presence of Au on the supports is not observed in the XRD patterns due to the loading being lower than 5 %.

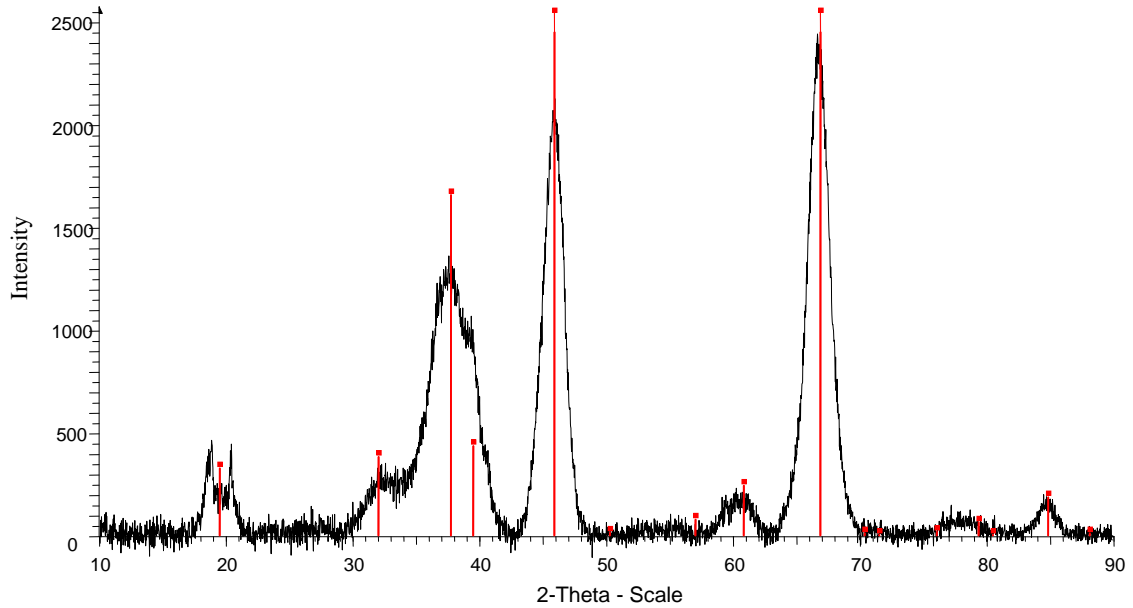


Figure 7.1: XRD pattern of 1% Au/Al₂O₃

The XRD pattern in Figure 7.1 was identified as γ -Al₂O₃ with peaks at the following 2θ values of 19.9, 32.1, 37.8, 39.5, 45.9, 60.8 and 69.9 for the planes of (111), (220), (311), (222), (400), (511) and (440) respectively (Lian et al., 2010).

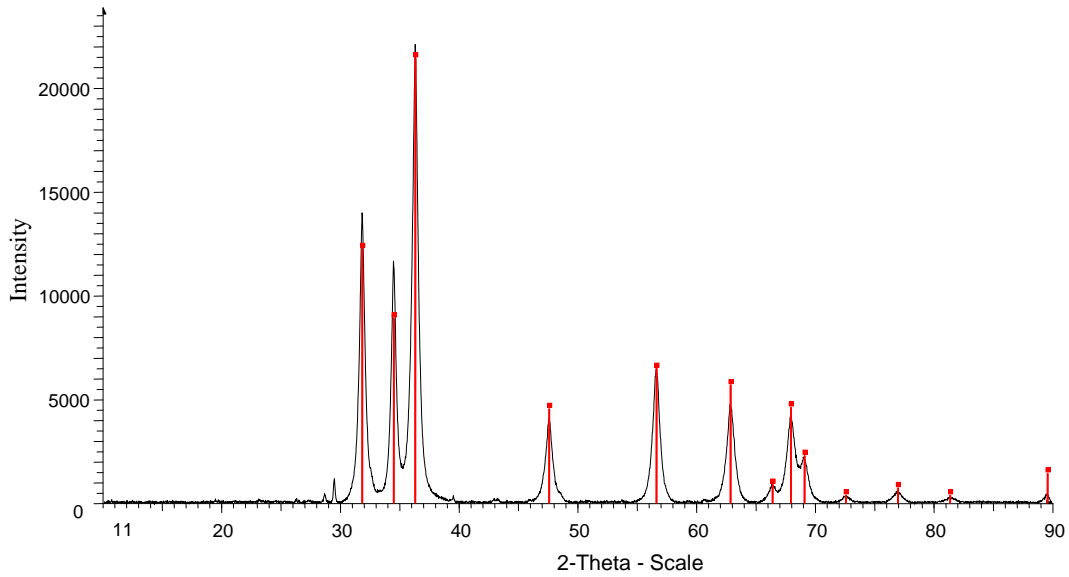


Figure 7.2: XRD pattern of fresh ZnO

The Au/ZnO profile peaks in Figure 7.2 also correlate with ZnO peaks generated by XPOW software (Downs et al., 1993) with major peaks at the 2θ angles of 31.75, 34.42, 36.26, 47.51, 56.54, 62.82, 66.30, 67.88, 69.01, 72.53, 76.88, 81.33 and 89.52 for the planes (100), (002), (101), (102), (110), (103), (200), (112), (201), (004), (202), (104) and (203) respectively.

The analysis of the Au/TiO₂ pattern in Figure 7.3 shows that TiO₂ is present in both the anatase and rutile phases. The anatase phase peaks (indicated as red) correlate to the XPOW software generated peaks that occur at the 2θ angles of 25.23, 36.86, 37.72, 38.46, 47.89, 53.77, 54.89, 61.92, 62.51, 68.59, 70.05, 74.83, 75.78, 82.41 and 82.87 for the planes (101), (103), (004), (112), (200), (105), (211), (213), (204), (116), (220), (215), (301), (224) and (312) respectively.

The rutile phase peaks (indicated as green) correlate to the XPOW generated peaks that occur at the 2θ angles of 27.45, 36.10, 39.21, 41.26, 44.06, 54.35, 56.65, 62.79, 64.08, 69.04, 72.45, 76.58, 79.87, 82.38, 84.29, 87.53 and 89.60 for

the planes of (110), (101), (200), (111), (210), (211), (220), (002), (301), (112), (311), (202), (212), (321), (400), (410) and (222) respectively.

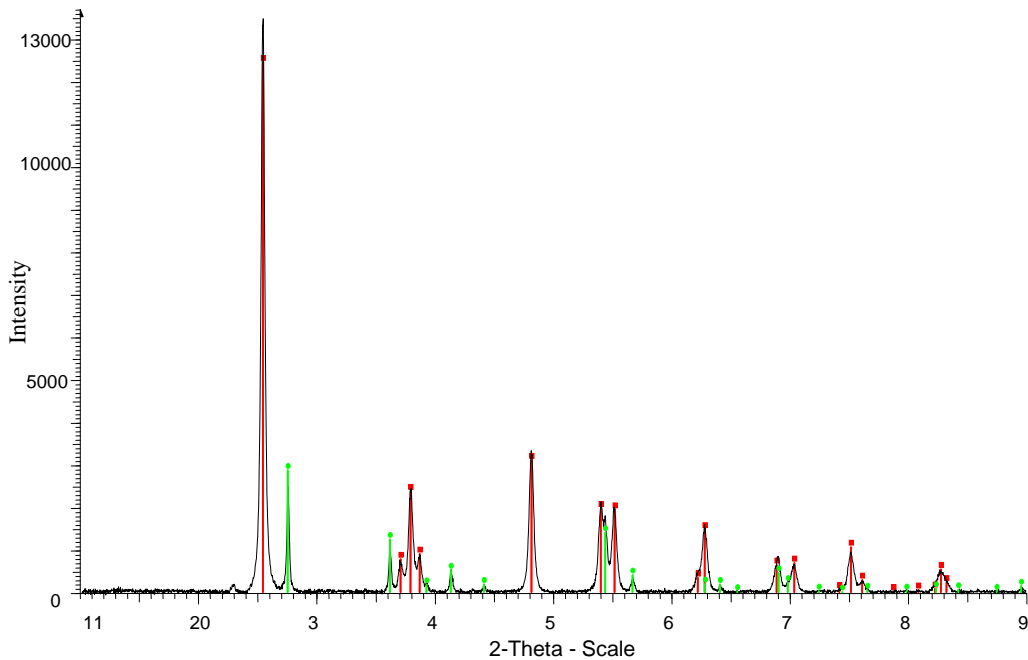


Figure 7.3: XRD patterns of fresh 1% Au/TiO₂ displaying the peaks for the anatase phase (red) and rutile phase (green)

7.1.3 Transmission Electron Microscopy (TEM)

The dispersion and particle size of the Au nanoparticles can be analysed from the TEM images as shown in Figures 7.4 to 7.6 and in Appendix B1 at a different magnification. The small dark spots are the Au nanoparticles supported on the larger grey metal oxide particles. The large dark spots in this image were due to support particles arranged on top of each other.

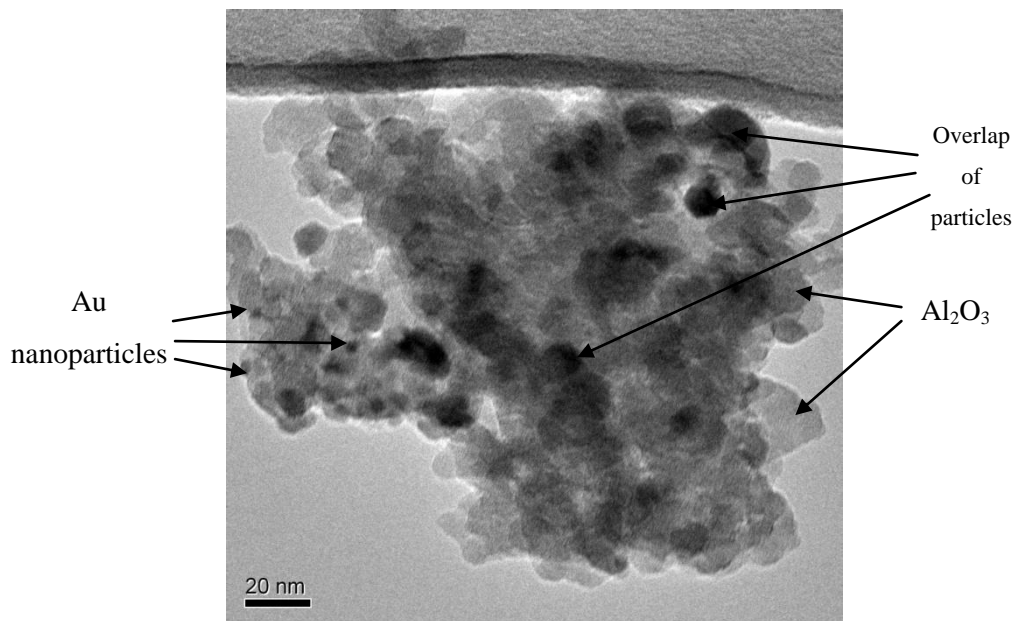


Figure 7.4: TEM image of Au/Al₂O₃

The Au nanoparticles on the Au/Al₂O₃ were not easily distinguishable at this resolution as compared to the images of Au/ZnO and Au/TiO₂. As seen from the image, there was an overlap of the catalyst particles resulting in the large dark spots shown in Figure 7.4. It was suspected that the thickness of the sample affected the visibility of the Au nanoparticles as the electron beam could not penetrate the sample.

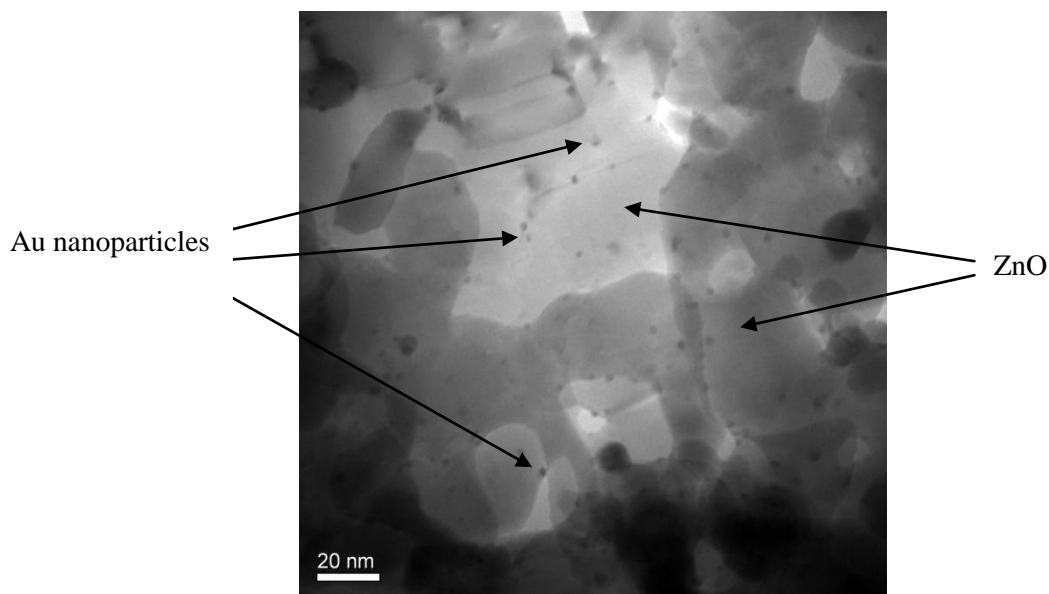


Figure 7.5: TEM image of Au/ZnO

The size of 105 Au clusters was measured using ImageJ software that generated a table of the measured particles, the mean and the standard deviation. The particles size distribution of this catalyst was then determined and plotted using Microsoft Excel. The Pivot table is shown in Appendix B1.

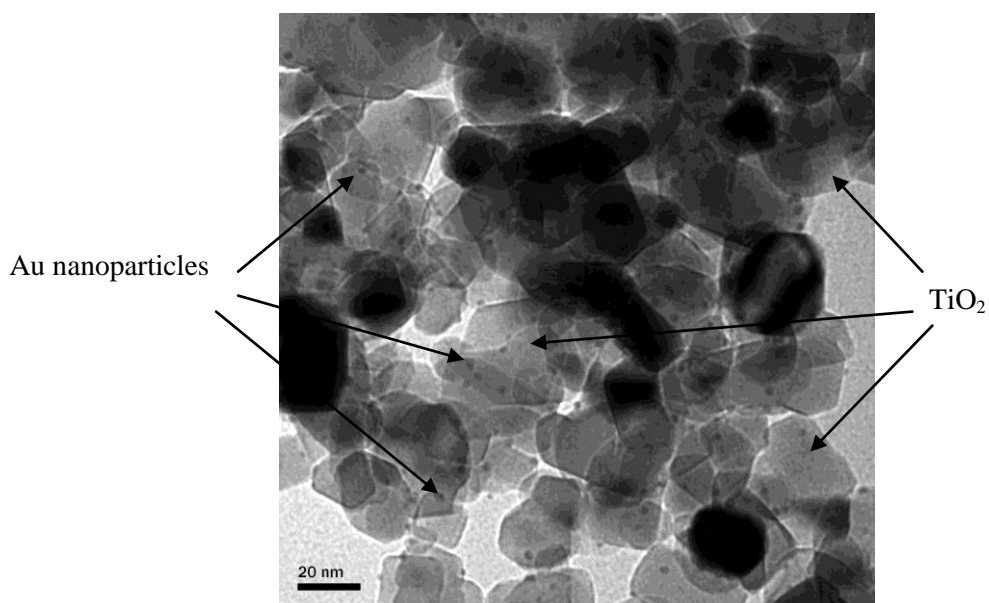


Figure 7.6: TEM image of Au/TiO₂

Chapter Seven: Characterization and Support Effects

For Au/TiO₂, the diameter of 100 Au clusters was measured using ImageJ software. The mean and standard deviation of the particles was used to determine the particle size distribution. The pivot table generated using this data in Microsoft Excel is presented in Appendix B1.

These TEM images show highly dispersed Au nanoparticles on larger support particles. The average particle size for Au/TiO₂ and Au/ZnO was determined to be 1.9 nm for 100 and 105 particles respectively. The particles size distribution curves are shown in Figure 7.7 and Figure 7.8. The number of Au nanoparticles on Au/Al₂O₃, which is the sample size, was too small to carry out an analysis on the particle size distribution. Therefore, an analysis of the small sample would not be a true representation of the particle size distribution of the catalyst.

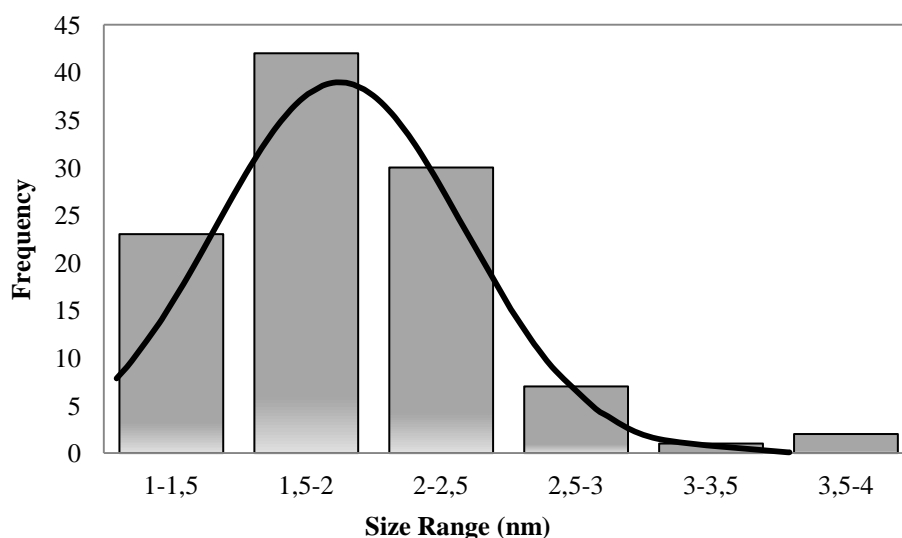


Figure 7.7: Au cluster size distribution for Au/ZnO

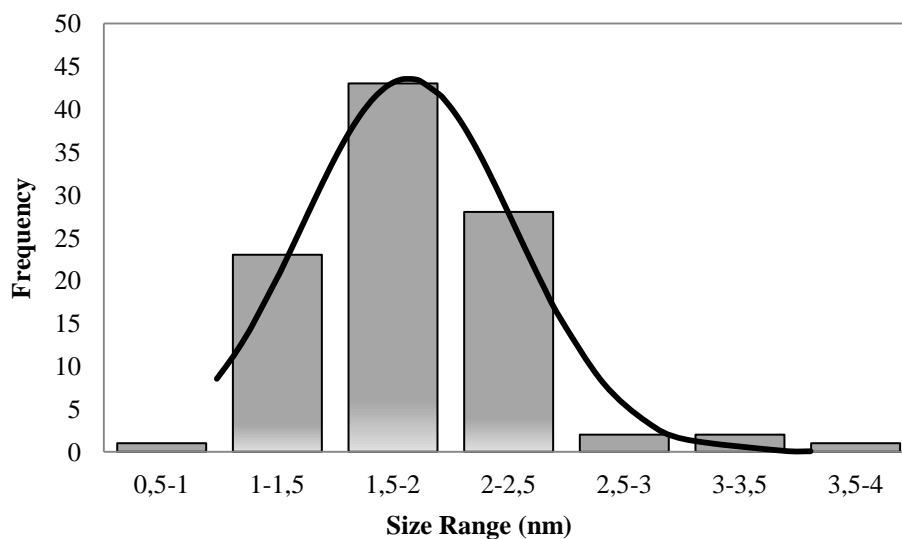


Figure 7.8: Au cluster size distribution for Au/TiO₂

7.2 Effect of Au nanoparticles and Reaction Temperature

The effect of catalytic Au nanoparticles was investigated by comparing the activity of the Au supported catalyst to the activity of the equivalent metal oxide support. The reduction of SO₂ by CO was done at a GHSV of 3 600 mL.g_{cat}⁻¹.h⁻¹, an SO₂ feed concentration of 2 000 ppm, a CO:SO₂ feed ratio of 3.75:1 with increasing reaction temperature from 50 to 300 °C over 51 hours on-stream. The percentage SO₂ conversion is calculated as shown in Equation 6.2, Section 6.4.

7.2.1 Activity of Au/Al₂O₃ and Al₂O₃

The conversion of SO₂ over Au/Al₂O₃ with a BET surface area of 224 m².g⁻¹ and Al₂O₃ is shown in Figure 7.9. At start up there was an initial high conversion of SO₂, approximately 95 % over Au/Al₂O₃. This was followed by a drastic drop in activity to an average of 1.4 %, with a slight increase every time the reactor temperature was increased. The activity of the supporting Al₂O₃ was much lower than that of Au/Al₂O₃. However the same trend in conversion was observed with a

high initial conversion of 10.4 %, followed by very low conversion. When the reactor temperature increases, there appears to be very high SO₂ desorption rates from the catalyst surface as shown by the negative conversion percentages. This was followed by some reaction occurring on the surface before SO₂ adsorbed on the surface again which became saturated.

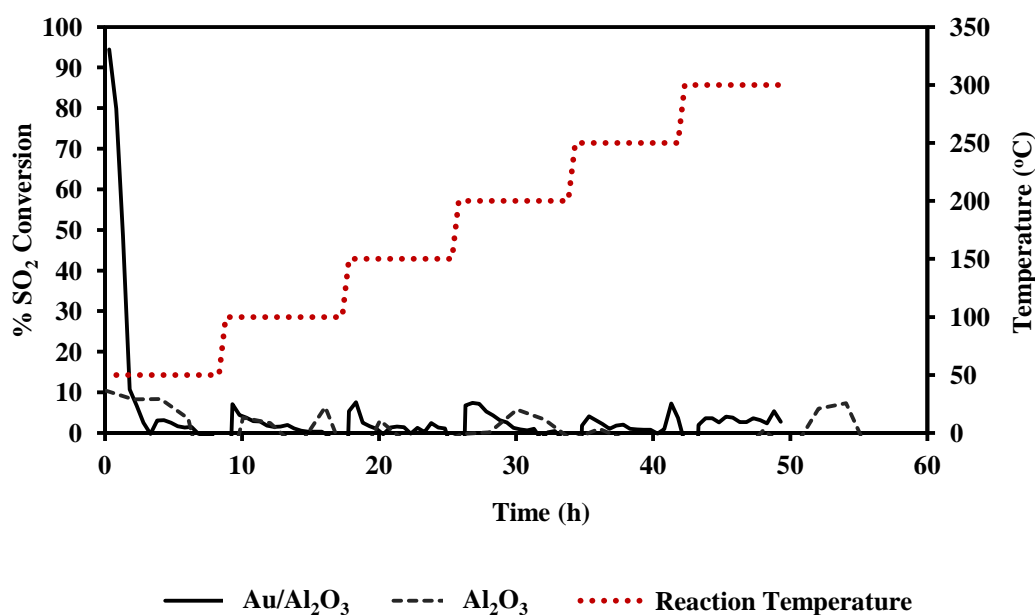


Figure 7.9: Activity test for Au/Al₂O₃ and Al₂O₃ for SO₂ reduction as temperature was increased in 50 °C steps at 8 h intervals at a GHSV of 3 600 mL.g_{cat}⁻¹.h⁻¹

Although γ -Al₂O₃ is the most catalytically active phase amongst the phases of alumina (Fierro, 2006), it is non-reducible. Studies into the adsorption of SO₂ by Al₂O₃ found that it is highly dependent on temperature; above 80 °C some of the SO₂ adsorbed irreversibly (Fellner et al., 2006). The adsorbed species on γ -Al₂O₃ were found to be both molecular and dissociated SO₂ (Dalla Lana, Karge & George, 1993). Thus, the behaviour of Al₂O₃ in the reduction of SO₂ was minimal with some desorption and reaction each time the reaction temperature was increased.

7.2.2 Activity of Au/ZnO and ZnO

Figure 7.10 shows the detailed conversion of SO₂ with time and temperature over Au/ZnO with a BET surface area of 38 m².g⁻¹ and the support ZnO. Upon start up, there was an initial conversion of SO₂ of 11 % which then decreased with time at 50 °C. The average conversion at each temperature remained relatively low, less than 4 %, except at the points when the reaction temperature increased. This shows that at start up, there was a high adsorption of SO₂ on the fresh catalyst surface resulting in less SO₂ molecules exiting the reactor. This was followed by a complete coverage of the surface resulting in very little to no reaction occurring on the surface. Once the reaction temperature increased, some SO₂ desorbed, cleaning the surface and allowing for further adsorption to occur before the surface was covered when the temperature stabilized. Activity tests over the support ZnO show that there was very little to activity over the support.

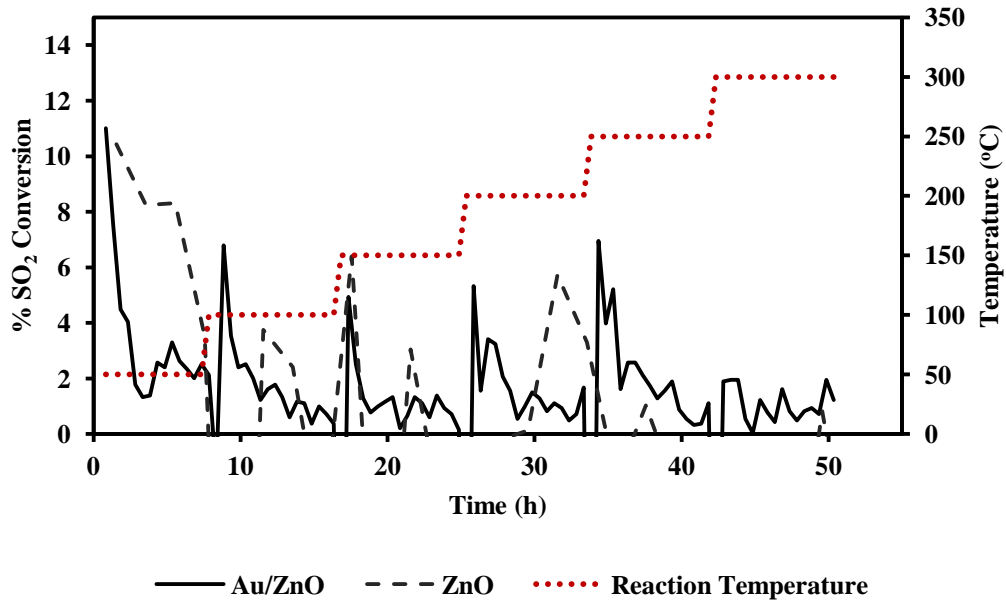


Figure 7.10: Activity test for Au/ZnO and ZnO for SO₂ reduction as temperature was increased in 50 °C steps at 8 h intervals at a GHSV of 3 600 mL.g_{cat}⁻¹.h⁻¹

The HRTEM images of fresh and after-reaction Au/ZnO samples, Figure 7.11, were compared and an amorphous substance was found on the surface of the Au/ZnO after-reaction. The surface was then further analysed by EDX to determine the atomic species on the surface and showed the presence of a sulphur species (Figure 7.12).

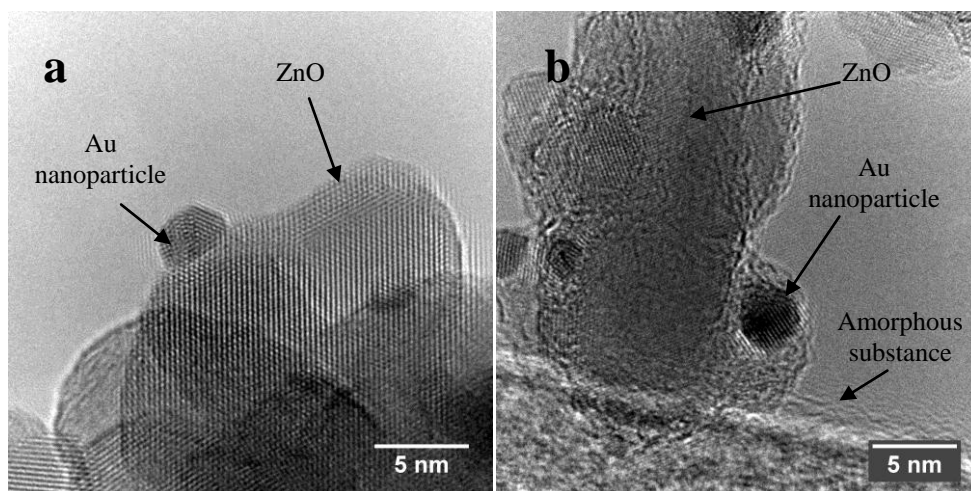


Figure 7.11: HRTEM images of (a) fresh and (b) after-reaction Au/ZnO

The alkaline nature of ZnO was assumed to be the major factor affecting the reactivity of Au/ZnO in the reduction of SO₂ by CO. The strong adsorption of SO₂ on the support surface inhibited the reaction between CO and SO₂ as shown by the low conversions of SO₂. The presence of Au on ZnO only slightly increased its activity.

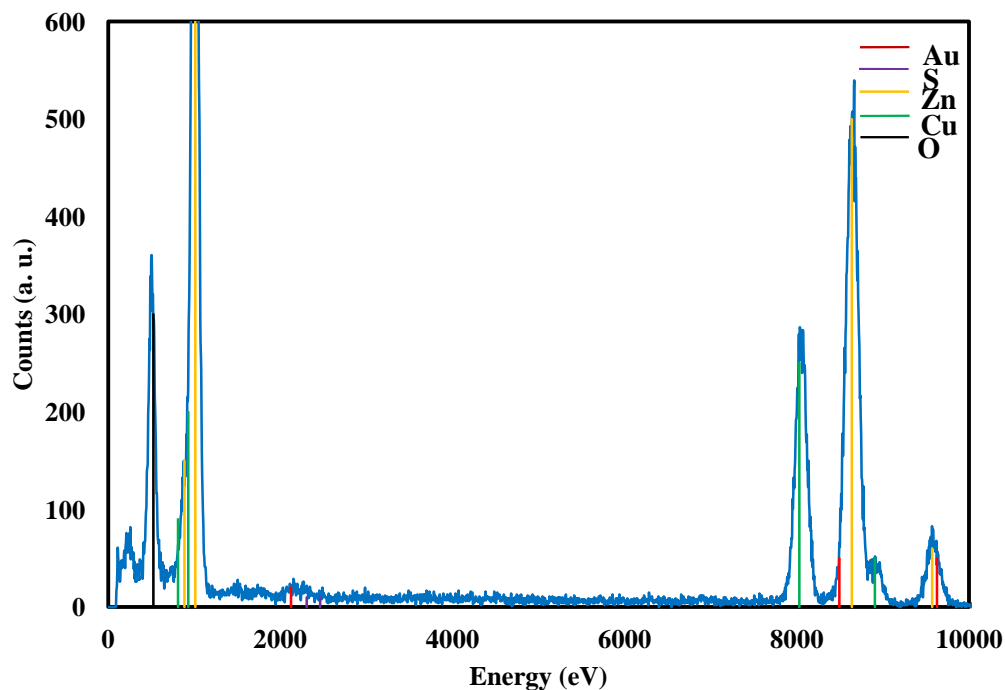


Figure 7.12: EDX analysis of after-reaction Au/ZnO showing presence of S species

7.2.3 Activity of Au/TiO₂ and TiO₂

Figure 7.13 shows the conversion of SO₂ with time and temperature over Au/TiO₂ and TiO₂. The highest conversion over Au/TiO₂ of an average of 86.4 % was achieved at 300 °C. This was followed by a significant decrease at 350 °C to an average of 13.7 %. This deactivation was found to be irreversible when the reaction temperature was lowered back to 300 °C.

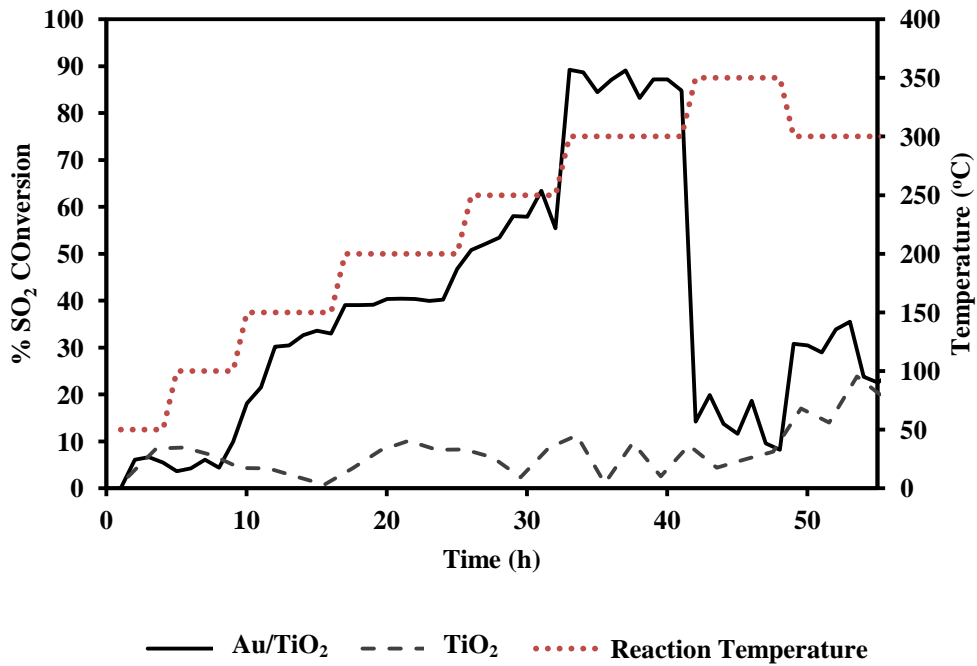


Figure 7.13: Activity test for Au/TiO₂ and TiO₂ for SO₂ reduction as temperature was increased in 50 °C steps at 8 h intervals at a GHSV of 3 600 mL.g_{cat}⁻¹.h⁻¹

Figure 7.14 shows the detailed activity of TiO₂ with increasing reaction temperature. As shown, the conversion of SO₂ increased as the temperature increased to a maximum of 24 %. This showed that Au nanoparticles on TiO₂ played a very important role in the reduction of SO₂ as shown by the low conversion achieved by the support as shown in Figure 7.14. With TiO₂ commonly used in the Claus reaction, there was adsorption of SO₂; however, the SO₂ appears not to dissociate to form elemental sulphur, although SO₄²⁻ is formed (Rodriguez et al., 2002).

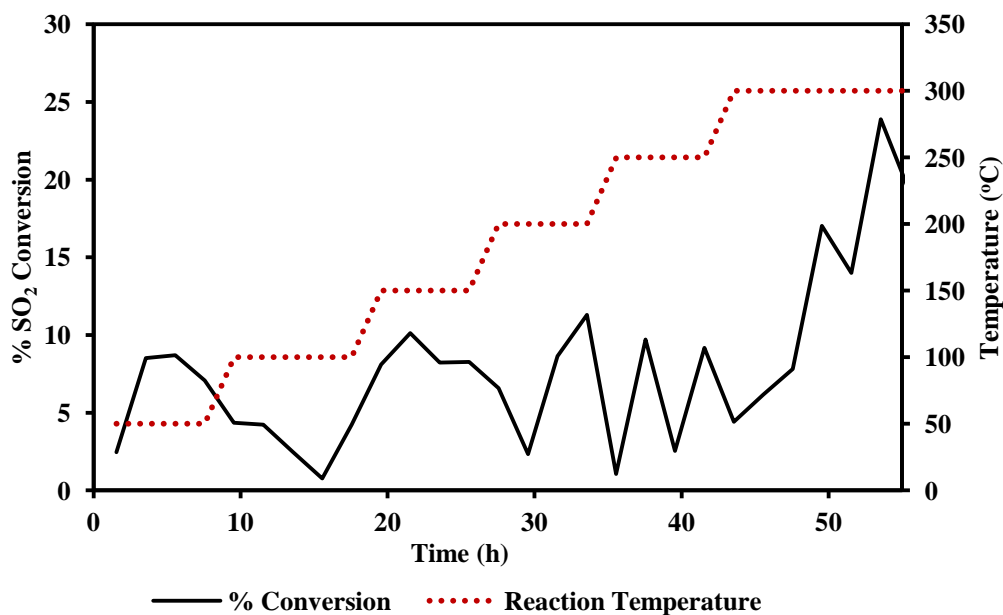


Figure 7.14: Activity test for TiO₂ for SO₂ reduction as temperature is increased in 50 °C steps at 8 h intervals at a GHSV of 3 600 mL.g_{cat}⁻¹.h⁻¹

It was suspected that the deactivation seen at temperatures above 300 °C was due to sintering of the catalyst resulting in larger non-active Au nanoparticles. The deactivation of the Au/TiO₂ could also be attributed to a change in the morphology of the Au cluster from hemispherical to spherical shape as seen in Figure 7.15. This offers less surface area for the adsorption and reaction of CO since it is thought that CO adsorbs and reacts at the interface between the Au particles and the support (Haruta, 2008). SO₂ however, has been reported to adsorb on the TiO₂ in close proximity to the Au nanoparticle (Rodriguez et al., 2002; Diebold, 2003). Similarly with Au/ZnO, there was an amorphous substance on the surface of the catalyst after the reaction. This was identified as a sulphur species by XPS analysis. Further research into the activity of Au/TiO₂ is presented in Chapter 8.

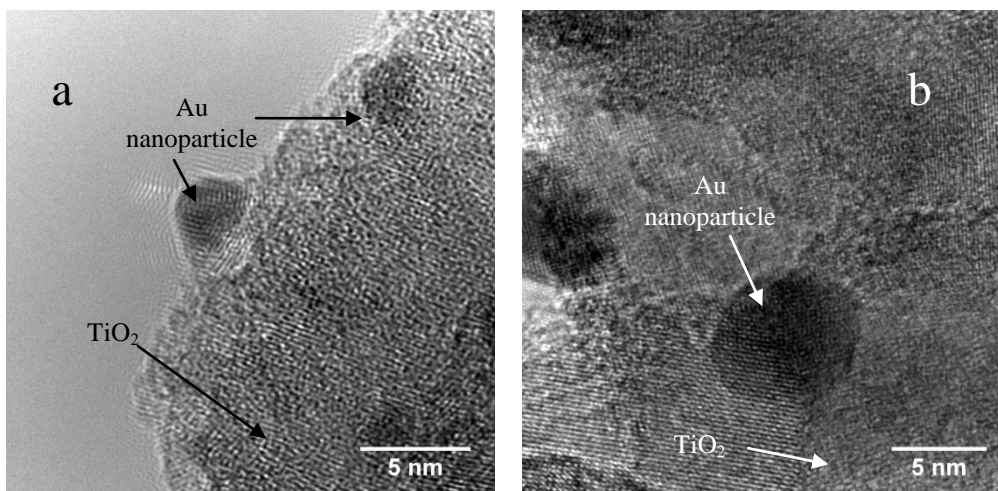


Figure 7.15: HRTEM images of (a) fresh and (b) after-reaction Au/TiO₂

7.3 Conclusion

The supports for Au nanoparticles studied here mainly compared the reducibility and acidity/basicity of the metal oxides. The activities of Au/ZnO and Au/Al₂O₃ were much lower than that of Au/TiO₂ at the reaction temperatures ranging from 50 °C to 300 °C. Au/TiO₂ had the highest activity at 300 °C and this was due to the reducible nature of TiO₂. It was suspected that the redox reaction mechanism (Ma et al., 1996) was followed in the reduction of SO₂, where the oxygen vacancies of the support act as active sites for SO₂ adsorption and subsequent dissociation. The CO molecule is primarily assumed to adsorb on the Au nanoparticle or Au-metal oxide interface, thus explains the low activity observed on Au/ZnO and Au/Al₂O₃ when the reactor temperature increased and SO₂ desorbed. The supporting metal oxides however, also showed lower activity in the reduction of SO₂ by CO. This confirmed that the addition of Au nanoparticles on the metal oxides enhanced their activity. Characterization by TEM and HRTEM showed that the Au nanoparticles were highly dispersed with a particle size less than 2 nm, which is characteristic for highly active Au-supported catalysts.

Chapter Seven: Characterization and Support Effects

Deactivation of Au/TiO₂ above 300 °C was attributed to sintering of the catalyst resulting in agglomeration of Au clusters as shown by HRTEM. It was concluded that Au-supported catalysts are active in the reduction of SO₂ but are highly dependent on the reducibility and acidity/basicity of the metal oxide support.

Chapter 8. Product Selectivity and Feed Ratio Effects

8.1 Analysis of Reaction Products

The reaction products were analysed mainly by the gas chromatography where calibration of the GC determined the retention time for each gas separated by the GC column. It was found that the exit gas stream of the reactor contained unreacted SO₂, unreacted CO, air impurity and product CO₂ with no other gaseous products. This can be seen in the GC peaks illustrated in Figure 8.1.

Elemental sulphur was observed crystallising at the exit point of the reactor into yellow crystals and amber needle-like crystals. These crystals were removed and analysed by XRD and HRTEM with EDS. The XRD peaks obtained are shown in Figure 8.2.

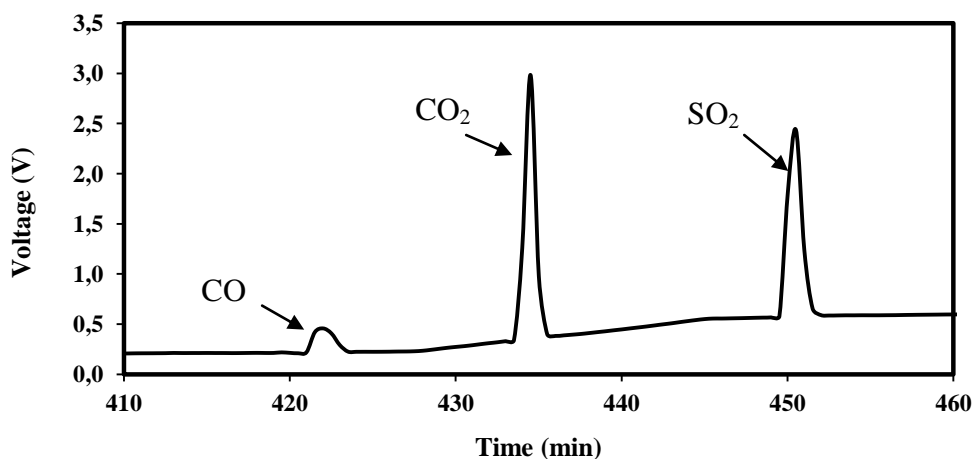


Figure 8.1: GC peaks of separated reactor exit gas stream for CO:SO₂ ratio of 3:1, reaction over Au/TiO₂ at 300 °C

The sulphur produced from this reaction was analysed ex situ using XRD and found to be S₈ as shown in the Figure 8.2. These peaks correlate to the S₈ peaks generated by XPOW software (Downs et al., 1993) shown in Appendix B.

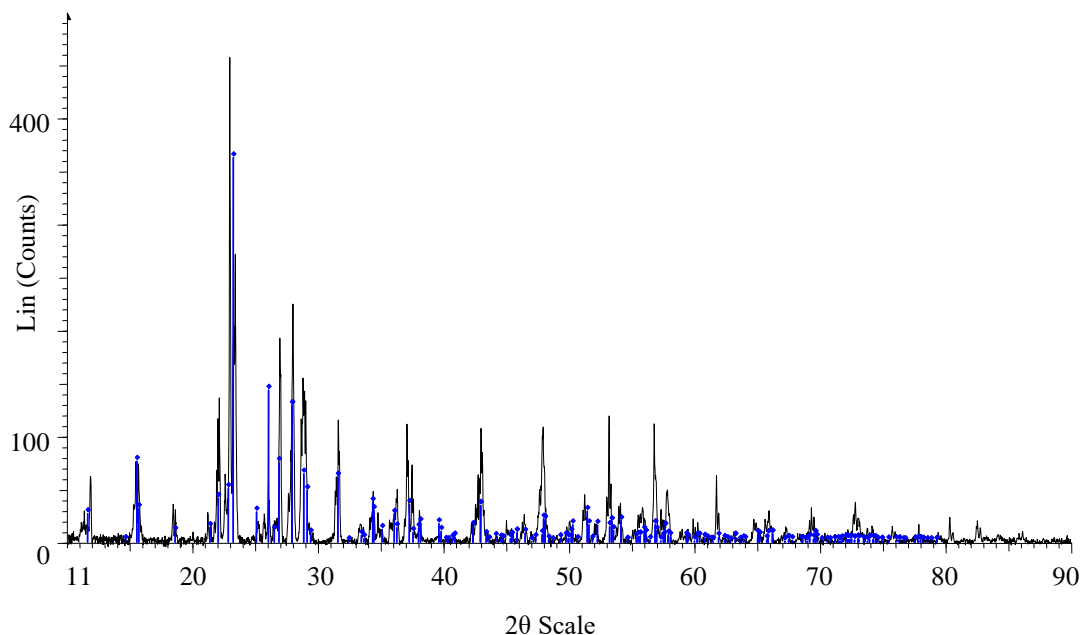


Figure 8.2: XRD peaks of sulphur product identified as S₈

Further analysis of the sulphur product by HRTEM and EDS is shown in Figure 8.3 and Figure 8.4. The EDS peaks also show peaks of Au, Ti and O as some of the catalyst particles mixed with the sulphur during the removal of the sulphur from the reactor. Copper (Cu) also appears in the EDS peaks of the sulphur analysis as it is the material supporting the sample for analysis.

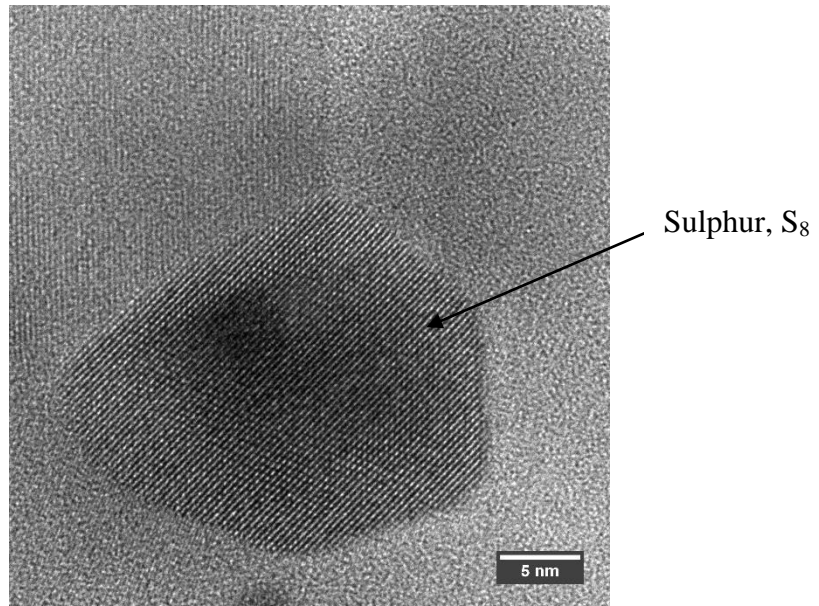


Figure 8.3: HRTEM image of sulphur product

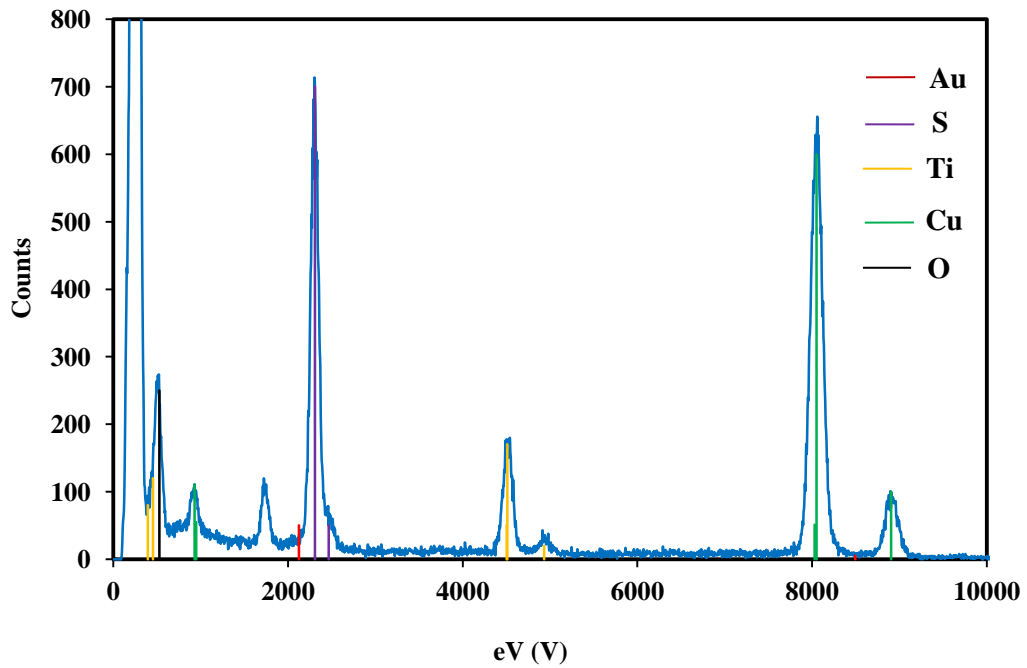


Figure 8.4: EDS peaks of the sulphur product sample

Chapter Eight: Product Selectivity and Feed Ratio Effects

Figure 8.4 shows the different peaks that are unique to each element and are identified as S, Ti, O, Au and Cu as detailed in Table 8.1 (“X-ray Data Booklet”, n.d.).

Table 8.1: EDS peaks from figure 7.4 for S, Ti, O, Au and Cu

Element	Peak Colour in Figure 8.4	Peak Position (eV)
Sulphur (S)	Purple	2306.6
		2307.8
		2464.0
Titanium (Ti)	Yellow	395.3
		452.2
		458.4
		4504.9
		4510.8
4931.8		
Oxygen (O)	Black	524.9
Gold (Au)	Red	2122.9
		8493.9
		9628.0
		9713.3
Copper (Cu)	Green	811.1
		929.7
		949.8
		8027.8
		8049.8
8905.3		

Previous studies have reported the production of a reaction intermediate COS (Haas & Khalafalla, 1973; Liu et al., 1996; et al., 1997; Wang et al., 2006; Han et al., 2008; Han et al., 2008) as explained in Section 3.4. As, stated in the Section 5.2, the production of COS mainly depends on the catalyst employed in the

reduction of SO₂ by CO. These studies used Fe supported on Al₂O₃ and SiO₂, fluorite oxides doped with Ni, Pt, Co and Cu, CoAl₂O₃, Fe₂O₃/Al₂O₃, SnO₂ and Sn-Zr based catalysts, respectively. Also, pre-sulphiding of the catalysts resulted in the presence of the active Cat [S] species that reacts with CO to produce COS.

The reaction by-product COS was not observed in any of the reaction exit gases in this study. It was thus assumed that over Au/TiO₂, the redox reaction mechanism was followed in the reduction of SO₂ by CO. The adsorption of S on Au has been reported to be weak at low S concentrations temperatures above 400 K (Rodriguez et al., 2003). Hence, the active species in the COS intermediate reaction, the metal sulphide Au [S], is not likely to be present on the catalyst surface. Therefore, on Au/TiO₂, SO₂ was reduced via the redox reaction mechanism which results in little or no COS produced.

8.2 Effect of Feed Ratio on Au-supported catalysts

The preliminary studies of this work showed that the highest SO₂ conversion was achieved at a SO₂ feed concentration of 2 000 ppm as shown in Appendix C.

The activity of Au-supported catalysts was tested at a constant SO₂ feed concentration of 2 000 ppm and changing feed ratio values as shown in Table 6.3 from Section 6.2.1. These were also compared to the supporting metal oxides as shown in Table 8.2.

Table 8.2: Effect of feed ratio on the conversion of SO₂ at a reaction temperature of 300 °C and SO₂ concentration of 2 000 ppm

Catalyst	Percentage SO ₂ Conversion			
	Feed Ratio			
	0.5	1	2	3
Au/TiO₂	34.90	57.59	77.23	66.17
Au/ZnO	2.64	9.83	6.95	7.64
Au/Al₂O₃	0.56	2.37	1.52	2.49
TiO₂	4.58	5.06	5.94	8.62
ZnO	1.23	1.69	1.22	2.03
Al₂O₃	0.59	0.48	0.61	0.72

At any given ratio, Au/TiO₂ shows the highest SO₂ conversions compared to Au/ZnO and Au/Al₂O₃. In concurrence with the results in Chapter 6, the supports show lower activities in comparison with the Au loaded catalysts with a maximum SO₂ conversion of 8.62 % over TiO₂. The detailed activity of Au/TiO₂ over a TOS of 72 h and a reaction temperature of 300 °C is shown in Figure 8.5. The highest conversion of 80.96 % was achieved when the feed ratio was 2 and the lowest at the feed ratio value of 0.5 with a maximum of 42.46 %. The analysis of variance was done for each feed ratio for all catalysts and the supports, and for the catalyst compared to the corresponding support.

As observed in Table 8.3, for 95 % confidence level, the p value is >> 0.05. Therefore, the conversion data for the different catalysts and metal oxides are not equal. The analysis of variance (ANOVA) data table for the comparison between each catalyst and its equivalent the metal oxide support is shown in Appendix C.

Table 8.3: ANOVA of the SO₂ conversions over the catalysts and the supports

Feed ratio	Source of Variation	SS	df	MS	F	P-value	F critical
0.5	Between Groups	33625,16	5	6725,03	1680,045	3,6E-167	2,2570
	Within Groups	840,6067	210	4,00289			
1	Between Groups	88919,13	5	17783,83	11228,04	8E-253	1,47281
	Within Groups	332,6141	210	1,583877			
2	Between Groups	164164,2	5	32832,83	1339,805	3,9E-157	1,47281
	Within Groups	5146,192	210	24,50567			
3	Between Groups	114187,5	5	22837,49	13257,98	3,6E-254	1,47325
	Within Groups	351,3995	204	1,722546			

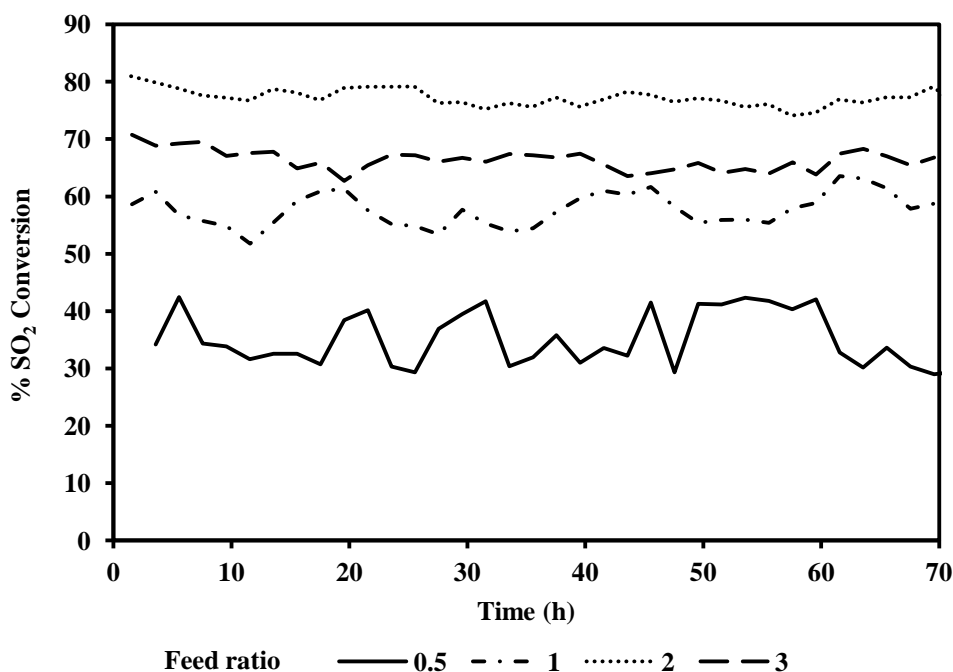


Figure 8.5: Effect of feed ratio on the activity of Au/TiO₂ at 300 °C, TOS of 72 h and GHSV of 3 600 mL.g_{cat}⁻¹.h⁻¹

Industrial flue gas concentrations of SO₂ are notably much lower than the ones previously investigated. The flow rates of the feed gases were adjusted to obtain

Chapter Eight: Product Selectivity and Feed Ratio Effects

an SO₂ and CO feed concentration of 420 ppm and 50 ppm respectively. The SO₂ conversion data for each catalyst and the support is shown in Table 8.4.

Table 8.4: Effect of reaction temperature on the conversion of SO₂ at a feed ratio of 0.12

Catalyst	Percentage SO ₂ Conversion					
	Reaction Temperature (°C)					
	50	100	150	200	250	300
Au/TiO ₂	83.89	78.21	79.92	81.02	81.94	79.56
Au/ZnO	5.68	6.27	7.56	6.95	7.02	6.52
Au/Al ₂ O ₃	3.59	2.13	2.98	2.33	2.69	3.01
TiO ₂	2.69	3.04	3.06	2.87	3.10	3.15
ZnO	1.16	1.25	1.33	1.45	1.56	1.49
Al ₂ O ₃	0.91	0.84	0.95	1.01	0.92	1.14

Table 8.4 shows the conversion for each catalyst as a function of temperature. At this low SO₂ feed concentration, the reaction temperature had a negligible effect on the activity of the catalysts. The activity of Au/TiO₂ at this feed ratio and varying reaction temperature, presented in Figure 8.6 shows the negligible effect of reaction temperature.

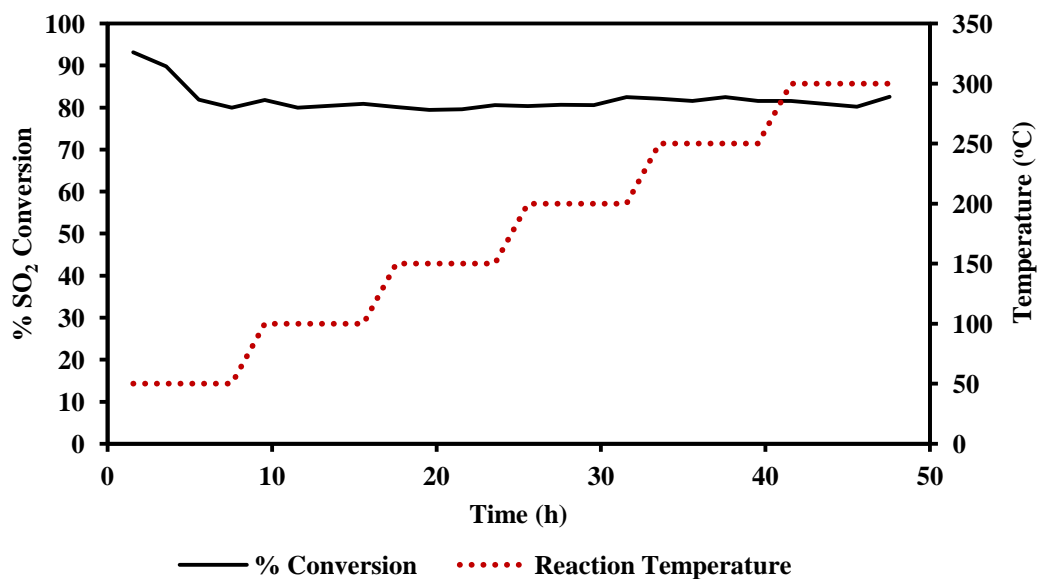


Figure 8.6: Effect of temperature on activity of Au/TiO₂ at a feed ratio of 0.12:1, GHSV of 3 600 mL.g_{cat}⁻¹.h⁻¹ and SO₂ feed concentration of 420 ppm.

The initial observation from these results is the higher conversions achieved over Au/TiO₂ compared to Au/Al₂O₃ and Au/ZnO. As explained in Chapter 5, the redox properties of the TiO₂ support aid in the reduction of SO₂. The results from the feed ratio tests show that the highest activities were achieved at a feed ratio of 2:1 with the lowest at 0.5:1. This trend can be explained by taking into account the reaction mechanism involved in the reduction of SO₂ over Au-supported catalysts. It was assumed that the redox mechanism was followed in the reduction of SO₂ due to the absence of COS from the exit gas stream and the availability of mobile oxygen vacancies on TiO₂. The catalytic active species in this mechanism are the oxygen vacancies on the metal oxide (Cat []) support where the adsorption of SO₂ occurs and the Au-metal oxide (Cat [O]) interface where the CO adsorbs. When CO was in excess, that is, the feed ratio of 3:1, the catalyst surface was reduced via Reaction 5.2a which generated the oxygen vacancies. The increase in the number of oxygen vacancies drove the reduction of SO₂ via Reactions 5.2b and 5.2c, thus leading to high SO₂ conversion rates. When CO was the limiting reactant, that is, when the feed ratio was 1:1 and 0.5:1, the Reactions 5.2b and

5.2c led to an excess of O atoms on catalyst surface since there was less CO available to reduce the surface. In turn, the conversion rate of SO₂ was decreased due to the limited oxygen vacancies available for its adsorption. The highest conversion of SO₂ was observed at the stoichiometric feed ratio of 2:1 where there were an equal number of active sites generated for the reduction of SO₂ and oxidation of CO. At the industrial flue gas feed ratio of 0.12:1, the concentrations of CO and SO₂ were so low that the conversion of SO₂ was relatively high at 81.3 % on average over the temperature range of 50 °C to 300 °C. Thus, it is assumed that in the industrial application of this research, more CO will need to be co-fed to the SO₂ reduction reactor to obtain higher SO₂ conversion rates.

8.3 Conclusion

The analysis of the reaction products showed that there was no COS produced with CO₂ and elemental sulphur as the main reaction products. The elemental sulphur condensed to form S₈ as identified by XRD and HRTEM with EDS techniques. This led to the conclusion that the redox reaction mechanism was followed mainly over Au/TiO₂ as this support has oxygen vacancies that make it easily oxidised and reduced and no COS was observed in the reactor exit line.

The optimum feed ratio to obtain the highest activity at a SO₂ feed concentration of 2 000 ppm was found to be CO:SO₂ equal to 2:1. At this feed ratio, there was a balance in the number of active sites generated for the reduction of SO₂ and the oxidation of CO. High SO₂ conversions were also observed at a feed ratio of 3:1 with lowest seen at a feed ratio of 0.5:1, where SO₂ was in excess. The reaction temperature was seen to have little effect on the conversion rates at the industrial feed ratio of 0.12:1 over Au/TiO₂ due to the very low concentration of SO₂. It is then concluded that to achieve close to complete conversion rates of SO₂, CO will need to be co-fed to flue gas to increase the reactor feed ratio from 0.12:1 to 2:1.

Chapter 9. Effect of time on-stream, pre-treatment and adding oxygen on Au/TiO₂

9.1 Introduction

Au nanoparticles supported on TiO₂ have been shown in Chapters 6 and 7 to be active for the reduction of SO₂ by CO ideally at 300 °C and low SO₂ concentrations. The Au/TiO₂ used in the preliminary studies was analysed after the reaction using XPS techniques and found to have 1 % of sulphur species on its surface. This raised a question of whether sulphur accumulates on the surface of the catalyst with time on-stream (TOS), poisoning the catalyst as the reaction proceeds. TOS is the length, in time, of the reaction.

Previous studies have analysed enhancing the activity of the catalyst by pre-treating with different gases (Ma et al., 1997; Zhuang et al., 2000; Chen & Weng, 2005; Wang et al., 2006; Han et al., 2008). These studies used individual and mixed gases such as H₂S, SO₂, He, CO for the pre-treatment step to enhance the activity of the catalyst tested.

Ruth et al., (2000) and Kim & Woo, (2006) investigated the poisoning effect of SO₂ on Au/TiO₂ for CO oxidation. They found that the presence of SO₂ reversibly poisons the catalyst by adsorbing on the O adsorption sites hence blocking the oxidation of CO. Given that flue gas contains O₂ it was necessary to investigate

the effect of co-feeding it into the reactor to determine whether it inhibits the reduction of SO₂.

9.2 Effect of Time-On-Stream

The Au/TiO₂ catalyst sample used in the preliminary studies was analysed by XPS and found to have an atomic concentration of 1 % of sulphur species on the surface. This was confirmed by an EDS analysis indicating the presence of sulphur species as shown in Figure 9.1.

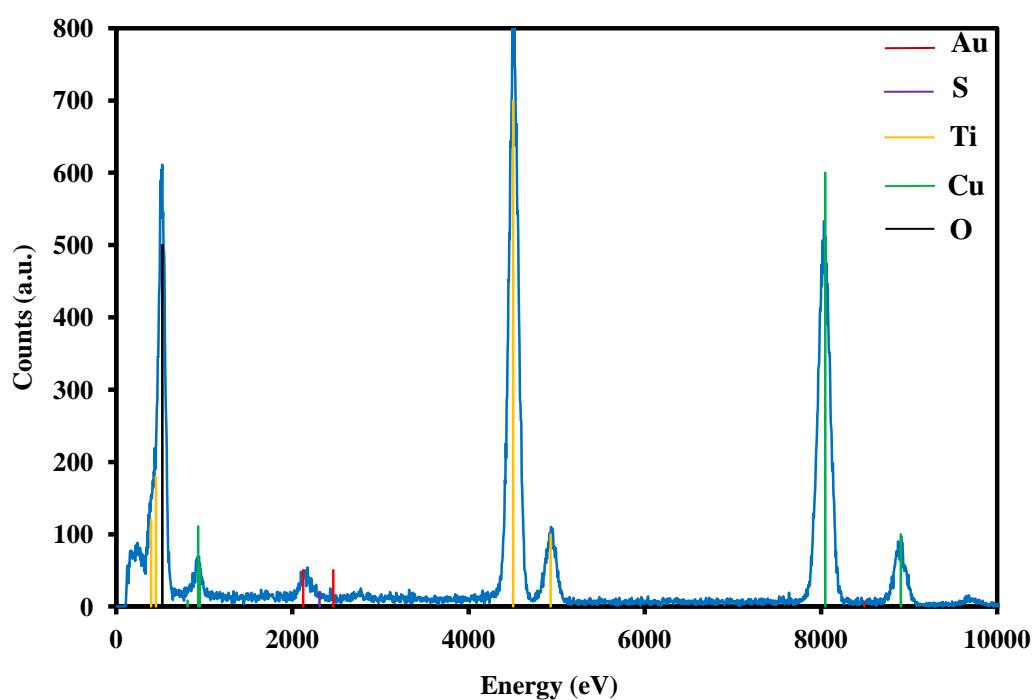


Figure 9.1: EDS analysis of after-reaction Au/TiO₂ (“a.u.” refers to arbitrary units)

The peaks shown in Figure 9.1 were identified as Au, Ti, O, S and Cu (“X-ray Data Booklet”, n.d.) as shown in Appendix B. The presence of Cu is a result of

the copper disc used to mount the catalyst for HRTEM analysis. The EDS energy peaks of Au/TiO₂ show the presence of sulphur with a peak at 2 306 eV.

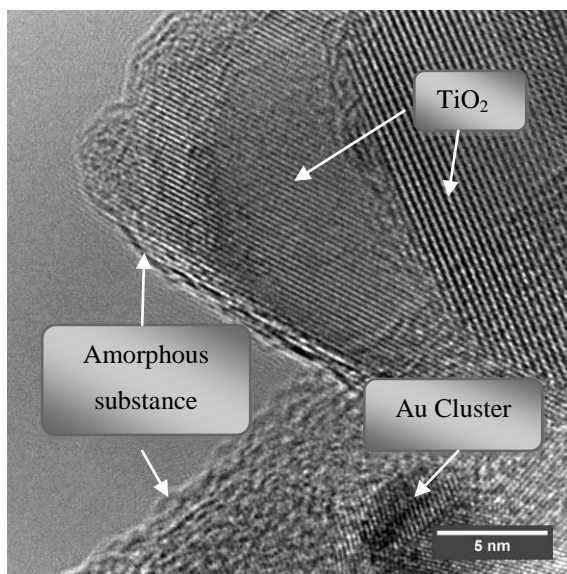


Figure 9.2: HRTEM image of an after-reaction Au/TiO₂ sample

Thus, further testing was done to identify the sulphur species and determine whether it accumulated on the surface of the catalyst. Three different Au/TiO₂ samples were used for SO₂ reduction by CO at a GHSV of 3 600 mL.g_{cat}⁻¹.h⁻¹ and a reaction temperature of 300 °C for a TOS of 24, 72 and 144 hours, separately. The surface of the catalyst was tested by XPS to determine the amount of sulphur on the surface and compared to a fresh Au/TiO₂ sample. Table 9.1 shows the XPS results and atomic percentages of Au, O, Ti, C and S for the four catalyst samples.

Table 9.1: XPS results of Au/TiO₂ at different TOS

TOS (h)	Atomic Concentration (%)				
	Au	O	Ti	C	S
0	1	55	26	18	0
24	1	58	25	15	1
72	1	58	26	14	2
144	1	58	26	15	1

For all four samples, the Au concentration remained steady at 1 % with Ti having a steady concentration of approximately 25 %. The concentration of sulphur on the surface was found to have increased by 1 % after 24 hours on-stream. The atomic surface concentration of oxygen increased by 3 % from the fresh catalyst to 58 % after 24 hours on-stream and remained constant with increasing TOS.

It is evident from Table 9.1 that there was no significant accumulation of sulphur on the catalyst surface with increasing TOS from 24 hours to 144 hours given that the XPS elemental error ranges from 2 % to 5 %. The 2p spectra peaks for sulphur show that it may be present on the catalyst surface in the form of SO_x as shown in Figure 9.3.

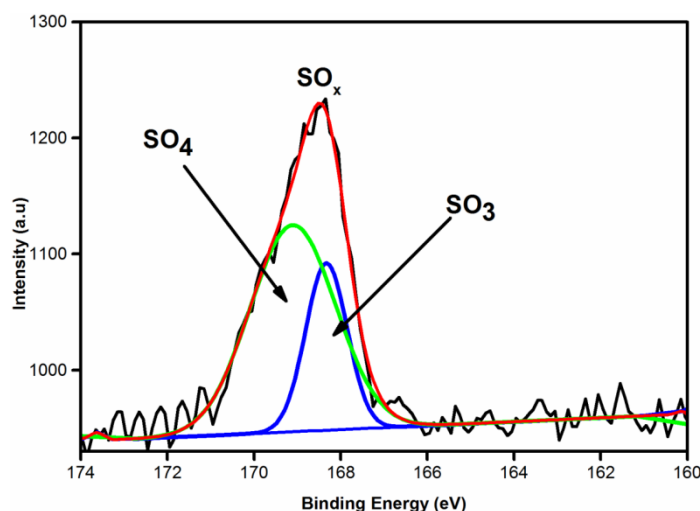


Figure 9.3: XPS analysis peak of S2p (“a.u.” denotes arbitrary units)

Chapter Nine: Effect of TOS, Pre-treatment and adding O₂ on Au/TiO₂

These XPS results offer further insight into the reaction mechanism followed for the reduction of SO₂ by Au/TiO₂. SO₂ adsorbed on the catalyst surface to form SO_x before being dissociated to elemental sulphur and oxygen which then combined to form the gaseous sulphur species and condensed outside the reactor after desorption. This observation concurs with the results obtained by Rodriguez et al., (2002) who showed how SO₂ adsorbs and dissociates on the surface of Au/TiO₂ using high-resolution photoemission spectroscopy and first principle density-functional slab calculations. They also showed that SO₂ adsorbs weakly on Au (which is non-reactive due to its nobility) and on TiO₂, SO₄ is formed upon adsorption which dissociates slightly when the temperature is increased. On Au/TiO₂, SO₂ formed SO₄ on the surface followed by a significant dissociation to elemental S, this demonstrates the effect Au nanoparticles have on the reactivity of TiO₂ (Rodriguez et al., 2002; Bond, Louis & Thompson, 2006).

From this observation, it was then hypothesized that in the reduction of SO₂, the molecule adsorbs on the TiO₂ site or the Au-TiO₂ interfacial site creating adsorbed SO₄ (or SO₃) species. The presence of Au aids the dissociation of SO₂ by increasing the mobility of oxygen vacancies in the metal oxide support between the bulk and surface (Haruta, 1997; Schubert et al., 2001) which could be the active site for SO₂ adsorption and subsequent dissociation. Once dissociated, the excess O on the surface oxidises the CO whose active site is either the Au nanoparticle or the Au-TiO₂ interface. This mechanism is similar to the redox mechanism (Ma, Fang & Ting Lau, 1996) that results in very low amounts or no COS generated as observed.

9.3 Effect of Pre-treatment

Introducing SO₂ to the catalyst prior to the reaction may increase its activity by presulphiding it and increasing the dissociation and oxidation rates of SO₂ and CO, respectively. This phenomenon is observed mainly when the COS reaction

Chapter Nine: Effect of TOS, Pre-treatment and adding O₂ on Au/TiO₂

intermediate reaction mechanism is followed (Haas & Khalafalla, 1973a; Paik, Kim & Chung, 1997; Zhuang et al., 2000; Chen & Weng, 2005). Pre-treatment of Au/TiO₂ was carried out by exposing to 0.5 vol % SO₂ at a flow rate of 15 mL.min⁻¹ for 1 hour at room temperature (approximately 25 °C) and at 300 °C. These temperatures were chosen based on the reaction temperature recorded for the lowest and highest activity on the reduction of SO₂. As observed in Chapter 7, any temperatures higher than 300 °C lead to deactivation of the catalyst. The activity of the pre-treated catalyst was tested at a CO:SO₂ feed ratio of 2:1, TOS of 51 hours and increasing reaction temperature from 50 to 300 °C and GHSV of 3 600 mL.g_{cat}⁻¹.h⁻¹. Figure 9.4 shows the effect of pre-treatment on the conversion of SO₂.

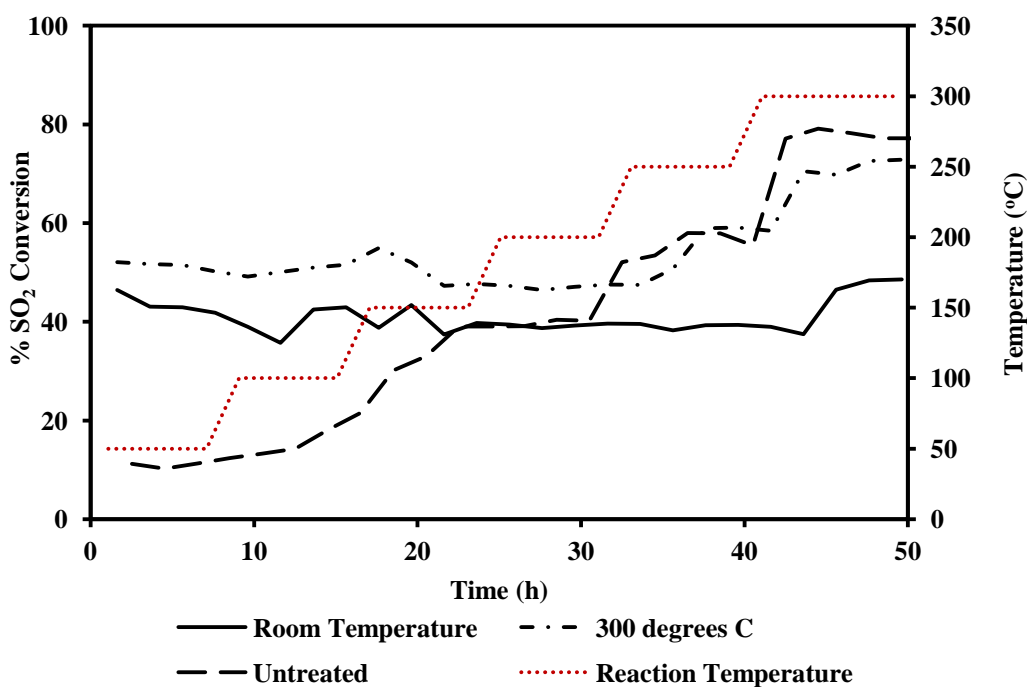


Figure 9.4: Effect of pre-treatment temperature on conversion of SO₂ with time over Au/TiO₂ at CO:SO₂ feed ratio of 2:1, as temperature was increased in 50 °C steps at 8 h intervals at a GHSV of 3 600 mL.g_{cat}⁻¹.h⁻¹

Chapter Nine: Effect of TOS, Pre-treatment and adding O₂ on Au/TiO₂

As the reaction temperature increased from 50 to 150 °C, the catalyst pre-treated at 300 °C was the most active with the untreated catalyst as the least active. Once the reaction temperature reached 250 °C, the activity of the untreated catalysts surpassed that of the 300 °C from an average of 55 % to an average of 78 % SO₂ conversion. The catalyst pre-treated at room temperature showed an average of 41 % SO₂ conversion with very little to no effect of the reaction temperature on the conversion.

It is evident from Figure 9.4 that pre-treating the catalyst in 0.5 vol% of SO₂ increased the activity at low reaction temperatures, less than 200 °C, with less influence at higher reaction temperatures. When comparing the activity of the Au/TiO₂ pre-treated at room temperature and at 300 °C, it was observed that the latter shows slightly higher activity with a significant increase when the reaction temperature reached 300 °C. Pre-exposing Au/TiO₂ to SO₂ leads to the formation of adsorbed SO_x species on the catalyst. As observed before, the percent conversion increased monotonically with reaction temperature thus, as the temperature increased, the rate of reduction of SO₂ increased for pre-treatment at 300 °C. The untreated catalyst had a light-off temperature of 250 °C, after 30 hours on-stream, and performed better at 300 °C than the pre-treated catalysts. It was assumed that the catalyst needed to be activated by exposure to SO₂ to show higher activity at low temperatures, hence the low activity at reaction temperatures less than 150 °C. Also, higher reaction temperatures activated the catalyst for SO₂ reduction as shown in Figure 9.4. It was suspected that pre-treatment at 300 °C with 0.5 vol% SO₂ led to the formation of pre-adsorbed SO_x on the catalyst which overcame the initial catalyst activation step in the reduction of SO₂, thus when the reaction commenced, even at low temperatures, a significant percentage of SO₂ was reduced compared to the untreated catalyst. This may play an important role in decreasing the amount of energy input required to activate Au/TiO₂ in the reduction of SO₂ by CO, since the pre-

treatment activates the catalyst for 1 hour at 300 °C, compared to the 30-hour in situ.

9.4 Effect of adding Oxygen to feed gas

It was important to investigate the activity of Au/TiO₂ for the reduction of SO₂ under oxidising conditions mainly since flue gas contains oxygen. Au/TiO₂ has also been reported to be an excellent catalyst for the oxidation of CO (Haruta, 2004b; Solsona et al., 2005) due to the redox properties of TiO₂ and its interactions with Au clusters (Bond, Louis & Thompson, 2006). Previous research has shown that the presence of SO₂ on Au/TiO₂ inhibits the oxidation of CO (Ruth et al., 2000; Kim & Woo, 2006) by adsorbing on the O₂ sites, hence, it was necessary to investigate the activity of this catalyst for the reduction of SO₂ in the presence of O₂.

The activity of Au/TiO₂ for SO₂ reduction in the presence of oxygen was measured by maintaining both the CO:O₂ and CO:SO₂ feed ratios at the stoichiometric ratio of 2:1. The percent conversions of CO, SO₂ and O₂ by Au/TiO₂ at reaction temperature of 300 °C are shown in Figure 9.5.

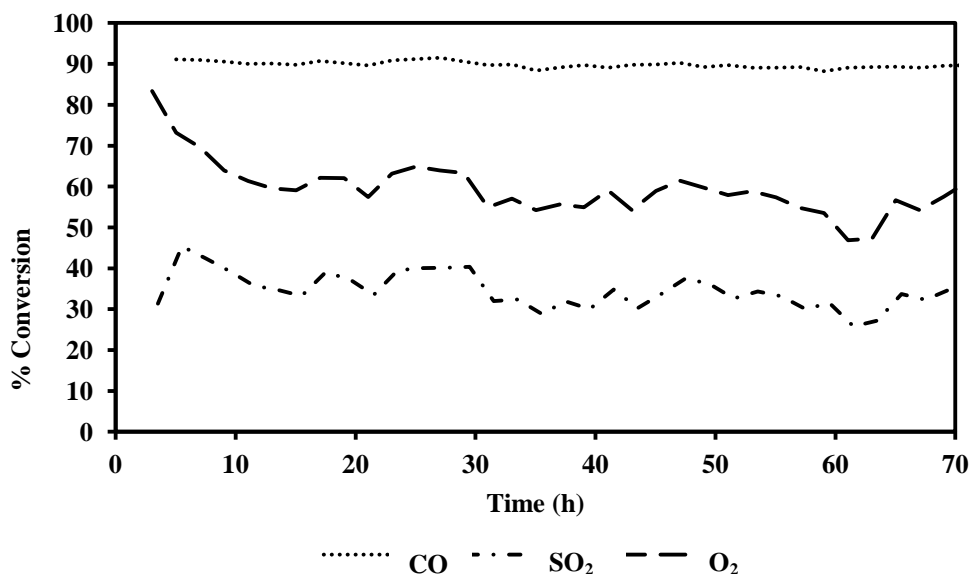


Figure 9.5: Conversion versus time over Au/TiO₂ at 300 °C, O₂ feed concentration of 2 000 ppm, CO concentration of 4 000 ppm and CO:SO₂ = 2:1

The introduction of O₂ to the reactor feed gas stream resulted in a drop in the percentage conversion of SO₂ to an average of 34.5 %. The percentage conversion of O₂ however was observed to be an average of 59.5 % under these reaction conditions. The Reactions 3.9 and 1.5 show that for every mole of O₂ and SO₂ that react, a total of 4 moles of CO are consumed. This explained the high conversion of CO in the presence of O₂, with direct CO oxidation occurring.

In order to determine whether the addition of O₂ lowered the activity of Au/TiO₂ for the reduction of SO₂ irreversibly, the O₂ feed was removed after 30 hours of reaction. The flow rate of He was increased in order to maintain the GHSV at 3 600 mL.g_{cat}⁻¹.h⁻¹. Figure 9.6 shows the effect of removing O₂ from the reactor feed 30 hours after the reaction commenced.

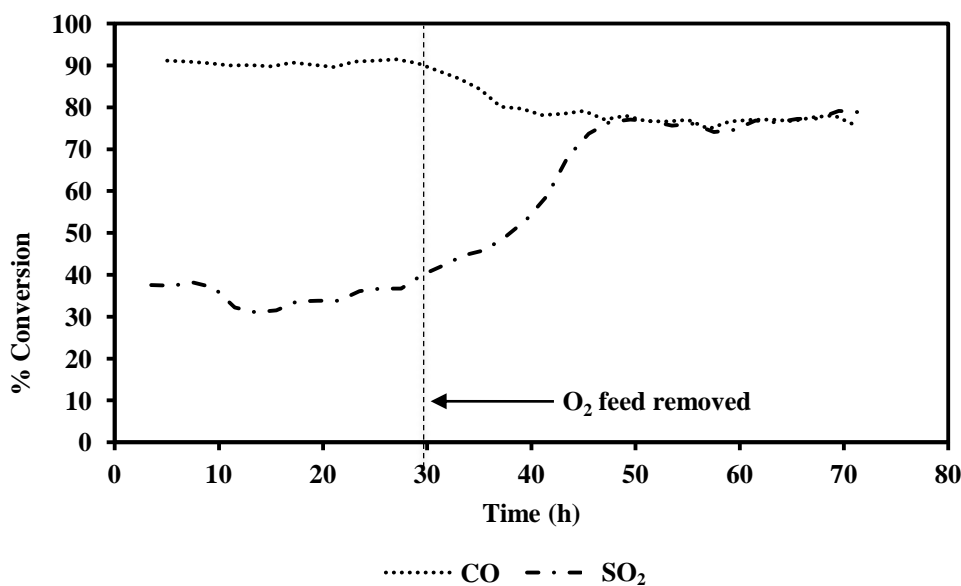


Figure 9.6: Effect of removal of O₂ from reactor feed gas on SO₂ and CO percentage conversion at CO:SO₂ = 2, 2 000 ppm O₂ and reaction temperature of 300 °C

As seen in Figure 9.6, once O₂ was removed from the feed gas, the conversion of SO₂ slowly increased from an average of 35.0 % to 75.9 % while the CO conversion showed a slight decrease from an average of 90.5 % to 77.1 %. This showed that the negative effect of the addition of O₂ to the feed gas stream in the reduction of SO₂ was reversible once O₂ is removed. Two competing reactions occur over Au/TiO₂, namely Reactions 3.9 (the reduction of SO₂ by CO or the oxidation of CO by SO₂) and 1.5 (oxidation of CO by O₂) under these conditions. It was suspected that O₂ and SO₂ compete for active sites as they may adsorb on the TiO₂ before dissociation (Kim & Woo, 2006). Despite SO₂ adsorbing more strongly than O₂ on TiO₂, O₂ reacts faster due to its lower bond dissociation energy of 498.4 kJ.mol⁻¹ (Darwent, 1970) and there is only one bond to break (Equation 9.1). On the other hand, SO₂ has two bonds to break (Equations 9.2) for dissociation with bond dissociation energies of 546.5 kJ.mol⁻¹ and 521.7 kJ.mol⁻¹ (Darwent, 1970), hence a lower conversion of SO₂ in the presence of O₂.



9.5 Conclusion

Au/TiO₂ was found to be very active in the reduction of SO₂ by CO to elemental sulphur with no generation of COS. The sulphur product did not accumulate on the catalyst surface with increasing time-on-stream as shown by XPS analysis of the catalyst surface over 144 hours. However, it was found that the sulphur species on the catalyst was in the form of SO_x which suggested that the redox reaction mechanism was followed in the reduction of SO₂ over Au/TiO₂. In the redox reaction mechanism, SO₂ adsorbs and dissociates on the metal oxide while the CO oxidation occurs on the Au and/or the Au-TiO₂ interface. The presence of Au on the TiO₂ aided in the dissociation of SO₂ by increasing the mobility of the oxygen vacancies between the bulk and surface of the support. In general, little or no COS is generated when the redox mechanism is followed, thus no COS was observed in the product gas in these experiments.

Previous studies have shown an improvement in activity by pre-treating the catalyst, specifically, presulphidation. This step leads to the formation of a metal-sulphur species that is active in the reduction of SO₂. It is important to note that in the literature, this pre-treatment step is followed by reduction via the COS intermediate mechanism where CO reacts with the metal-sulphur species to form COS. Pre-treatment of Au/TiO₂ with 0.5 % of SO₂ by volume for an hour at room temperature and 300 °C improved the activity of the catalyst at low reaction temperatures (less than 150 °C). Conversely, the untreated catalysts showed

higher activities at higher reaction temperatures, above 150 °C. This may be due to the fact that the redox reaction mechanism is followed over Au/TiO₂ with the formation of a SO_x species on TiO₂ as the first step in the reaction. As demonstrated by Rodriguez et al., (2002), doping SO₂ on Au/TiO₂ leads to the formation of S via SO_x on the TiO₂ which results in an excess of O adatoms on the surface. These excess O adatoms are then involved in the subsequent oxidation of CO, probably via the same mechanism as CO oxidation over Au/TiO₂.

The addition of O₂ to the reactor feed gas reduced the conversion of SO₂ by competing with SO₂ for the adsorption sites on TiO₂. With the advantage of having lower bond dissociation energy and one double bond to break, compared to two bonds and higher bond dissociation energies of SO₂, the presence of O₂ resulted in a large decrease in SO₂ conversion. The conversion of CO was very high because of the presence of oxygen in the reactor, meaning that O₂ and SO₂ were competing to react with CO or that O₂ and SO₂ were competing for adsorption sites. The adverse effect of O₂ was reversible to some extent as seen when its flow into the reactor was stopped leading to an increase in the conversion of SO₂. Given that flue gas contains O₂, among other components, it may be necessary to co-feed CO to achieve the best results in optimising the performance of Au/TiO₂ for SO₂ reduction. The selectivity of Au/TiO₂ for SO₂ reduction under oxidising conditions could be improved by using other reducing agents or by pre-treatment. As shown in this chapter, pre-treatment of the catalyst with SO₂ produces adsorbed SO_x, which in turn is assumed can improve the selectivity of Au/TiO₂ for SO₂ reduction even under oxidising conditions.

Summary and Conclusions

The discovery of gold supported nano catalysts and their high activities for a variety of reactions motivated their use in the reduction of SO₂ by CO. Three catalysts were chosen for comparison based on the acidity and redox properties of the supporting metal oxide, that is; Au supported on an acidic metal oxide (Au/ γ -Al₂O₃), basic metal oxide (Au/ZnO) and an easily reducible metal oxide (Au/TiO₂). Chapter 7 reports the characterization and comparison of the supporting metal oxide of these industrially manufactured AUROLite™ gold supported catalysts. The characterisation showed Au clusters on larger metal oxide particles with a particle size of 1.8 nm, which have been reported by the literature to be highly active. However, to prove that loading Au nanoparticles onto the metal oxide support produced a highly active catalyst, the activities of the loaded catalysts were also compared to the activities of the metal oxides. This enhancement of the activity of the metal oxide was only significant in the case of Au/TiO₂ where TiO₂ had an SO₂ conversion 60 % less than that of Au/TiO₂. The activity over Au/Al₂O₃ and Au/ZnO in comparison to the metal oxides was very low. This shows that the nature of the support plays an important role determining the activity of the catalyst other than just supporting the Au nanoparticles. Unlike the alkaline ZnO and acidic γ -Al₂O₃, TiO₂ is an easily reducible metal oxide with oxygen vacancies that are involved in the reduction of SO₂. On Au/ZnO and Au/Al₂O₃, SO₂ adsorbed strongly on the surface with a slight desorption when the

Summary and Conclusions

reaction temperature increased. This slight desorption allowed for the reaction to occur briefly on the surface before it was full saturated again once the temperature stabilised. To further test this, other reducible metal oxides, such as oxides of iron, cobalt and cerium, could be tested as they are more reducible than TiO₂. However, further in-situ analysis will be required to study the adsorption interaction of the SO₂ and the catalyst.

The reaction tests showed that the optimum reaction temperature for high SO₂ conversion rates was 300 °C. Au/TiO₂ had a very high activity, 86.4 % SO₂ conversion, compared to Au/ZnO and Au/Al₂O₃ (less than 2 %) at a reaction temperature of 300 °C. When the reaction temperature was increased above 300 °C over Au/TiO₂, the activity dropped irreversibly to 13 %. The HRTEM images comparing the catalyst before and after the reaction showed that the shape of the Au nanoparticles had changed from hemispherical particles to slightly more spherical particles. As explained in Chapter 4, this may have been the main reason why the activity Au/TiO₂ dropped irreversibly to a low SO₂ conversion of 13 %.

The investigation into the effect of SO₂ feed concentrations and CO:SO₂ feed ratio showed that lower SO₂ concentrations yield higher conversions over Au/TiO₂ at 300 °C. The highest conversions at a set SO₂ feed concentration of 2 000 ppm were achieved at the feed ratio of 2:1, which is the stoichiometric ratio. However, this ideal feed ratio may not be easily achievable with the actual flue gas ratio of

CO:SO₂, which also depends on the composition of the coal burnt and the combustion conditions. As such, it could be necessary to co-feed CO if this catalyst is developed for industrial applications.

Chalom (2009) showed that Au/TiO₂ converted SO₂ in its reduction using CO but did not identify the reaction products. This work showed two main reaction products; CO₂ and elemental sulphur which condensed at the exit of the reactor. The analysis of the gaseous products using gas chromatography showed no other gaseous product, specifically COS. This led to the conclusion that the redox mechanism proposed by previous research, as shown in Chapter 5, is followed over Au/TiO₂. This mechanism suggested that the SO₂ to form SO₄ adsorbed on the oxygen vacancies on TiO₂ in close proximity to the Au nanoparticle. The Adsorbed SO₄ dissociates into S and leaves the surface in gaseous form (Rodriguez et al., 2002). CO preferentially oxidises on the Au-TiO₂ interface and thus may not react with S to form COS, hence there was no COS production observed. Coupling the GC with mass spectrometry may confirm the products of the reaction.

For a TOS of 144 hours, it was found that there was no accumulation of S species on Au/TiO₂. However, these results may not be accurate given that the XPS elemental error is within the range of 2 to 5 % and the surface S concentration was

Summary and Conclusions

reported to be below 2 %. As such, it is recommended that a more sensitive technique should be used, also, to increase the TOS.

Pre-treatment of Au/TiO₂ was done with 0.5 vol% SO₂ at room temperature and at 300 °C as shown in Chapter 9. Comparing these pre-treated catalysts to an untreated catalyst showed that there was an increase in activity at reaction temperatures less than 150 °C. Above 150 °C, the untreated catalyst performed better than the pre-treated catalysts. Therefore, the activity of Au/TiO₂ was only improved by the pre-treatment step at low reaction temperatures. It was assumed that this was due to the pre-adsorption of SO₂ as SO_x, where x is 2, 3 or 4, on the catalyst surface that overcame the first activation barrier of the reduction of SO₂ by CO. The pre-treatment temperatures and SO₂ concentrations could be varied to determine the optimum pre-treatment conditions.

The addition of oxygen in the reduction of SO₂ by CO decreased the percentage conversion of SO₂. The CO conversion was approximately 90 % as it was oxidised by reactions with both O₂ and SO₂. The decline in SO₂ conversion was shown to be reversible once the oxygen feed was removed. This was assumed to be due to O₂ and SO₂ competing for adsorption sites, while SO₂ with larger bond dissociating energies than O₂ had lower conversion rates in the presence of O₂. Under the conditions tested, CO was the limiting reactant, thus, a CO co-feed may be required for the industrial applications of this work.

Summary and Conclusions

This work has shown that Au/TiO₂ catalyses the reduction of SO₂ using CO as the reducing agent. It has also, to a limited extent, shown that COS is not produced by the reaction. However, more a sensitive analysis is recommended to simultaneously identify the reaction products.

It was suggested that increasing the Au loading from 1 wt% could yield a more active catalyst than the ones used in this research. However, increasing the loading may increase the deactivation of the catalyst, unless the support has a very large surface area. Therefore, investigating the chemical and/or physical mixtures of Au supported on a metal oxide with a large surface area and an easily reducible metal oxide would be recommended.

It is recommended that this work can be used as a foundation for developing Au-supported catalysts used to mitigate air pollution. Therefore, an in depth market study for the economic viability should be done before the development of this catalyst. The market study could include, amongst other factors; a commodity study of sulphur, comparing the reagent prices of current SO₂ abatement methods to the ones required in this study.

References

About 49M. 2014. Available: <http://www.49m.co.za/1024-1500/about>. [20 September 2014]

Azar, M., Caps, V., Morfin, F., Rousset, J., Piednoir, a, Bertolini, J. & Piccolo, L. 2006. Insights into activation, deactivation and hydrogen-induced promotion of a Au/TiO₂ reference catalyst in CO oxidation. *Journal of Catalysis*. 239(2):307–312. [18 April 2004]

Berga, L. 2016. The Role of Hydropower in Climate Change Mitigation and Adaptation: A Review. *Engineering*. 2(3):313–318. [15 April 2017]

Bond, G.C., Louis, C. & Thompson, D.T. 2006. *Catalysis by Gold*. V. 6. London: Imperial College Press.

Busca, G. 2006. The Surface Acidity and Basicity of Solid Oxides and Zeolites. In *Metal Oxides Chemistry and Applications*. J.L.G. Fierro, Ed. Florida. 247–318. CRC Press

Cant, N.W. & Fredrickson, P.W. 1975. Silver and Gold Catalyzed Reactions of Carbon Monoxide with Nitric Oxide and with Oxygen. *Journal of Catalysis*. 37:531–539.

Chalom, L.A. 2009. *SO₂ Abatement Using Gold Catalysts* Degree of Master of Science in Engineering. University of the Witwatersrand.

Chandel, S.S. & Agarwal, T. 2017. Review of current state of research on energy storage, toxicity, health hazards and commercialization of phase changing materials. *Renewable and Sustainable Energy Reviews*. 67:581–596.

References

- Chen, C. & Weng, H. 2005. Nanosized CeO-supported metal oxide catalysts for catalytic reduction of SO₂ with CO as a reducing agent. *Applied Catalysis B: Environmental*. 55(2):115–122.
- Chen, C.-L., Wang, C.-H. & Weng, H.-S. 2004. Supported transition-metal oxide catalysts for reduction of sulfur dioxide with hydrogen to elemental sulfur. *Chemosphere*. 56(5):425–31.
- Dalla Lana, I.G., Karge, H.G. & George, Z.M. 1993. Dissociative Adsorption of Sulfur Dioxide on Gamma Alumina Investigated by TPD and Mass Spectrometry. *Journal of Physical Chemistry*. 97:8005–8011.
- Darwent, B. 1970. *Bond Dissociation Energies.pdf*. Available: <http://www.nist.gov/data/nsrds/NSRDS-NBS31.pdf> [29 April 2016].
- Devoe, H. 2014. *Thermodynamics and Chemistry*. 2nd ed. Available: <http://www2.chem.umd.edu/thermobook/>. [21 July 2016]
- Diebold, U. 2003. The surface science of titanium dioxide. *Surface Science Reports*. 48:53–229.
- Downs, R.T., Bartelmehs, K.L., Gibbs, G. V. & Boisen, M.B. 1993. Interactive software for calculating and displaying X-ray or neutron powder diffractometer patterns of crystalline materials. *American Mineralogist*. 78:1104–1107.
- Fellner, P., Jurisova, J., Khandl, V., Sykorova, A. & Thonstad, J. 2006. Adsorption of SO₂ on Alumina. *Chemical Papers*. 60(4):311–314.
- Fierro, J.L.G. Ed. 2006. *Metal Oxides Chemistry and Application*. Florida: CRC Press.

References

- Flytzani-stephanopoulos, M., Zhu, T. & Li, Y. 2000. Ceria-based catalysts for the recovery of elemental sulfur from SO₂-laden gas streams. *Catalysis Today*. 62:145–158.
- Foster, P. 2013. Now for the downside of fracking. *The Telegraph*. 20 February. Available: www.telegraph.co.uk/earth/energy/9883362/Now-for-the-downside-of-fracking.html. [21 November 2015]
- Giorgio, S., Henry, C., Pauwels, B. & Van Tendeloo, G. 2001. Au particles supported on (110) anatase-TiO₂. *Materials Science and Engineering: A*. A297(1–2):197–202.
- González-Roubaud, E., Pérez-Osorio, D. & Prieto, C. 2017. Review of commercial thermal energy storage in concentrated solar power plants: Steam vs. molten salts. *Renewable and Sustainable Energy Reviews*. 80:133–148.
- Goodman, D.W. 2004. Catalysis by Supported Gold Nanoclusters. In *Dekker Encyclopedia Of Nanoscience and Nanotechnology*. New York: Marcel Dekker. Inc. 611–621.
- Guney, M.S. 2016. Solar power and application methods. *Renewable and Sustainable Energy Reviews*. 57:776–785.
- Haas, L.A. & Khalafalla, S.E. 1973a. Kinetic Evidence of a Reactive of SO₂ with Intermediate CO in Reduction. *Journal of Catalysis*. 29:264–269.
- Haas, L.A. & Khalafalla, S.E. 1973b. Catalytic Thermal Decomposition of Carbonyl Sulfide and Its Reaction with Sulfur Dioxide. *Journal of Catalysis*. 30:451–459.
- Han, G.B., Park, N.-K., Ryu, S.O. & Lee, T.J. 2008. Catalytic reduction of sulfur dioxide using hydrogen or carbon monoxide over Ce_{1-x}Zr_xO₂ catalysts for the recovery of elemental sulfur. *Catalysis Today*. 131:330–338.

References

- Han, G.B., Park, N.-K., Yoon, S.H. & Lee, T.J. 2008. Catalytic reduction of sulfur dioxide with carbon monoxide over tin dioxide for direct sulfur recovery process. *Chemosphere*. 72:1744–1750..
- Han, G.B., Park, N.-K., Yoon, S.H., Lee, T.J. & Yoon, K.J. 2008. Synergistic catalysis effect in SO₂ reduction by CO over Sn-Zr-based catalysts. *Applied Catalysis A: General*. 337:29–38.
- Han, G.B., Park, N.-K. & Lee, T.J. 2009. Effect of O₂ on SO₂ reduction with CO or H₂ over SnO₂-ZrO₂ Catalysts. *Industrial & Engineering Chemistry Research*. 48:10307–10313.
- Hanaor, D.A.H. & Sorrell, C.C. 2010. Review of the Anatase to Rutile Phase Transformation. *Journal of Material Science*. 46(4):855–874.
- Haruta, M. 1997. Size and support dependency in the catalysis of gold. *Catalysis Today*. 36:153–166.
- Haruta, M. 2004a. Gold as a novel catalyst in the 21st century: Preparation, working mechanism and applications. *Gold Bulletin*. 37(1–2):27–36.
- Haruta, M. 2004b. Nanoparticulate Gold Catalysts for Low-Temperature CO Oxidation. *Journal of New Materials for Electrochemical Systems*. 7:163–172.
- Haruta, M. 2008. Relevance of Metal Nanoclusters Size Control in Gold (0) Catalytic Chemistry. In *Metal Nanoclusters in Catalysis and Materials Science: The Issue of Size Control*. 183–199. Amsterdam. Elsevier
- Haruta, M., Kobayashi, T., Sano, H. & Yamada, N. 1987. Novel Gold Catalysts for the Oxidation Of Carbon Monoxide at a Temperature far below 0 °C. *Chemistry Letters*. 405–408.

References

Haruta, M., Yamada, N., Kobayashi, T. & Iijima, S. 1989. Gold Catalysts Prepared by Coprecipitation for Low-Temperature Oxidation of Hydrogen and of Carbon Monoxide. *Journal of Catalysis*. 115:301–309.

Heinsohn, R.J. & Kabel, R.L. 1999. *Source and Control of Air Pollution*. New Jersey: Prentice-Hall, Inc.

Hutchings, G.J. 1985. Vapor Phase l-hydrochlorination of Acetylene : Correlation of Catalytic Activity of Supported Metal Chloride Catalysts. *Journal of Biotechnology*. 96:292–295.

Hutchings, G.J. 2004. New Directions in Gold Catalysis. *Gold Bulletin*. 37(1–2):3–11.

IEA report. 2017. Available:

<http://www.iea.org/statistics/statisticssearch/report/?country=SOUTHAFRIC&product=electricityandheat&year=2014> [23 August 2017].

Ilieva, L., Pantaleo, G., Nedyalkova, R., Sobczak, J.W., Lisowski, W. & Kantcheva, M. 2009. Environmental NO reduction by CO over gold catalysts based on ceria supports, prepared by mechanochemical activation, modified by Me³⁺ (Me = Al or lanthanides): Effect of water in the feed gas. *Applied Catalysis B: Environmental*. 90:286–294.

Kannan, N. & Vakeesan, D. 2016. Solar energy for future world: - A review. *Renewable and Sustainable Energy Reviews*. 62:1092–1105..

Khalafalla, S.E. & Haas, L.A. 1972. Active sites for catalytic reduction of SO₂ with CO on alumina. *Journal of Catalysis*. 24(1):115–120.

Khalafalla, S.E., Foerster, E.F. & Haas, L.A. 1971. Catalytic Reduction of Sulfur Dioxide on Iron-Alumina Bifunctional Catalysts. *Industrial & Engineering Chemistry Product Research and Development*. 10(2):133–137.

References

- Kim, M.R. & Woo, S.I. 2006. Poisoning effect of SO₂ on the catalytic activity of Au/TiO₂ investigated with XPS and in situ FT-IR. *Applied Catalysis A: General*. 299:52–57.
- Kim, H., Won Park, D., Chul Woo, H. & Shik Chung, J. 1998. Reduction of SO₂ by CO to elemental sulfur over Co₃O₄-TiO₂ catalysts. *Applied Catalysis B: Environmental*. 19(3–4):233–243.
- Klimont, Z., Smith, S.J. & Cofala, J. 2013. The last decade of global anthropogenic sulfur dioxide: 2000–2011 emissions. *Environmental Research Letters*. 8(1):14003.
- Ku, T., Chen, M., Li, B., Yun, Y., Li, G. & Sang, N. 2017. Synergistic effects of particulate matter (PM_{2.5} and sulfur dioxide (SO₂ on neurodegeneration via the microRNA-mediated regulation of tau phosphorylation. *Toxicol. Res*. 6(1):7–16.
- Kummu, M. & Sarkkula, J. 2008. Impact of the Mekong River Flow Alteration on the Tonle Sap Flood Pulse. *A Journal of the Human Environment*. 37(3):185–192.
- Lai, S.Y., Zhang, H. & Ng, C.F. 2004. Deactivation of Gold Catalysts Supported on Sulfated TiO₂-ZrO₂ Mixed Oxides for CO Oxidation During Catalytic Decomposition of Chlorodifluoromethane (HCFC-22). *Catalysis Letters*. 92(3–4):107–114.
- Lepsoe, R. 1940. Chemistry of Sulfur Dioxide Reduction, Kinetics. *Industrial & Engineering Chemistry*. 32(7):910–918.
- Li, X., Zhu, P., Wang, F., Wang, L. & Tsang, S.C. 2008. Simultaneous Catalytic Reductions of NO and SO₂ by H₂ over Nickel-Tungsten Catalysts. *Journal of Physical Chemistry*. 112:3376–3382.

References

- Lian, J., Ma, J., Duan, X., Kim, T., Li, H. & Zheng, W. 2010. One-step ionothermal synthesis of α -Al₂O₃ mesoporous nanoflakes at low temperature. *Chemical communications (Cambridge, England)*. 46:2650–2652.
- Liu, W., Wadia, C. & Flytzani-stephanopoulos, M. 1996. Transition metal / fluorite-type oxides as active catalysts for reduction of sulfur dioxide to elemental sulfur by carbon monoxide. *Catalysis Today*. 28:391–403.
- Ma, J., Fang, M. & Ting Lau, N. 1996. On the Synergism between La₂O₂S and CoS₂ in the Reduction of SO₂ to Elemental Sulfur by CO. *Journal of Catalysis*. 158(1):251–259.
- Ma, J., Fang, M. & Lau, N.T. 1997. The catalytic reduction of SO₂ by CO over lanthanum oxysulphide. *Applied Catalysis A: General*. 150:253–268.
- Mansfield, T.A. 1998. Stomata and plant water relations: does air pollution create problems? *Environmental pollution (Barking, Essex : 1987)*. 101(1):1–11.
- Masters, G.M. 1998. *Introduction to environmental engineering and science*. 2nd ed. New Jersey: Prentice-Hall, Inc.
- Moma, J.A. 2007. Carbon Monoxide Oxidation over Titanium Dioxide Supported Gold Catalysts. Doctor of Philosophy in Science. University of the Witwatersrand.
- Mulligan, D.J. & Berk, D. 1989. Reduction of sulfur dioxide with methane over selected transition metal sulfides. *Industrial & Engineering Chemistry Research*. 28:926–931.
- National Environment Management: Air Quality Act [No. 39 of 2004]*. 2005. V. 476.
- Available:https://www.environment.gov.za/sites/default/files/legislations/nema_amendment_act39.pdf. [20 November 2015]

References

- De Nevers, N. 2000. *Air Pollution Control Engineering*. 2nd ed. New York. McGraw-Hill International Editions.
- NIST Standard Reference Database Number 69*. 2010. Available: <http://webbook.nist.gov/chemistry/> [12 February 2010].
- NIST Webbook*. n.d. Available: <http://webbook.nist.gov/> [01 June 2011].
- Novacheck, J. & Johnson, J.X. 2017. Diversifying wind power in real power systems. *Renewable Energy*. 106:177–185.
- Okay, V.C. & Short, W.L. 1973. Effect of Water on Sulfur Dioxide Reduction by Carbon Monoxide. *Ind. Eng. Chem. Process Des. Develop.* 12(3):291–294.
- Paik, S.C. & Chung, J.S. 1995. Selective catalytic reduction of sulfur dioxide with hydrogen to elemental sulfur over Co-Mo/Al₂O₃. *Applied Catalysis B: Environmental*. 5(3):233–243.
- Paik, S.C., Kim, H. & Chung, J.S. 1997. The catalytic reduction of SO₂ to elemental sulfur with H₂ or CO. *Catalysis Today*. 38:193–198.
- Park, N.-K., Park, J.Y., Lee, T.J., Baek, J.-I. & Ryu, C.K. 2011. Catalytic reduction of SO₂ over Sn–Zr based catalysts for DSRP under high pressure. *Catalysis Today*. 174(1):46–53.
- Parker, S.C. & Campbell, C.T. 2007. Reactivity and sintering kinetics of Au/TiO₂ (110) model catalysts : particle size effects. *Topics in Catalysis*. 44(1–2):3–13.
- Patel, E.M. 2012. Practical Considerations in the Implementation of Emissions Reduction Solutions at Eskom's Coal Fired Power Plant. In *4th EU-SA Clean Coal Technologies Working Group Meeting*. 1–33. Available: [http://www.energy.gov.za/files/4thEUSouthAfricaCleanCoalWorkingGroup/Practical Considerations in the Implementation of Emissions Reduction Solutions in](http://www.energy.gov.za/files/4thEUSouthAfricaCleanCoalWorkingGroup/Practical%20Considerations%20in%20the%20Implementation%20of%20Emissions%20Reduction%20Solutions%20in%20Coal%20Fired%20Power%20Plants.pdf)

SA Coal Fired Power Plant Final.pdf. [20 August 2017]

Querido, R. & Short, W.L. 1973. Removal of Sulfur Dioxide from Stack Gases by Catalytic Reduction to Elemental Sulfur with Carbon Monoxide. *Industrial & Engineering Chemistry Process Design and Development*. 12(1):10–18.

Raphulu, M., Mcpherson, J., Patrick, G., Ntho, T., Mokoena, L., Moma, J. & Lingen, E. Van Der. 2009. CO oxidation : Deactivation of Au/TiO₂ catalysts during storage. *Gold Bulletin*. 42(4):328–336.

Rase, H.F. 2000. *Handbook of Heterogeneous Catalysts*. Texas. CRC Press.

Ray, B.T. 1995. *Environmental Engineering*. Boston: PWS Publishing Company.

Reddy, B.M. 2006. Redox Properties of Metal Oxides. In *Metal Oxides Chemistry and Applications*. J. Fierro, Ed. Florida: CRC Press. 215–246.

Ren, G., Liu, J., Wan, J., Guo, Y. & Yu, D. 2017. Overview of wind power intermittency: Impacts, measurements, and mitigation solutions. *Applied Energy*. 204:47–65.

Ren, X., Sun, R., Meng, X., Vorobiev, N., Schiemann, M. & Levensis, Y.A. 2017. Carbon, sulfur and nitrogen oxide emissions from combustion of pulverized raw and torrefied biomass. *Fuel*. 188:310–323.

Rivolta Hernández, M., Figueroa Murcia, C., Gupta, R. & de Klerk, A. 2012. Solvent–Coal–Mineral Interaction during Solvent Extraction of Coal. *Energy & Fuels*. 26(11):6834–6842.

Rodriguez, A., Liu, G., Jirsak, T., Hrbek, J., Chang, Z., Dvorak, J. & Maiti, A. 2002. Activation of Gold on Titania : Adsorption and Reaction of SO₂ on Au/TiO₂ (110). *J.Am.Chem.Soc.* 124(110):

Rodriguez, A., Dvorak, J., Jirsak, T., Liu, G., Hrbek, J., Aray, Y., Gonza, C.,

References

- York, N., et al. 2003. Coverage Effects and the Nature of the Metal - Sulfur Bond in S/Au (111): High-Resolution Photoemission and Density-Functional Studies. *J.Am.Chem.Soc.* 125(1):276–285.
- Rossi, M., Pina, C. Della, Falletta, E. & Matarrese, R. 2008. Gold Nanoparticles : From Preparation to Catalytic Evaluation. In *Metal Nanoclusters in Catalysis and Materials Science: The Issue of Size Control*. 253–262. Amsterdam. Elsevier
- Ruth, K., Hayes, M., Burch, R., Tsubota, S. & Haruta, M. 2000. The effects of SO₂ on the oxidation of CO and propane on supported Pt and Au catalysts. *Applied Catalysis A: General*. 24:L133–L138.
- Sarlis, J. & Berk, D. 1988. Reduction of Sulfur Dioxide with Methane over Activated Alumina. *Industrial & Engineering Chemistry Research*. 27(10):1951–1954.
- Schnelle, K.B. & Brown, C.A. 2002. *Air Pollution Control Handbook*. Florida. CRC Press.
- Schubert, M.M., Hackenberg, S., van Veen, A.C., Muhler, M., Plzak, V. & Jurgen Behm, R. 2001. CO Oxidation over Supported Gold Catalysts—“Inert” and “Active” Support Materials and Their Role for the Oxygen Supply during Reaction. *Journal of Catalysis*. 197(1):113–122.
- Seifried, D. & Witzel, W. 2010. *Renewable Energy -The Facts*. Earthscan. [20 April 2016]
- Shikina, N. V, Khairulin, S.R., Yashnik, S.A., Teryaeva, T.N. & Ismagilov, Z.R. 2015. Direct Catalytic Reduction of SO₂ by CH₄ over Fe-Mn Catalysts Prepared by Granulation of Ferromanganese Nodules. *Eurasian Chemico-Technological Journal*. 17:129–136.

References

- Singh, V.K. & Singal, S.K. 2017. Operation of hydro power plants-a review. *Renewable and Sustainable Energy Reviews*. 69(November 2015):610–619.
- Singh, R.I., Brink, A. & Hupa, M. 2013. CFD modeling to study fluidized bed combustion and gasification. *Applied Thermal Engineering*. 52(2):585–614.
- Soares, J.M.C. & Bowker, M. 2005. Low temperature CO oxidation on supported and unsupported gold compounds. *Applied Catalysis A: General*. 291(1–2):136–144.
- Solsona, B., Conte, M., Cong, Y. & Hutchings, G. 2005. Unexpected promotion of Au / TiO₂ by nitrate for CO oxidation. *Chemical communications (Cambridge, England)*. 2351–2353.
- Sovacool, B.K. 2014. Cornucopia or curse? Reviewing the costs and benefits of shale gas hydraulic fracturing (fracking). *Renewable and Sustainable Energy Reviews*. 37:249–264.
- Stein, W.H. & Buck, R. 2017. Advanced power cycles for concentrated solar power. *Solar Energy*. 152:91–105.
- Strauss, W. 1972. *Air Pollution Control Part II*. W. University of M. Strauss, Ed. John Wiley and Sons, Inc.
- Terblanche, P. 1998. *Vaal Triangle Air Pollution Health Study*. Pretoria: MRC.
- Thornton, S.L. 2014. *Encyclopedia of Toxicology*. Elsevier. DOI: 10.1016/B978-0-12-386454-3.01229-X.
- Tripathi, P., Deng, F., Scruggs, C., Chen, Y. & Huang, Steven, K. 2017. Effect of Particulate Matter 2.5 on the Expression and DNA Methylation Pattern of Asthma-Related Genes in Bronchial Epithelial Cells. In *American Thoracic Society*. American Journal of Respiratory and Critical Care Medicine.

References

- Vesilind, P. & Morgan, S. 2004. *Introduction to Environmental Engineering*. 2nd ed. New York. Thompson Books
- Vesilind, P.A., Pierce, J.J. & Weiner, R.F. 1994. *Environmental Engineering*. 3rd ed. Butterworth-Heinemann.
- Wang, C.-H., Lin, S.-S., Hwang, W.-U. & Weng, H.-S. 2002. Supported Transition-Metal Oxide Catalysts for Catalytic Reduction of SO₂ with CO as a Reducing Agent. *Industrial & Engineering Chemistry Research*. 41:666–671.
- Wang, C.-H., Lin, S.-S., Sung, P.-C. & Weng, H.-S. 2003. Catalytic reduction of SO₂ over supported transition-metal oxide catalysts with C₂H₄ as a reducing agent. *Applied Catalysis B: Environmental*. 40(4):331–345
- Wang, G., Bing, L., Yang, Z. & Zhang, J. 2014. Selective catalytic reduction of sulfur dioxide by carbon monoxide over iron oxide supported on activated carbon. *Turkish Journal of Chemistry*. 38(1):70–78.
- Wang, X., Wang, A., Li, N., Wang, X., Liu, Z. & Zhang, T. 2006. Catalytic Reduction of SO₂ with CO over Supported Iron Catalysts. *Industrial & Engineering Chemistry Research*. 45(13):4582–4588.
- Wei, J., Guo, X., Marinova, D. & Fan, J. 2014. Industrial SO₂ pollution and agricultural losses in China: evidence from heavy air polluters. *Journal of Cleaner Production*. 64(2014):404–413.
- Wu, K.-C., Tung, Y.-L., Chen, Y.-L. & Chen, Y.-W. 2004. Catalytic oxidation of carbon monoxide over gold/iron hydroxide catalyst at ambient conditions. *Applied Catalysis B: Environmental*. 53(2):111–116..
- X-ray Data Booklet*. n.d. Available: http://xdb.lbl.gov/Section1/Table_1-3.pdf [20

April 2016]

Xu, X., Song, C., Wincek, R., Andresen, J.M., Miller, B.G. & Scaroni, A.W. 2003. Separation of CO₂ from Power Plant Flue Gas Using a Novel CO₂ “Molecular Basket” Adsorbent. *Fuel Chemistry Division Preprints*. 48(1):162–163.

Yen, F.T. 1999. *Environmental Chemistry: Essentials of Chemistry for Engineering Practice*. Vol 4A ed. Prentice Hall, PTR.

Yin, Y., Chevallier, F., Ciais, P., Broquet, G., Fortems-Cheiney, A., Pison, I. & Saunois, M. 2015. Decadal trends in global CO emissions as seen by MOPITT. *Atmospheric Chemistry and Physics*. 15(23):13433–13451.

Yu, B. & Xu, L. 2016. Review of ecological compensation in hydropower development. *Renewable and Sustainable Energy Reviews*. 55:729–738.

Yu, H., Ming, H.A.I., Gong, J., Li, H., Huang, H.U.I., Pan, K., Liu, Y., Kang, Z., et al. 2013. Facile synthesis of Au / ZnO nanoparticles and their enhanced photocatalytic activity for hydroxylation of benzene. *Bull. Mater. Sci.* 36(3):367–372.

Yu, J., Yu, Q., Jin, Y. & Chang, S. 1997. Reduction of Sulfur Dioxide by Methane to Elemental Sulfur over Supported Cobalt Catalysts. *Industrial & Engineering Chemistry Research*. 36(6):2128–2133.

Yunus, M. & Iqbal, M. 1996. *Plant Response to Air Pollution*. England: John Wiley and Sons Ltd.

Zerrahn, A. 2017. Wind Power and Externalities. *Ecological Economics*. 141:245–260.

References

- Zhang, L., Qin, Y. hong, Chen, B. zhen, Peng, Y. guang, He, H. bing & Yuan, Y. 2016. Catalytic reduction of SO₂ by CO over CeO₂-TiO₂ mixed oxides. *Transactions of Nonferrous Metals Society of China (English Edition)*. 26(11):2960–2965.
- Zhao, H., Luo, X., He, J., Peng, C. & Wu, T. 2015. Recovery of elemental sulphur via selective catalytic reduction of SO₂ over sulphided CoMo/γ-Al₂O₃ catalysts. *Fuel*. 147(x):67–75.
- Zhao, Y., Liu, Z. & Jia, Z. 2007. Elementary sulfur recovery by H₂-regeneration of SO₂-adsorbed CuO/Al₂O₃—Effect of operation parameters. *Chemical Engineering Journal*. 134(1–3):11–15.
- Zhaoliang, Z., Jun, M. & Xiyao, Y. 2003. Separate / simultaneous catalytic reduction of sulfur dioxide and / or nitric oxide by carbon monoxide over titanium – tin solid solution catalysts. *Chemical Engineering Journal*. 95:15–24.
- Zhu, T., Dreher, A. & Flytzani-Stephanopoulos, M. 1999. Direct reduction of SO₂ to elemental sulfur by methane over ceria-based catalysts. *Applied Catalysis B: Environmental*. 21(2):103–120.
- Zhu, T., Kundakovic, L., Dreher, A. & Flytzani-Stephanopoulos, M. 1999. Redox chemistry over CeO₂-based catalysts: SO₂ reduction by CO or CH₄. *Catalysis Today*. 50(2):381–397.
- Zhuang, S.-X., Magara, H., Yamazaki, M., Takahashi, Y. & Yamada, M. 2000. Catalytic conversion of CO, NO and SO₂ on the supported sulfide catalyst: I. Catalytic reduction of SO₂ by CO. *Applied Catalysis B: Environmental*. 24(2):89–96.
- Zhuang, S.-X., Yamazaki, M., Omata, K., Takahashi, Y. & Yamada, M. 2001.

References

Catalytic conversion of CO, NO and SO₂ on supported sulfide catalysts II. Catalytic reduction of NO and SO₂ by CO. *Applied Catalysis B: Environmental*. 31(2):133–143.

Appendix A: Research Methods

A.1 Thermodynamic Calculations

The values of the reaction equilibrium constant were calculated using Equation 3.3.

$$K_a = \exp\left(-\frac{\Delta G_{rxn}}{RT}\right) \quad (3.3)$$

The values of ΔG_{rxn} for temperatures varying from 298.15 K to 6 000 K were calculated by Equation A.1

$$\Delta G = \Delta H - T\Delta S \quad (A.1)$$

Where ΔH and ΔS is the enthalpy and entropy change of the reaction and calculated as shown in Equations A.2 and A.3 (Sandler, 2006).

$$\Delta H_{rxn}^{\circ}(T, 1bar) = \sum_i \nu_i \Delta H_{f,i}^{\circ}(25^{\circ}\text{C}, 1bar) + \sum_i \nu_i \int_{T=25^{\circ}\text{C}}^T C_{P,i}^{\circ} dT \quad (A.2)$$

$$\Delta S_{rxn}^{\circ}(T, 1bar) = \sum_i \nu_i \Delta S_{f,i}^{\circ}(25^{\circ}\text{C}, 1bar) + \sum_i \nu_i \int_{T=25^{\circ}\text{C}}^T \frac{C_{P,i}^{\circ}}{T} dT \quad (A.3)$$

Where $C_{P,i}^{\circ}$ is the heat capacity of species i in its standard state.

The Shomate equation (A.4) was used to find the heat capacities of the substances at any temperature T (“NIST Standard Reference Database Number 69”, n.d.).

$$C_p = A + BT + CT^2 + DT^3 + \frac{E}{T^2} \quad (A.4)$$

Where A, B, C, D, E and F are constants specific to each gas in determining the value of C_p . From this data and equations, the value of ΔG_{rxn} for each reaction at

temperatures ranging from 298.15 K to 6 000 K were calculated and used to determine the relationship between temperature T and the $\log_{10} K_a$.

A.2 Gas Mixtures and Feed Compositions

The synthetic gas mixture used to investigate the activity of the catalyst was supplied via AFROX gas cylinders with the following certified compositions

- 1 vol% (10 000 ppm) SO₂ in He
- 2 vol% (20 000 ppm) CO in He
- Pure He
- 1 vol% (10 000 ppm) O₂ in He

The feed concentration of SO₂ into the reactor was maintained at 2 000 ppm (unless otherwise specified) with the CO feed concentration varied accordingly to increase the CO:SO₂ feed ratio from 0.5:1 to 8:1. The flow rates required to obtain each feed ratio were calculated from the cylinder concentration while maintaining the gas-hourly-space-velocity (GHSV) of 3 600 mL.g_{cat}⁻¹.h⁻¹ as demonstrated.

The final feed concentrations of each gas after mixing can be expressed as shown in Equation A.5

$$C_{x,f} = C_{x,i} \times \frac{V_x}{V} \quad (\text{A.5})$$

Where; C_x is the concentration of each gas x

V_x is the volumetric flow rate of each gas x

V is the total volumetric flow rate

f is the final state

i is the initial state

The feed ratio FR is defined as

$$FR = \frac{C_{CO,f}}{C_{SO_2,f}} \quad (A.6)$$

The equations A.5 and A.6 were combined to calculate the volumetric flow rate of each gas CO and SO₂ as shown in Equation A.7.

$$V_{CO} = V \times \frac{C_{CO,f}}{C_{CO,i}}$$

$$V_{SO_2} = V \times \frac{C_{SO_2,f}}{C_{SO_2,i}} \quad (A.7)$$

Diving the two equations and combining with the feed ratio yields

$$V_{CO} = FR V_{SO_2} \frac{C_{SO_2,i}}{C_{CO,i}} \quad (A.8)$$

This equation was used to calculate the volumetric flow rate of CO given the initial/cylinder concentration of each gas ($C_{x,i}$) and the setting the values for and the SO₂ volumetric flow rate.

For the addition of oxygen, a new feed ratio FR^o is defined which relates the feed concentration of CO to the feed concentration of O₂. This ratio is kept at the stoichiometric ratio of 2:1 in the oxidation of CO.

$$FR^o = \frac{C_{CO,f}}{C_{O_2,f}} \quad (A.9)$$

Upon rearranging and substituting FR^o into the equation A.5 for O₂, equation A.6 is obtained and can be used to evaluate the volumetric flow rate of O₂.

$$V_{O_2} = \frac{V_{CO} \times C_{CO,i}}{R^o \times C_{O_2,i}} \quad (\text{A.10})$$

A.3 Mass Balance Calculations

A simple steady state reaction mass balance can be used to determine amount of reactants and products that exit the reactor via the equation A.11

$$\text{Amount OUT} = \text{Amount IN} + \text{Amount GENERATED} - \text{Amount REACTED} \quad (\text{A.11})$$

For all reactants, the amount generated is typically zero as they react in the reaction unless a side reaction produces that particular reactant. In the same manner, the amount of products reacted is also zero unless they also react via a side reaction.

The stoichiometric reaction below shows the relation between products and reactants for a single reaction.

$$\frac{\text{Amount of reactant } i \text{ reacted}}{v_i} = \frac{\text{Amount of product } j \text{ generated}}{v_j} \quad (\text{A.12})$$

In order to determine the amount of reactants consumed by the reaction a baseline concentration of the reactants had to be established by analysing the reactor feed in the absence of a catalyst for 24 hours. This resulted in a series of peaks generated by Clarify™ software that were integrated to determine each peak area, which was equivalent to the feed concentration of each gas. The peak areas for each specific gas (identified by retention time) were statistically summed up and a mean value was determined that corresponds to the feed volumetric concentration. CO had a retention time of 4 min while SO₂ had a retention time of approximately 6 min once the GC oven reached 200 °C.

The volumetric flow rate can be converted to a molar flow rate via the ideal gas equation with the assumption that the gases behave ideally as shown.

$$PV = \dot{n}RT \quad (\text{A.13})$$

Where P is the atmospheric pressure in Johannesburg, South Africa, V is the volumetric flow rate, \dot{n} is the molar flow rate, R is the ideal gas constant and T is the temperature (room temperature).

This equation can be rearrange to give the conversion factor for converting between volumetric and molar flow rates.

$$\frac{\dot{n}}{V} = \frac{P}{RT} = \frac{0.85 \text{ atm}}{82.05746 \text{ cm}^3 \cdot \text{atm} \cdot \text{K}^{-1} \cdot \text{mol}^{-1} \times 293.15 \text{ K}} = 3.53 \times 10^{-5} \text{ mol} \cdot \text{cm}^{-3} \quad (\text{A.14})$$

Appendix B: Characterization Results

B.1 TEM Images

The following images are the TEM images of the fresh catalysts, Au/TiO₂, Au/ZnO and Au/Al₂O₃ and a different magnification than that shown in Chapter 6.

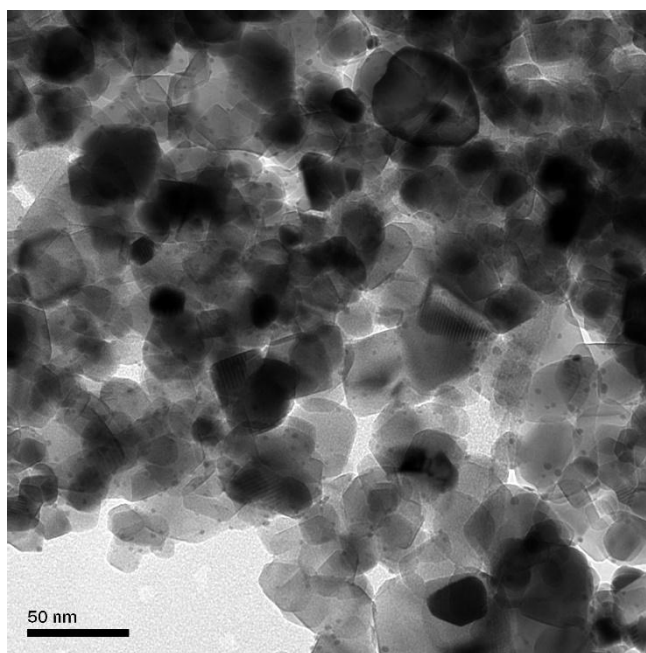


Figure B1: TEM image of Au/TiO₂

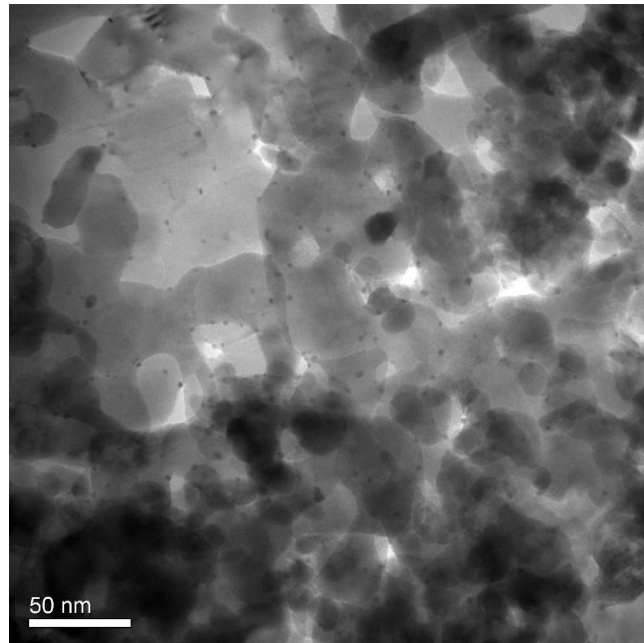


Figure B2: TEM image of Au/ZnO

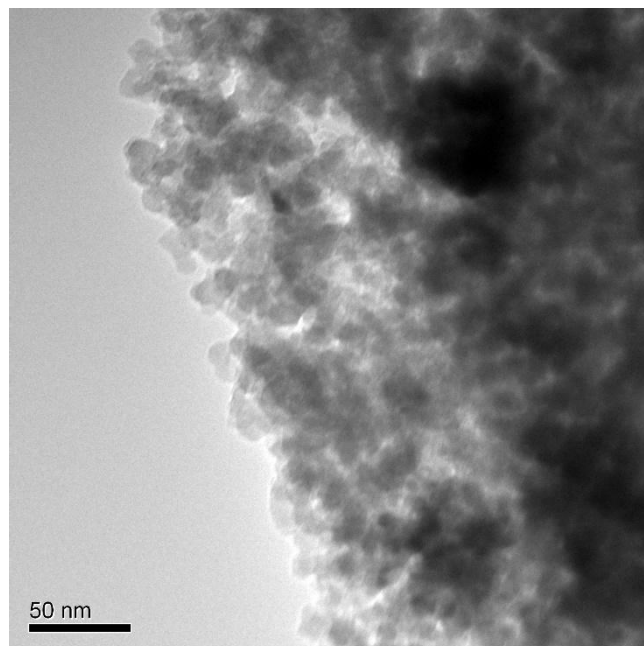


Figure B3: TEM image of Au/Al₂O₃

The particle size distribution was determined by measuring the diameter of each Au nanocluster using ImageJ 1.44p software. This generated a table of the diameter of each particle analysed, the mean and standard deviation of each set of data (Table B3). For Au/ZnO, 105 particles were analysed and the pivot table is shown in Table B1. 100 Au nanoparticles were analysed on Au/TiO₂ and the pivot table is shown in Table B2.

Table B1: Pivot table for 105 Au nanoparticles on Au/ZnO

Row Labels	Values Frequency	%
1-1,5	23	21,90%
1,5-2	42	40,00%
2-2,5	30	28,57%
2,5-3	7	6,67%
3-3,5	1	0,95%
3,5-4	2	1,90%
Grand Total	105	100,00%

Table B2: Pivot table for 100 Au nanoparticles on Au/TiO₂

Row Labels	Values Frequency	%
0,5-1	1	1,0%
1-1,5	23	23,0%
1,5-2	43	43,0%
2-2,5	28	28,0%
2,5-3	2	2,0%
3-3,5	2	2,0%
3,5-4	1	1,0%
Grand Total	100	100,0%

Table B2: Mean and Standard deviation for Au/ZnO and Au/TiO₂

	105 Au on Au/ZnO	100 Au on Au/TiO ₂
Mean	1,873	1,816
SD	0,461	0,458
Min	1,047	0,988
Max	3,540	3,555

B.2 XRD Analysis

The sulphur sample from the reaction products was identified as S₈ using XRD techniques. Table B1 shows the peaks for the corresponding 2θ values for S₈ generated by XPOW software.

Table B1: 2θ values and peaks used in identifying S_8

2θ	Intensity	d-Spacing	H	K	L
11.48	6.61	7.7078	1	1	1
15.39	14.86	5.7566	1	1	3
15.56	6.16	5.6964	0	2	2
18.44	1.74	4.8122	2	0	2
21.19	2.06	4.1935	1	1	5
21.89	11.88	4.0603	2	2	0
22.69	13.81	3.9186	1	3	1
23.08	100.00	3.8539	2	2	2
24.94	6.62	3.5699	1	3	3
25.85	38.72	3.4464	0	2	6
26.34	2.72	3.3836	2	2	4
26.72	22.66	3.3360	3	1	1
27.72	24.86	3.2181	2	0	6
27.72	11.32	3.2178	0	4	0
27.77	12.89	3.2125	1	1	7
28.68	21.06	3.1129	3	1	3
28.95	15.15	3.0838	1	3	5
29.18	1.10	3.0606	0	0	8
31.41	19.35	2.8482	0	4	4
33.30	2.14	2.6905	3	3	1
33.50	1.21	2.6749	2	4	2
34.16	11.73	2.6244	1	3	7
34.27	2.58	2.6167	4	0	0
34.92	3.80	2.5693	3	3	3
35.90	8.30	2.5017	2	4	4
36.12	4.53	2.4868	1	5	1
37.06	14.57	2.4259	3	1	7
37.37	2.42	2.4061	4	0	4
37.84	4.44	2.3778	4	2	2
37.98	5.13	2.3690	3	3	5
39.37	7.24	2.2885	0	2	10
40.68	1.77	2.2177	0	4	8
42.09	3.72	2.1467	1	1	11
42.73	7.37	2.1162	3	1	9
42.80	8.83	2.1130	0	6	2
43.14	2.25	2.0968	2	2	10
43.98	1.71	2.0589	5	1	1
44.36	1.30	2.0419	2	4	8
45.16	1.87	2.0078	3	5	3
45.61	4.14	1.9889	4	0	8
46.34	3.58	1.9593	2	6	2

Appendix B: Characterization Results

47.17	1.48	1.9269	4	4	4
47.67	1.72	1.9078	3	5	5
47.78	8.25	1.9037	5	1	5
47.87	3.07	1.9002	4	2	8
47.91	1.25	1.8988	0	6	6
49.52	1.25	1.8407	1	5	9
49.69	1.17	1.8348	1	1	13
49.94	2.20	1.8261	2	4	10
50.03	4.96	1.8232	2	2	12
51.26	15.56	1.7823	3	5	7
52.08	8.99	1.7562	5	3	5
53.02	7.35	1.7270	6	0	2
53.15	5.12	1.7232	0	4	12
53.17	2.38	1.7226	4	2	10
53.28	1.36	1.7193	3	3	11
53.98	10.55	1.6986	1	7	5
55.15	2.42	1.6653	2	6	8
55.26	1.17	1.6624	1	5	11
55.46	2.44	1.6569	5	3	7
55.78	7.17	1.6481	3	5	9
55.94	1.11	1.6438	3	1	13
56.70	3.48	1.6234	6	2	4
56.72	6.10	1.6231	3	7	1
56.81	1.91	1.6206	5	5	1
57.25	1.74	1.6091	4	0	12
57.36	6.07	1.6063	2	2	14
57.60	2.50	1.6003	1	1	15
57.80	2.59	1.5953	3	7	3
59.11	2.39	1.5628	4	4	10
60.00	1.64	1.5419	2	6	10
60.22	1.81	1.5368	4	6	6
60.50	2.39	1.5303	0	0	16
61.66	2.65	1.5043	1	5	13
62.25	1.31	1.4915	2	8	4
63.01	2.61	1.4752	6	2	8
63.68	1.16	1.4613	7	1	3
64.78	3.51	1.4392	4	4	12
64.89	1.17	1.4369	5	3	11
64.96	1.53	1.4356	6	4	6
65.62	2.79	1.4228	2	6	12
65.69	1.25	1.4213	7	1	5
65.85	1.60	1.4183	4	2	14
65.86	2.35	1.4182	1	1	17
67.30	1.29	1.3913	7	3	3

68.94	1.01	1.3620	4	8	2
69.00	1.23	1.3611	1	9	5
69.25	1.11	1.3567	7	3	5
69.42	1.48	1.3539	1	3	17
69.44	4.34	1.3534	6	6	0
72.34	2.76	1.3062	3	9	3
72.76	2.55	1.2997	6	4	10
72.83	1.17	1.2987	6	2	12
73.74	2.23	1.2849	5	7	7
74.24	1.35	1.2775	3	9	5
75.81	1.83	1.2549	8	2	4
77.24	1.04	1.2351	6	0	14
79.46	1.76	1.2061	8	4	2
82.55	1.16	1.1687	5	9	3
82.62	1.22	1.1678	7	5	9
88.87	1.28	1.1011	7	7	7
89.67	1.34	1.0934	5	1	19

B.3 XPS Analysis

The XPS analysis of the after reaction Au/TiO₂ catalyst used in the preliminary studies is shown in Figure B4.

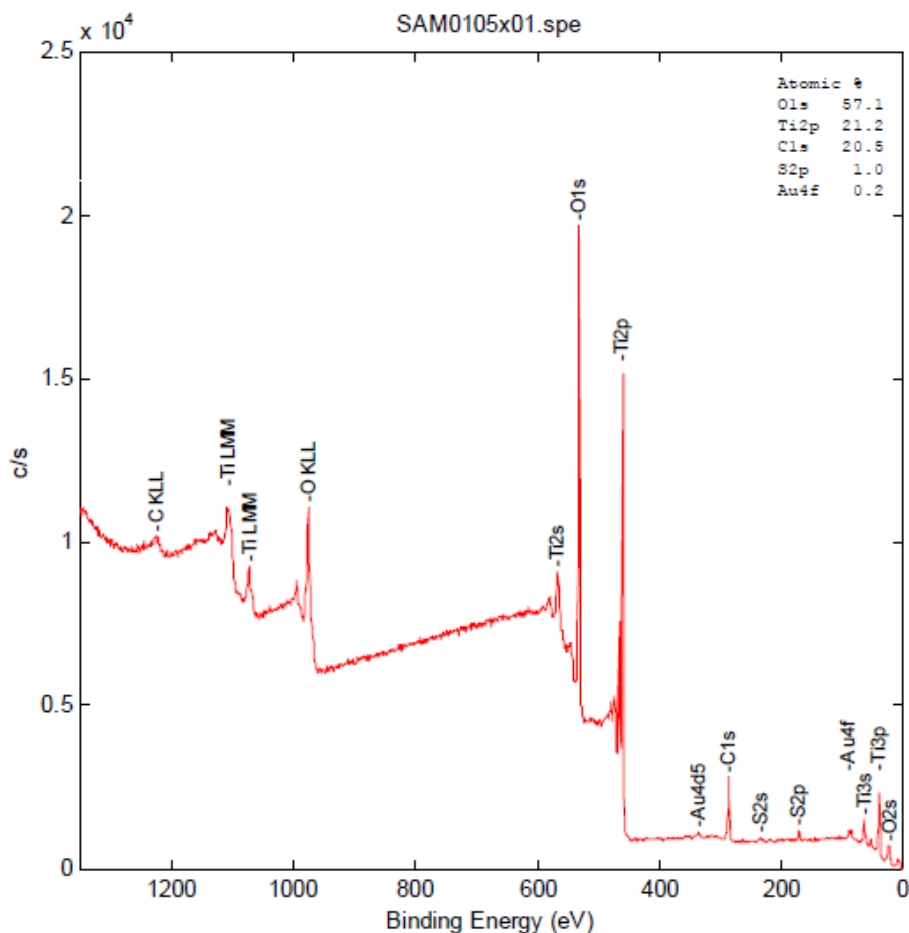


Figure B4: XPS analysis of after-reaction Au/TiO₂ showing presence of 1 % sulphur on the surface.

B.4 EDS Peaks

Table B1: EDS peaks of Au, O, Ti, S and Cu adapted from (“X-ray Data Booklet”, n.d.)

Element	Line	Peak Position (eV)
Sulphur (S)	K α_2	2306.6
	K α_1	2307.8
	K β_1	2464.0
Titanium (Ti)	L1	395.3
	L $\alpha_{1,2}$	452.2
	L β_1	458.4
	K α_2	4504.9
	K α_1	4510.8

Appendix B: Characterization Results

	$K\beta_{1,3}$	4931.8
Oxygen (O)	$K\alpha_{1,2}$	524.9
Gold (Au)	$M\alpha_1$	2122.9
	L1	8493.9
	$L\alpha_2$	9628.0
	$L\alpha_1$	9713.3
Copper (Cu)	L1	811.1
	$L\alpha_{1,2}$	929.7
	$L\beta_1$	949.8
	$K\alpha_2$	8027.8
	$K\alpha_1$	8047.8
	$K\beta_{1,3}$	8905.3

Appendix C: Reaction Tests

C.1 Effect of varying SO₂ feed concentrations

In the preliminary investigations into the effect of feed ratio on the reduction of SO₂, the feed ratio was only be adjusted by varying both feed concentrations of CO and SO₂ simultaneously.

The SO₂ and CO feed concentrations were varied as shown in table C.1 while maintaining the GHSV at 3 600 mL.g_{cat}⁻¹.h⁻¹ and a catalyst weight of 0.5 g unless otherwise adjusted to 1 g.

Table C1: SO₂ and CO feed ratios and concentrations

Feed Ratio	Feed Concentration (ppm)	
	SO ₂	CO
2	5 000	10 000
4	3 333	13 333
6	2 500	15 000
8	2 000	16 000

Table C2: Effect of feed ratio on the conversion of SO₂ at a reaction temperature of 300 °C

Catalyst	SO ₂ conversion			
	Feed Ratio			
	2	4	6	8
Au/TiO ₂	24.81	35.09	55.28	70.08
Au/ZnO	3.52	22.98	33.89	10.30
Au/Al ₂ O ₃	1.78	3.37	1.85	2.56
TiO ₂	8.87	6.65	7.54	12.32
ZnO	1.09	1.00	2.03	1.56
Al ₂ O ₃	0.63	0.55	0.42	0.61

The effect of feed ratio, in Table C1, on the conversion of SO₂ over Au/ZnO at increasing reaction temperature is shown in Figure C1. The reaction temperature does not have any effect on the activity of Au/ZnO.

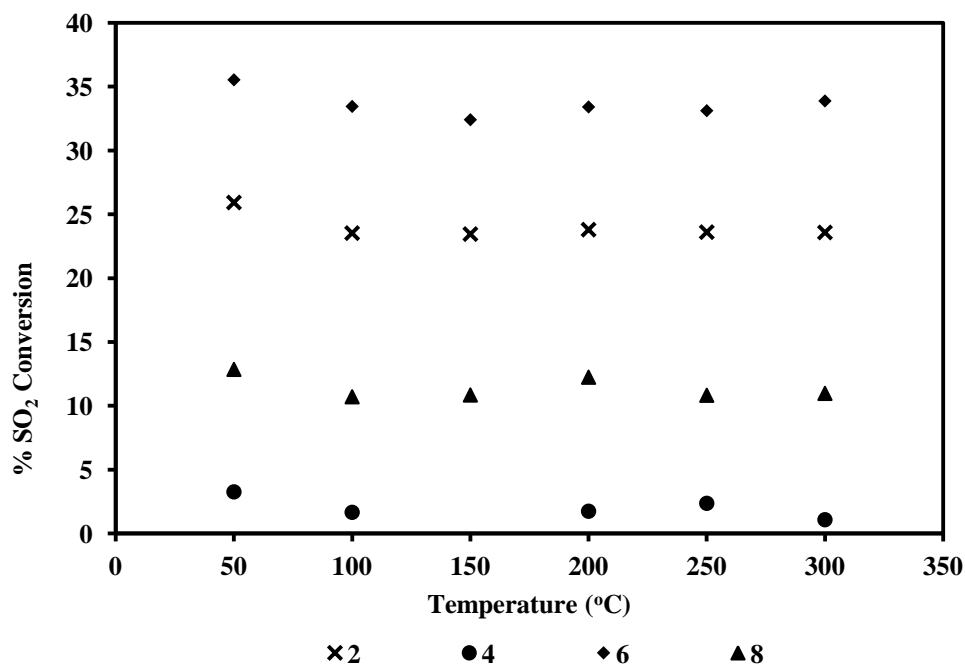


Figure C1: Effect of feed ratio and reaction temperature on the conversion of SO₂ over 0.5 g Au/ZnO at GHSV of 3 600 mL_{g_{cat}}⁻¹.h⁻¹

The effect of feed ratio, in Table C1, on the conversion of SO₂ over Au/TiO₂ at increasing reaction temperature is shown in Figure C2.

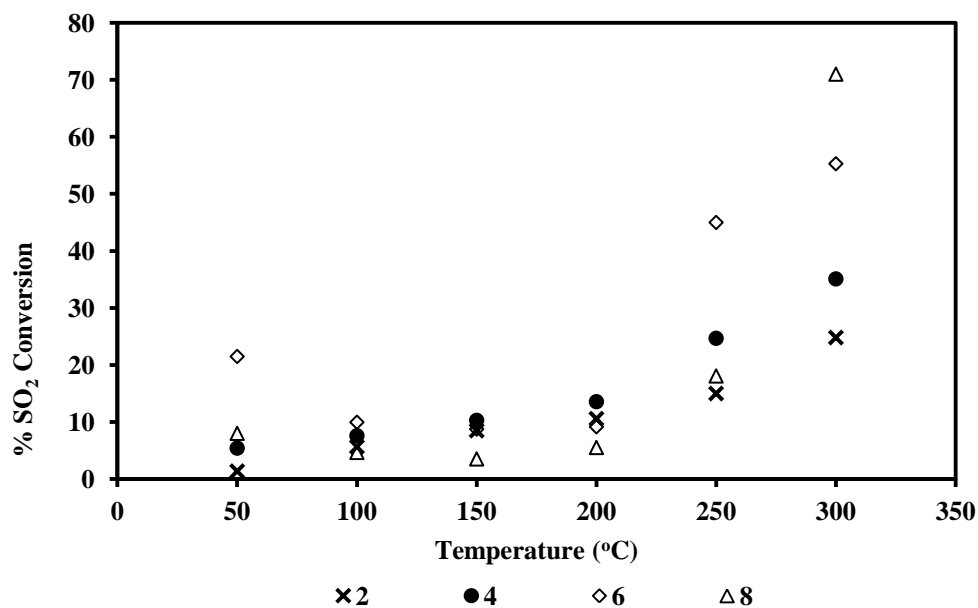


Figure C2: Effect of feed ratio and reaction temperature on the conversion of SO₂ over 0.5 g Au/TiO₂ at GHSV of 3 600 mL.g_{cat}⁻¹.h⁻¹

ANOVA Tables

Table C3:SUMMARY for Feed ratio = 0.5:1

Groups	Count	Sum	Average	Variance
Au/Al ₂ O ₃	36	20,213	0,561472	0,022588
Au/ZnO	36	95,17	2,643611	0,554841
Au/TiO ₂	36	1266,837	35,18991	22,176
Al ₂ O ₃	36	21,248	0,590222	0,024161
ZnO	36	44,37	1,2325	0,319654
TiO ₂	36	164,71	4,575278	0,920088

ANOVA

Source of Variation	SS	df	MS	F	P-value	F crit
Between Groups	33625,16	5	6725,032	1680,045	3,6E-167	2,257066
Within Groups	840,6067	210	4,002889			
Total	34465,77	215				

Table C4: SUMMARY for Feed ratio = 1:1

<i>Groups</i>	<i>Count</i>	<i>Sum</i>	<i>Average</i>	<i>Variance</i>
Au/Al ₂ O ₃	36	85,37143	2,371429	0,276921
Au/ZnO	36	354,0024	9,8334	0,567336
Au/TiO ₂	36	2077,792	57,71645	8,236302
Al ₂ O ₃	36	17,39582	0,483217	0,006227
ZnO	36	60,94851	1,693014	0,11213
TiO ₂	36	182,2109	5,061414	0,304346

ANOVA

<i>Source of Variation</i>	<i>SS</i>	<i>df</i>	<i>MS</i>	<i>F</i>	<i>P-value</i>	<i>F crit</i>
Between Groups	88919,13	5	17783,83	11228,04	8E-253	1,472809
Within Groups	332,6141	210	1,583877			
Total	89251,74	215				

Table C5: SUMMARY for Feed ratio = 2:1

<i>Groups</i>	<i>Count</i>	<i>Sum</i>	<i>Average</i>	<i>Variance</i>
Au/Al ₂ O ₃	36	54,7285	1,520236	0,088474
Au/ZnO	36	250,3446	6,954017	1,769063
Au/TiO ₂	36	2780,36	77,23223	2,3341
Al ₂ O ₃	36	98,86531	2,746258	31,63365
ZnO	36	83,60867	2,322463	9,064479
TiO ₂	36	124,9037	3,469547	102,1443

ANOVA

<i>Source of Variation</i>	<i>SS</i>	<i>df</i>	<i>MS</i>	<i>F</i>	<i>P-value</i>	<i>F crit</i>
Between Groups	164164,2	5	32832,83	1339,805	3,9E-157	1,472809
Within Groups	5146,192	210	24,50567			
Total	169310,3	215				

Table C6: SUMMARY for Feed ratio = 3:1

<i>Groups</i>	<i>Count</i>	<i>Sum</i>	<i>Average</i>	<i>Variance</i>
Au/Al ₂ O ₃	35	86,9965	2,485614	1,976875
Au/ZnO	35	267,371	7,639171	2,654223
Au/TiO ₂	35	2323,2	66,37714	3,3079
Al ₂ O ₃	35	25,2173	0,720494	0,217511
ZnO	35	71,0345	2,029557	0,588534
TiO ₂	35	301,6706	8,619161	1,590235

ANOVA

<i>Source of Variation</i>	<i>SS</i>	<i>df</i>	<i>MS</i>	<i>F</i>	<i>P-value</i>	<i>F crit</i>
Between Groups	114187,5	5	22837,49	13257,98	3,6E-254	1,47325
Within Groups	351,3995	204	1,722546			1
Total	114538,9	209				